IMPLEMENTATION OF THE UNIVERSITY OF MISSOURI TERAWATT TEST STAND AND THE STUDY OF A LARGE, MULTICHANNELING, LASER TRIGGERED GAS SWITCH

A Dissertation presented to the Faculty of the Graduate School

University of Missouri – Columbia

In Partial Fulfillment

Of the Requirements for the Degree

Doctorate of Philosophy

Electrical Engineering

By

KEITH ROBERT LECHIEN

Committee
Dr. John M. Gahl, Chairman
Dr. Ken Struve, Member
Dr. Scott Kovaleski, Member
Dr. Mark Prelas, Outside Member
Dr. Bill Miller, Outside Member

MAY 2006

The undersigned, appointed by the Dean of the Graduate School, have examined the dissertation entitled.

IMPLEMENTATION OF THE UNIVERSITY OF MISSOURI TERAWATT TEST STAND AND THE STUDY OF A LARGE, MULTICHANNELING, LASER TRIGGERED GAS SWITCH

Presented by Keith LeChien

A candidate for the degree of Doctor of Philosophy

And hereby certify that in their opinion it is worthy of acceptance.

Dr. John Gahl, Professor, Electrical Engineering, University of Missouri-Columbia

Dr. Ken Struve, Adjunct Faculty, Electrical Engineering, Sandia National Laboratories

Dr. Scott Kovaleski, Assistant Professor, Electrical Engineering, University of Missouri-Columbia

Dr. Mark Prelas, Professor, Nuclear Engineering, University of Missouri-Columbia

Dr. William Miller, Professor, Nuclear Engineering, University of Missouri-Columbia

Acknowledgements

I would like to thank the members of the committee for their insight and assistance throughout this work.

I extend special thanks to Dr. John Gahl whose door is always open and who is always willing to discuss research.

I extend special thanks to Dr. Ken Struve of Sandia National Laboratories for support of this work.

I extend special thanks to Rob Sharpe and Dr. Juan Elizondo at Sandia National Laboratories. Rob acquired the equipment used for this work and provided invaluable technical help. Juan's correspondence was extremely helpful in designing the system used to test the switch.

I extend special thanks to Andrew Benwell for much needed assistance and willingness to brainstorm.

I extend special thanks to Shawn Bryan, Paul Glaser, Tim Evans, Zach Korenak, Ramasamy Ravindran, Mike Lombardo, Mike Hutsel, Brandon Morgan, Bill Baldridge, and Tyler Nickell. These undergraduate assistants made this research possible.

I extend special thanks to my parents, Robert and Barbara. I have always understood the importance of education because of their support.

Table of Contents

List of Figures

List of Tables

IMPLEMENTATION OF THE UNIVERSITY OF MISSOURI TERAWATT TEST STAND AND THE STUDY OF A LARGE, MULTICHANNELING, LASER TRIGGERED GAS SWITCH

Keith R. LeChien

Dr. John Gahl, Dissertation Supervisor

ABSTRACT

The University of Missouri Terawatt Test Stand is one of the world's largest university operated pulsed power facilities. It was developed and implemented, for a fraction of similar facilities cost, under the supervision of the author. The test stand was routinely operated at up to 200 kA at approximately 200 ns FWHM and 600 kV into appropriate loads. The test stand provides a valuable resource for pulsed power experimentation in areas ranging from component evaluation to wire array physics.

The laboratories original initiative was to research 2.5 MV laser triggered gas switches. Experiments were conducted in voltage ranges from 800 kV to 2.5 MV, with peak currents of over 175 kA, using air and SF_6 as fill gases. These parameters, along with electrode type, configuration, and size were varied to experimentally understand multichanneling and low inductance configurations for large laser triggered gas switches. This effort discovered that for very low impedance gas switching, avenues of drastic redesign of existing switches must be explored as opposed to modest design changes to meet stringent impedance requirements for future inertial confinement fusion programs. From this initiative, novel results were obtained that may be utilized for the future design of large, low inductance gas switches.

Chapter 1
Introduction

The University of Missouri Terawatt Test Stand (MUTTS) began assembly in January 2003 and was operational on April 22, 2004. The test stand consists of a 100 kJ Marx bank with a maximum theoretical charge voltage of 3 MV, that feeds intermediate storage capacitors that are switched with a laser triggered gas switch into a dummy load. The test stand is capable of supplying a >250 kA damped sinusoidal wave with a FWHM pulse width of 200 ns into the appropriate low impedance load. The test stand has gone through two major development phases and has supported thirteen students including one Ph.D., two Masters, and ten undergraduates. The test stand serves as one of the nations largest university operated pulsed power drivers.

A. Purpose of Research

The primary purpose of the test stand is to evaluate large, multichanneling, laser triggered gas switches with low inductance geometries. This will aid in the understanding of these switches for future very low inductance designs. MUTTS was fitted with a 2.7 MV multichanneling laser triggered gas switch called Rimfire designed at Sandia National Laboratories. The long term goal of the research at MUTTS is to improve the multichanneling reliability of these switches as well as improve jitter when the switches are scaled to larger voltages and electrodes are either increased in number or in diameter. It is also to achieve a more fundamental understanding of the effects of laser triggering on multichanneling and switch impedance. Multichanneling is important for two main reasons:

1) a reduction of electrode wear and 2) reduced impedance. The test facility provides a high voltage/high current test bed for a number of experiments that are easily scalable to large accelerators. The results are directly applicable to the requirements of the ZR accelerator at Sandia National Laboratories [1].

One obstacle in developing large accelerators based on Marx bank technology like that of ZR is switching the energy downstream of the initial energy storage section in a fast, reliable way. Thirty-six Marx banks on ZR slow charge intermediate storage capacitors. Energy is switched using individually laser triggered Rimfire gas switches that feed self-breaking water switches. Those switches feed transmission lines to the wire array load. The self-breaking water switches are present because the individually triggered gas switches do not switch fast enough (too highly inductive) to provide sufficient pulse compression to drive wire array loads. Lifetime performance limitations of the low inductance water switches fuels the desire to optimize more robust, faster, laser triggered gas switches. Gas switching is inherently superior to water switching because it is easier to work with logistically, has significantly reduced acoustic shock, and easier triggering methods, etc. Eliminating water self break switches, with a triggered gas switch, has a number of advantages such as: 1) reduced jitter, 2) increased timing/trigger control, and 3) reduced mechanical damage that is caused by the water switch shock wave. It is the goal of MUTTS to investigate ways to lower inductance in previously designed gas switches and perhaps eliminate the need for water based switching altogether.

We have previously investigated the requirement that, although multichannel breakdown may occur in the cascade section, a lack of symmetric and uniform breakdown will lead to higher switch inductance than is possible if symmetric breakdown occurred [2]. A lack of consistent and repeatable multichanneling performance may prevent the switch

from having the lowest possible inductance, thus affecting the risetime. Initial results indicated the need to encourage channel formation in a symmetric distribution on each cascade electrode eliminating azimuthal current flow in the electrodes. Methods were investigated for iterating small changes of currently designed switches rather than entire electrode redesigns because of the proven performance of the large gas switches [3,4]. We have also investigated the effects of electrode type, size, switch fill gas and fill gas pressure on multichanneling in both a laser triggered mode and in a self break environment and how the switches impedance is affected by a given parameter.

Rimfire has been extensively studied but with limited fundamental understanding fueling the research effort on scaled versions of the switch [4,5,6,7]. The switch investigated, depicted in Fig. 1-1, is scaled from a Sandia designed 4 MV Rimfire. It consists of a ten gap self-break section (called the "cascade section", Fig. 1-1, item 7) and a long single channeling trigger gap ("trigger section", Fig. 1-1, item 3) that is designed to utilize SF_6. In self-break mode the trigger gap is allowed to over volt with no applied trigger pulse. In laser-triggered mode, triggering is controlled by a pulsed (5 ns) frequency quadrupled Nd:YAG laser (266 nm, 30 mJ).

B. Dissertation Overview

This dissertation covers a wide range of subjects from development and design of system components to, switch testing, data analysis, and paper summaries. It starts with a review of papers and chronicles the high voltage switch program at Sandia National Laboratories that led to the development of the multistage Rimfire laser triggered gas switch. **Chapter 2: Rimfire Switch History** serves as a history that lays the foundation for the importance of Rimfire research conducted in this dissertation. The focus of this chapter is

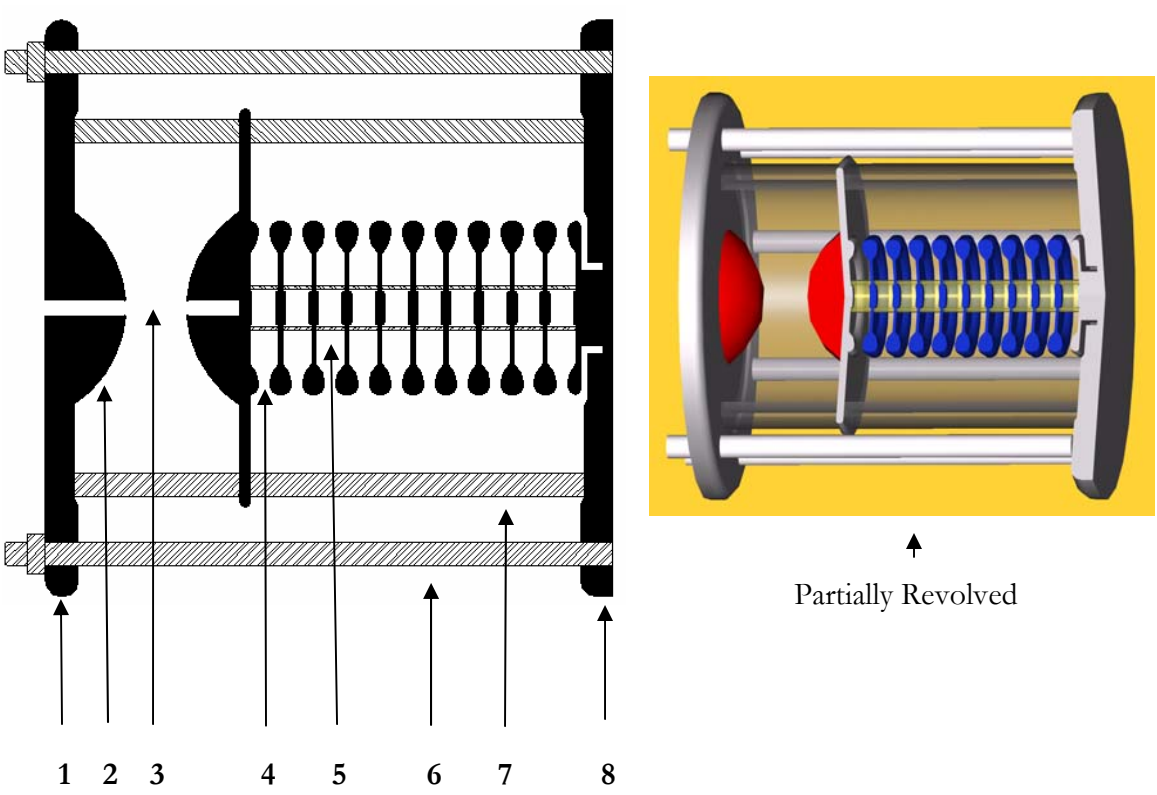

Fig. 1-1. 2.5 MV Rimfire. 1) Load end (aluminum), 2) trigger electrode with hole for laser (stainless/Mallory), 3) trigger gap (gas dielectric), 4) cascade gap, ten total (gas dielectric, stainless electrodes), 5) cascade spacer (acrylic), 6) tie rod (nylon), 7) gas envelop (PMMA acrylic), 8) I-Store/high voltage end (aluminum).

to highlight how the results of experimentation influenced Rimfire design progression over its' 20 year history. This section does not describe the programs on which Rimfire was implemented, but rather how a multigap concept was designed to meet the requirements for each machine.

Initial development, design, and implementation of the test stand are described in **Chapter 3: Development of the University of Missouri Terawatt Test Stand**. In the first phase, a two intermediate store design was considered and self-break switch data were collected, mostly with air as the fill gas. This chapter describes the design and initial experimental results which were used to obtain operational parameters for all subsequent

testing. This portion of the research was extremely crucial not only for gaining experience with the machine itself, but in the implementation of pulsed power design techniques in general.

The first switch data obtained were operating the switch in self-break mode and it is presented in **Chapter 4: Self-Break Data**. There are three separate sets of electrode trials presented. All data were taken at either ±30 kV Marx charge (1MV peak at the I-Store) or ±40 kV Marx charge (1.4 MV peak at the I-Store). All data are in self break mode using air as the fill gas. Analysis of self-break data was approached with the mission of obtaining proper experimental setup and a parameter space for the laser trigger data. Therefore, data are presented in a manner that was aimed toward guiding the MUTTS program in the direction of laser triggered experiments. Electrode configurations that were tested included arrangements of discrete conductors that acted as field enhancement points with the purpose of forcing a specific number of channels or channel arrangement.

Laser trigger experiments are described in **Chapter 5: Laser Trigger Data**. This chapter covers the phase II redesign of MUTTS beginning with test stand design for implementation of the laser system. This chapter presents the results from cascade electrode radius experiments and an electrode configuration using field enhancement holes in an SF_6 environment. Data were collected in a voltage range of 1.6 – 2.4 MV. Data are presented for air triggered arrangements and compared to SF_6 results. Effects of gas pressure on multichanneling are also presented. An impedance analysis of all data is presented.

An investigation into higher pressure SF_6 switch testing was conducted because of the lack of consistency in previously published work and the possibility at the time of fabricating a switch utilizing elevated SF_6 pressure. Pulsed SF_6 gas switching has been studied for decades, but little data exist for pressures above 50 psig. Experiments on high

pressure SF_6 – Argon breakdown were conducted as the natural progression of Rimfire testing was taking place and they are presented in **Chapter 6: SF_6 Breakdown – Experimental Analysis**. This chapter presents a collection of previous work regarding high pressure SF_6 and SF_6 – Argon break down and compares it to the data collected on MUTTS. Experimental work was conducted to determine how viable these mixtures would be to the development of a new switch. There are three parts to this chapter; 1) a brief discussion of impulse gas breakdown, 2) experimental data collected on the breakdown of SF_6 – Argon gas mixtures at elevated pressures, and 3) a summary of very high pressure gas switching and how the previous research relates to experimental data collected. This section served as a guide for the design of a new switch presented in **Chapter 7: New Switch Designs**.

Chapter 7: New Switch Designs describes a design process for large Rimfire-like SF_6 gas switch that is a result of the lessons learned throughout all of the other aspects presented in this dissertation. It is an investigation into a reduced inner to outer conductor ratio and reduced length 2 MV switch. This switch addresses the low inductance issue to provide a very fast switch that could potentially replace water switches on machines like Z. It also addresses a problem with the location of the gas envelope on current Rimfire designs.

Experimental results are summarized in **Chapter 8: Conclusions**. This chapter serves as a bulleted list of conclusions based on research, data, and experimental analysis. It contains references to locations within the document where evidence for each conclusion may be located and, where appropriate, references to other researchers' work.

A final **Appendix** chapter coordinates several pieces of data, photographs, and details items that were too cumbersome to be presented within the main dissertation body. This section contains equations, calculations, and experimental data that address assumptions that were made when designing the first phase of the test stand and for other

purposes. This section contains critical information that is useful as a reference for future machine and multichannel switch design.

Chapter 2
Rimfire Switch History

The following chapter is a paper study that chronicles the high voltage switch program at Sandia National Laboratories that led to the development of the multistage Rimfire laser triggered gas switch. A list of conclusions drawn by the authors about Rimfire gas switching is listed after a summary of each paper. The focus of this chapter is to highlight how the results of experimentation influenced Rimfire design progression. This section does not describe the programs on which Rimfire was implemented (Proto II [8], PBFA I [9], HERMES III [10], SATURN [11], PBFA II [12], Z [13], ZR [5]), but rather how a multigap concept was designed to meet the requirements of each machine. Most experiments conducted in the past on Rimfire switches were focused on evaluating a component that would work for a given setup. Very few experiments were conducted at a basic understanding level, or with the ability to iterate switch parameters, which is why research continues today at the University of Missouri Terawatt Test Stand.

The first particle beam fusion accelerator at Sandia (PBFA I) was equipped with a single gap, electrically triggered trigatron with a trigger pin installed in the center of the anode electrode. The 11 cm, SF_6 filled gap had a self-breakdown voltage of 2.9 MV at 60 psia [5]. The switches runtime, or the time from application of trigger voltage to conduction of current, was 90 ns when a 60 kV pulse was applied to the trigger pin. The jitter, or shot to shot variation in runtime, of this switch was 2.5 ns. Triggering a similar 2.5 MV switch with a 120 mJ UV laser pulse reduced the jitter to 0.5 ns. An upgrade to PBFA I, called PBFA II, required thirty six, 6 MV gas switches. It was determined that more than doubling

the single gap trigatron operating voltage would double the inductance, unacceptably increasing the jitter and requiring unacceptably high laser trigger energy. It was concluded that a new switch was needed to meet the requirements of PBFA II. A multistage concept was considered and was first implemented on PBFA I because its' multistage design allowed a relatively straight forward scaling to PBFA II voltages.

The first multistage concept considered, depicted in Fig. 2-1, consisted of an electrically triggered gap in series with 14 smaller cascade gaps [14]. The switch was operated at 3 MV in its' initial implementation. Switch operating inductance was determined to be 70 nH. The fields in the triggered gap were 275 kV/cm and for the cascade gaps the field ranged from 265 kV/cm to 295 kV/cm with the highest field occurring opposite the trigger section. Thin plates extended into the outer housing that supported the multistage cascade section. The plates also provided field shaping for the cascade and trigger sections. Thirty percent of the total voltage was distributed across the trigger section. The self-break voltage exhibited a rather large spread of 400 kV at 40 psia and 600 kV at 60 psia. Switch

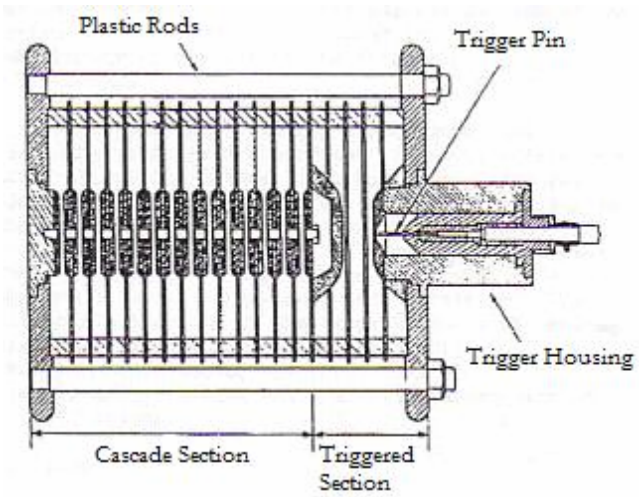

Fig. 2-1. First multigap concept utilized on a large accelerator at Sandia consisting of one electrically triggered gap and fourteen self break cascade gaps [5].

jitter was 2.5 ns. A faster rising trigger pulse lead to a smaller spread in jitter per switch and the jitter decreased slightly with increasing switch pressure. A similar switch, designed for 6 MV operation and a laser trigger, failed at 4 MV because of flashover on the housing dielectric. This was due to oscillating voltages between the resonant circuit set up between each electrode, the dielectric spacing, and the subsequent electrode. This particular multistage design was abandoned because program direction required larger operating voltages than the switch was able to accommodate without housing flashovers [5].

The subsequent design that eliminated electrodes extending into the dielectric was called Rimfire and was first introduced in 1985 [5]. The first implementation, a 6 MV, 500 kA design, consisted of a laser triggered gap in series with 16 multistage, cascaded gaps and is depicted in Fig. 2-2. Field shapers were implemented in the dielectric housing, but the electrodes themselves were pulled entirely into the gas envelope to eliminate problems in earlier designs. The driving factors of this design were to remove the cascaded electrodes from the outer housing, to lower the gap to gap capacitance, and to reduce the runtime of the switch. With a 25 mJ, 248 nm, 20 ns FWHM, KrF laser trigger pulse the jitter for one

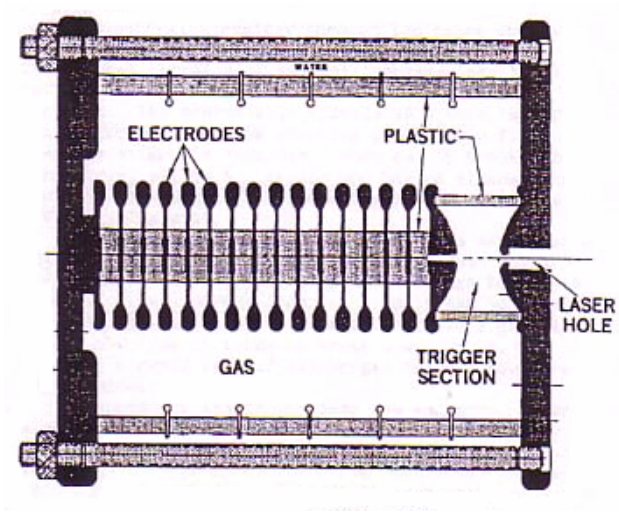

Fig. 2-2. The first version of Rimfire [14]. One laser triggered gap and sixteen self break cascade gaps.

switch was 0.4 ns. The laser created an ionization path a few centimeters long in the triggered gap. The switch had a runtime of 20 ns and showed a low dependence on self-breakdown voltage. The inductance of the switch was 400 nH, 100 nH of which came from the spark channels.

The switch was designed to operate with 325 kV in each cascade gap and 1.25 MV, or 21% of full voltage, across the triggered gap. Each electrode's field enhancement factor was approximately 1.1 giving a total field of 284 kV/cm per gap. The peak trigger field was approximately 300 kV/cm. The maximum fields experienced by any plastic surface were 115 kV/cm. As a result of initial testing, several conclusions were drawn about the initial Rimfire concept:

- Cascade design is important for fast switching because it allows short conduction lengths and relatively small capacitances between stages.
- Cascade field uniformity is very important because it insures each gap is equally ready to fire at the time of triggering. This allows a cascade breakdown to initiate in the gap closest the trigger and to "cascade" to the other end.
- Uniform fields between the cascade and triggered section insure that triggering will be dictated by the overvolting of the triggered gap and not by spurious high fields in the cascade section. This reduces jitter and the probability of prefire.
- The ringing current in each stage between multiple arcs is beneficial because it allows the arcs to self sustain and encourages multichanneling.
- The jitter of the total switch is approximately equal to that of the trigger gap if the first cascade gap is overvolted by a factor of four or more.
- The trigger gap should be short enough to be dominated by the laser spark length.
- Shielding all triple points from UV is necessary for lifetime considerations.

The scalability of the Rimfire concept, one of its' cornerstones, was more thoroughly investigated in 1987 [15]. The goal of these experiments was to investigate reliability that was measured in the jitter and probability of failure caused by prefires. Weibull statistics were used to determine the prefire limits of the Rimfire switch depicted in Fig. 2-2. These statistics describe probability distributions that are non-Gaussian and skewed toward lower values. Implementing the statistical distribution formula, calculated Rimfire pre-breakdown fields, and experimental prefire data from Hermes III and the Demon accelerators, a relationship was developed between the prefire rate and the maximum electric fields that a Rimfire switch may withstand. For a prefire rate of 0.003% (individual switch failure rate chosen for a 36 switch system reliability of 90%), the maximum electric field is related to switch pressure by,

$$\frac{E}{P} < 82 - 3.5P \qquad for \quad P < 4\ bars \qquad \text{Eq. 2-1}$$

where E is in kV/cm and P is in bars. This describes the relationship between prefire rate and undesired over-voltage of a cascade gap being the cause of the prefire. The statistical uncertainty of this relationship was ± 6% for 50 samples and ± 4% for 200 samples.

A similar statistical method was used to determine the prefire likelihood due to insulator flashover field. Data taken from the Demon accelerator indicated that the flashover prefire limit was related to the pressure by,

$$\frac{E_{ins}}{P} < 25\ \frac{kV}{cm\ bar} \qquad \text{Eq. 2-2}$$

for a 0.003% prefire level. The statistical sampling uncertainty was ± 15%. Both Demon and PBFA data indicated that if the reduced trigger field, E_t/p, was below 50 kV/(cm bar),

the prefires were caused by untriggered gap to gap breakdown and with a reduced trigger field above 50 kV/cm-bar, prefires were caused by insulator flashover.

The jitter of the switch was determined to be related to the laser trigger energy, laser pulse width, laser sparking length, percentage of total voltage across triggered gap, and laser power density. The trigger field limit, based on data from PBFA I was,

$$\frac{E_t}{P_{trig}} > 46 \ \frac{kV}{cm\ bar} \qquad \text{Eq. 2-3}$$

for a jitter of roughly 2ns. A test was conducted to determine the effect of trigger gap voltage on jitter. The trigger gap was replaced by several cascade gaps all of the same length and therefore with the same impressed voltage. One of those gaps was laser triggered. The jitter in this setup was unacceptably high at 10 ns for an E_t/P of 50 kV/cm-bar. It was concluded that a large trigger gap was necessary to have acceptable switch jitter. Several additional conclusions were drawn from prefire and statistical analysis.

- At least twenty to thirty percent of the switch voltage should appear across the triggered section for acceptable jitter.
- The pulse width of the laser should be on the order of the laser gap closure time.
- Electric field enhancements should be minimized (and certainly be lest than 2) for low jitter in the trigger and cascade sections.
- The cascade section evenly grades the fields and has a reduced field compared to the one gap trigatron.
- Laser spark lengths should be no less than 10-30% of the trigger gap length.

The Rimfire concept was implemented on Hermes III in 1987 [16]. The switch was a 2.4 MV, laser triggered, SF_6 filled version with a RMS jitter of 2 ns and is depicted in Fig. 2-3. The switch was triggered with a 15 mJ KrF laser with a FWHM of 30 ns. Thirty two percent of the triggered voltage appears across the triggered gap with peak electric fields below 200 kV/cm.

Two different trigger electrode types were used, one flattened and one rounded. The jitter for the rounded electrodes at 70% of self break was 2 ns while the jitter for the flatter electrodes 80% of self break was 2.5 ns. The focused laser beam created low level ionization throughout the length of the gap and a denser laser plasma for a few cm. The field distribution was non-uniform with the fields in the cascade section varying from 170 kV/cm to 190 kV/cm. The following conclusions were made as a result of the Hermes tests:

- Insulator field rings may prevent tracking the entire length of the switch.
- The switches runtime was shorter when the switch was submerged in oil as opposed to water because of the faster propagation velocity of the breakdown wave in the

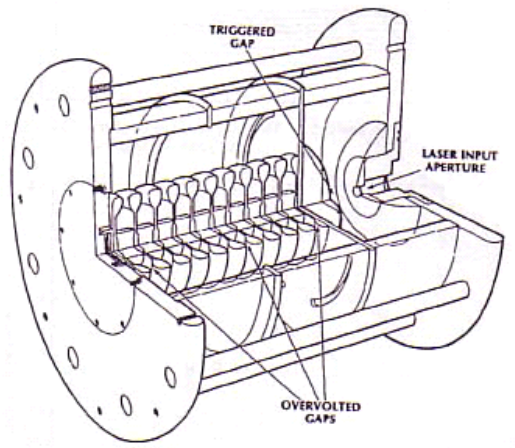

Fig. 2-3. HERMES III Rimfire implementation [16]. One laser triggered gap and ten self break cascade gaps.

lower dielectric constant oil.

With the Rimfire switch implemented in many of the large accelerators at Sandia, a shift was made to understand the complexities caused by the laser trigger on switching characteristics. A set of experiments was conducted on a 5 MV PBFA II switch like the one depicted in Fig. 2-2 [17]. This switch exhibited a 30 ns runtime and a 1 ns jitter. The average field for these experiments in the cascade section was 230 kV/cm with 22% of the voltage across the triggered gap. The first self breaking gap formed one to two arcs while the remaining gaps formed an average of four arcs. Delay associated with the cascade section was much larger for the first gap to break than for other gaps. Cascade gaps broke down sequentially, starting with the triggered gap. Increasing laser energy to 60 mJ did not significantly affect the jitter of the cascade section, but it did improve the jitter in the trigger section. The switch runtime and jitter was most dramatically affected by the reduced trigger field (E_t/P) and it depicted in Fig. 2-4.

A detailed account of Rimfire switch operation on Hermes III was presented in 1989

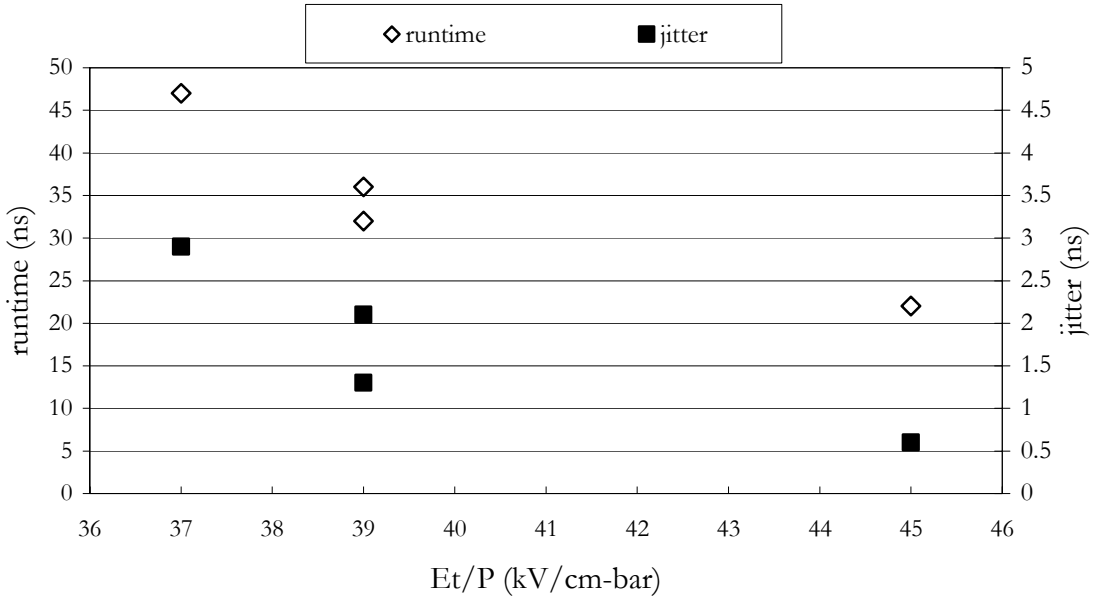

Fig. 2-4. Runtime and jitter as a function of reduced trigger field [17].

[10]. The version tested was 2.4 MV with a 1-sigma jitter (a 1-sigma jitter calculation assumes a Gaussian distribution and it is found by taking the spread of the runtimes and dividing by 3) of 2 ns for 70-75% self break. This did not change appreciably up to 90% of self break. The switch was triggered with a 10-30 mJ, 30 ns FWHM KrF laser. Shortening the laser pulse width from 26 ns to 15 ns had no effect on switch runtime. Decreasing the laser energy from 15 mJ to 7 mJ with a 15 ns FWHM affected the runtime slightly, perhaps a few nanoseconds for the whole switch.

The cascade section was shorted to emphasize the effect it had on the runtime of the switch. The trigger section alone could be triggered down to 35% of the self breakdown voltage. The trigger section was noted to close fully in 8 ns for 75% self break and that is why laser pulse width and energy had little effect on the runtime. It was concluded that a desirable Rimfire laser triggered switch would posses the following characteristics:

- Low jitter (sub nanosecond).
- Low prefire rate (one failure in several hundred shots).
- Minimal laser trigger requirements (30 mJ in a couple nanoseconds).

An experimental study of laser breakdown of the Rimfire switch was conducted in 1991 [6]. The KrF laser energy was varied from 5-60 mJ in a 22 ns FWHM pulse. It was hypothesized that a spark should be visible in the triggered gap wherever the power density exceeded 5 GW/cm^2 at 3 bars. Under these conditions, a spark was observed to be approximately 2 cm long which was 50% of the gap length. Three phases of laser triggered breakdown were noted in these experiments. First, there was a dim stage in which a fast discharge appeared within a few nanoseconds of laser arrival. Second, this stage was followed by a brighter phase in which the laser spark was visible and the entire channel heated. Channel heating dropped the resistance. Third, a current carrying phase began in

which the conduction current heated the channel further. These experiments confirmed that the jitter increases substantially when the gap closure time, or the first two stages, becomes longer than the laser pulse width. As trigger energy increased, the dependence of closure time on self break voltage was reduced. Focusing the laser in the middle of the gap had the lowest jitter as opposed to focusing it near the anode or cathode.

It was determined that two principle mechanisms dominate laser-SF6 interaction: multi-photon ionization and photo detachment (UV photons detach electrons from the negative ions). In a laser triggered gap, the SF_6 attachment rate and SF_6 photo detachment rate are comparable. As temperatures increase due to ohmic heating, thermal ionization becomes more significant. As this process occurs, electron density and temperature rise significantly and the gap is considered closed. Simulations showed completion of these phases was found to be 60 ns after laser arrival.

A 6 MV Rimfire was installed on the Advanced Pulsed Power Research Module (APPRM) at Sandia for investigation of the next generation pulsed power technologies in 2001 [3]. The focus of the first round of experiments was on switching runtime and jitter. The first of two switches tested was a hybrid design that incorporated the best of Russian and Sandia electrically triggered multigap switch design techniques. It consisted of a multigap cascade section that was in parallel with the main laser triggered gap. The trigger gap was isolated from switching voltages via a 4 μH isolation inductor.

The switch was electrically triggered and was implemented with several trigger configurations. With a 55.6 mm triggered gap, the runtime was 190 ns with unacceptable jitter. The trigger pin was moved to allow a 45.6 mm triggered gap. This reduced the runtime to between 147 and 156 ns. The final configuration had a 27.4 mm triggered gap. Trigger runtime was 31 ns with a jitter of 2 ns. The cascade section had a runtime of 39 ns

with a 3 ns jitter, providing a full switch jitter of 4 ns. A 5.8 MV Rimfire with 10.16 cm (4") radius electrodes and running in self-break was compared to the hybrid design. It was found to have a runtime of 24 ns and a jitter of 1.3 ns.

Several alternative designs were tested in 2003 [4]. These designs were pursued to address problematic failure modes of tracking the acrylic gas envelopes. Depicted in Fig. 2-5, the designs included a 6 MV baseline, a modified baseline, and a cantilevered design. The baseline operated at 4 MV and was originally fitted with 10.16 cm radius electrodes. Those electrodes were quickly determined to cause very high radial fields because of their close proximity to the gas envelope. Electrode radius was reduced to 6.67 cm (2.625") and in turn the radial fields at the envelope were reduced. The switch tracked on the cascade envelope housing after twelve shots.

The modified baseline was operated at 4.5 MV and did not experience any failures in

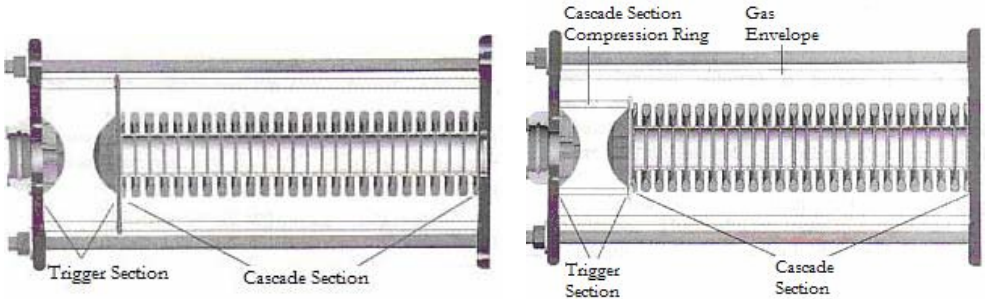

a) Baseline b) Modified Baseline

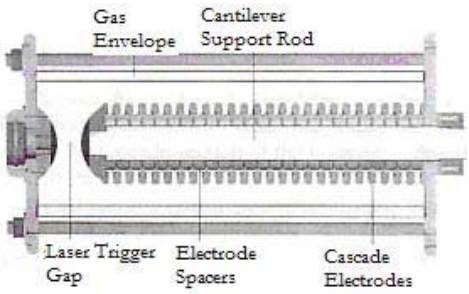

c) Cantilevered

Fig. 2-5. 6 MV alternative Rimfire designs [4].

18 shots on a test stand called Z-20 designed to represent a 20º slice of the ZR machine at Sandia. The modified baseline was tested for 50 shots at 5.4 MV in a different test bed that was called STB. Two tracking occurred on the trigger envelope and this design was abandoned for a cantilevered approach that did not require a trigger support envelope. The cantilevered switch was tested to 4.9 MV and failed once in 50 shots. The failure occurred on a cascade separator insulator without destruction and with a pressure adjustment, testing could continue.

A hybrid Rimfire design was introduced for the purpose of addressing high impedance/erosion problems in the long single channeling trigger section. These designs depicted in Fig. 2-6 required the implementation of an isolation inductor like the Russian/Sandia switch tested in 2001 [3]. The first attempt at a Rimfire hybrid trigger resulted in failures of the multigap trigger section insulator after 20 shots, although the

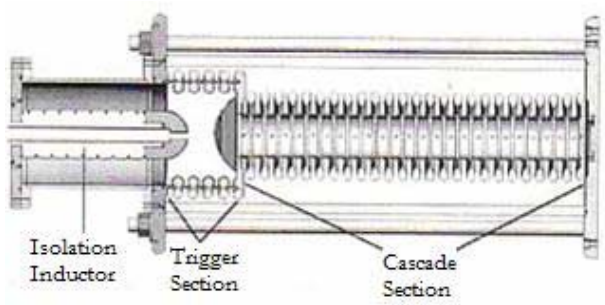

a) Trial 1

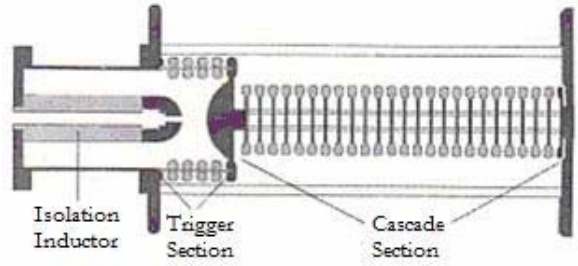

b) Trial 2

Fig. 2-6. 6 MV Hybrid Rimfire [4].

switch experienced similar runtimes as the baseline to 4.9 MV. The switch was redesigned to reduce this likelihood. A second design was implemented that required shorting the first cascade gap because of a post fabrication design change. This caused the fields to be non uniform and to be higher in the second cascade gap than in the trigger. As a result, the jitter was higher than acceptable and this design was abandoned.

With many years of experimental data for Rimfire conducted on several machines at Sandia, comprehensive modeling of the switch was initiated in 2003 [7]. The focus of the modeling was to provide a comprehensive picture of the electrical operation and to aid in determining causes of failure. The requirements for the hybrid trigger Rimfire at this time were a 0.2% probability of prefire with a 2.5 ns jitter. Arcs in the trigger and cascade section were modeled as a constant radius varying conductivity arc that switched from off to on in less than 3 ns. Modeling confirmed "cascade" breakdown initiating at the triggered end and ending at the opposite end. It also confirmed runtimes that were rather close to experimental values in both an oil and water dielectric exterior. The model also determined an appropriate value for isolation inductor that would have minimal effect on the breakdown wave, but still force multichanneling in the hybrid section. The model showed quantitatively the following issues.

- The hybrid trigger section initiates after the cascade section breakdown wave reflects back to the trigger section.
- The cascade runtime is 9 ns in oil and 19 ns in water.

In October 2005, the Rimfire switch program began a rejuvenated effort to understand the complexities of gas switching by exploring basic science. A massive joint effort between Sandia, several universities (including Missouri-Columbia), and industry was forged to bring experts from diverse backgrounds to work toward one common goal: to

understand the basic science governing laser triggered gas switches so a reliable switch may be developed that meets the needs of the evolving ZR program.

The very first multigap design implemented in 1985 at Sandia had flashover problems on the gas envelope. Twenty years later the problem of unacceptable flashing frequency of the gas envelope still exists. A reliable design is required for the ZR program by mid 2007. This is no trivial undertaking. The studies conducted at MUTTS represent the state of the art for the Rimfire switch program and are directly applicable to the future development of these switches and large pulsed power machines.

Chapter 3

Development of the University of Missouri Terawatt Test Stand

The test stand was constructed in two phases. Initially, a two intermediate store design was implemented and self-break switch data were collected, mostly with air as the fill gas. These data were collected for shots #1 through #141 and a shot log for these data is found in Table 9-3. In the second phase, the test stand was redesigned to accommodate the laser triggering system. This chapter describes the first phase and the settings that were used for self-break testing.

A. Phase I: High Energy Test Stand

The first phase of MUTTS consisted of a Marx bank, two intermediate store capacitors, a Rimfire switch, and a dummy load [18]. The Marx bank consists of 32, 0.7 μF, 100 kV Aerovox capacitors shown in Fig. 3-1 (additional pictures of this setup are depicted in Fig. 9-3). The Marx is arranged in 4 rows of 8 capacitors per row [19]. It is charged by a ± 100 kV, 50 mA Peschel Instruments dc power supply. The Marx is switched using 16 Physics International T508 spark gaps that are triggered by an erected mini-Marx. The mini-Marx consists of 8, 150 nF, 50 kV Maxwell capacitors that trigger the first two rows of the four row Marx. The mini-Marx is bipolar charged using two 50 kV Glassman High Voltage power supplies, one positive and one negative. The mini-Marx is triggered by a fast rising Physics International TG-70, which is triggered using a PT-55 made by Pacific-Atlantic

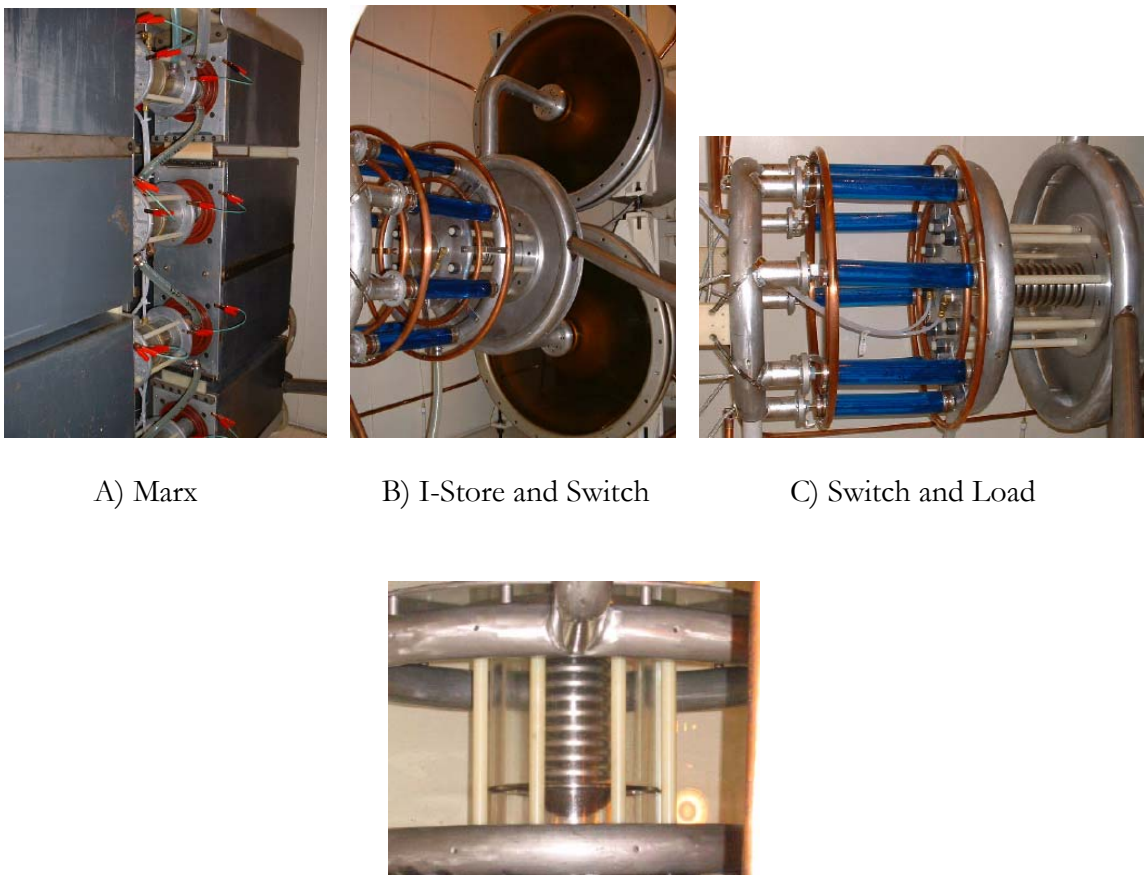

A) Marx B) I-Store and Switch C) Switch and Load

D) Switch

Fig. 3-1. Phase I of the University of Missouri Terawatt Test Stand.

Trading Co. Inc. The PT-55 is triggered by a PT-003 which is pulsed with a 500 ns, 7 V signal.

The load section, shown in Fig. 3-1, item C, was designed to accommodate both the resistance requirement of 4 Ω and to allow optical access for the laser. The symmetric array nature of the load also reduced the inductance. The load consisted of eight $CuSO_4$ water resistors that were 33 cm (13") long and 5.08 cm (2") in diameter. Each resistor had a nominal resistance of 32 Ω for an equivalent resistance of 4 Ω. It was experimentally determined as the resistors were made that the maximum conductivity we could expect from

our deionized water/copper sulfate solution was 50 mS/cm. A comprehensive design of the load is described in more detail in a following section.

Designed for 3.2 MV, the water filled intermediate stores (referred to as "I-Store" or "IS"), depicted in Fig. 3-1, item B, have a practical peak voltage of 2.7 MV resulting in a Marx maximum charge voltage of 70 kV for reliable operation [20]. Deionized water is constantly circulated through the intermediate stores, which are connected via hosing in series, to keep the resistivity above 10 MΩ-cm. With a very low inductance switch, the Marx is capable of delivering 2 MV at 500 kA into a 4 Ω load. Thus 1 TW is possible, however, in practice it has yet to be achieved. A simplified equivalent circuit of the Marx, intermediate store and load is depicted in Fig. 3-2. The series equivalent inductance and resistance for this model were previously obtained for Proto II [8]. The switch is modeled in a variety of ways as more detailed circuit simulations were implemented. Other implementations are described in the following chapters.

The University obtained a 4 MV Rimfire that needed to be scaled to a 2.7 MV version. The major effect of this decrease in voltage is the reduction in the number of cascade gaps from 17 to 10 and a repositioning of the trigger side field shaper. The following is a list that contains the stipulations that were utilized to scale the switch down in

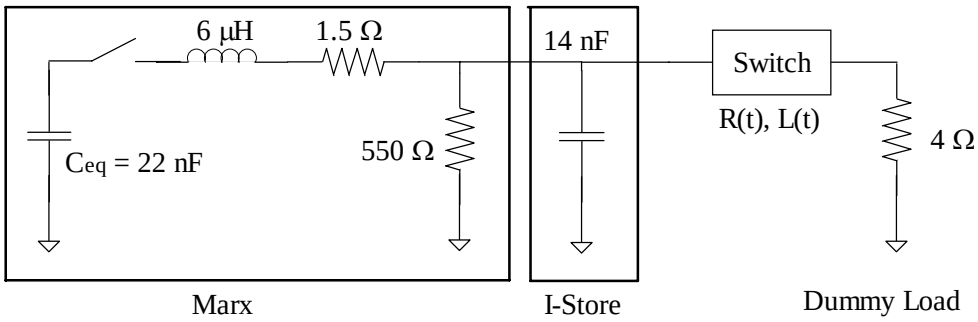

Fig. 3-2. Simplified equivalent circuit.

voltage. This section presents design stipulations and criteria, so the results are good to within sufficient design accuracies. These stipulations are a result of the physical space that was available, extensive design experience, and previous performance of Rimfire switches.

The maximum pulsed voltage allowed on the intermediate store is 2.7 MV. For a static full voltage (2.7 MV) the electric field should be 210-220 kV/cm in each of the ten cascade gaps. A uniform profile across all gaps is preferred [21]. The voltage distributed in the trigger section must have 20 to 30 percent or more of the voltage, or a range of 540 kV to 810 kV.

The original Proto II field shapers are used on both the load side and the intermediate store side. Fields across the load Tygon (or any plastic) must not exceed 100 kV/cm to reduce the risk of surface flashover [21] (see Appendix Section B). This means the load must be at least 33 cm (13") in length. A cylindrically symmetric load design is preferred for laser access. A voltage range of 2.4 MV – 2.7 MV is preferred, rather than always operating at peak voltage. Six return copper conductors are to be used to simulate a full coaxial geometry. This is a result of space constraints. The electric field must not exceed 400 kV/cm in the bulk oil [4]. The switch should be operated below 50 psig of SF_6.

The first step was to analyze the pulse charge characteristics of the intermediate store. Using an equivalent circuit of the Proto II Marx (Fig. 3-2), the charge voltage on the intermediate store rises to 2.7 MV with a 10%-90% rise time of 350 ns with a 90 kV charge on the Marx (Fig. 3-3). A voltage of roughly 180 kV is seen across each cascade gap and approximately 850 kV is distributed in the trigger section. The switch is filled with SF_6 with no independent pressure volumes for the trigger and the cascade section. Each section will experience the same breakdown fields. The appropriate pulsed breakdown pressure may be

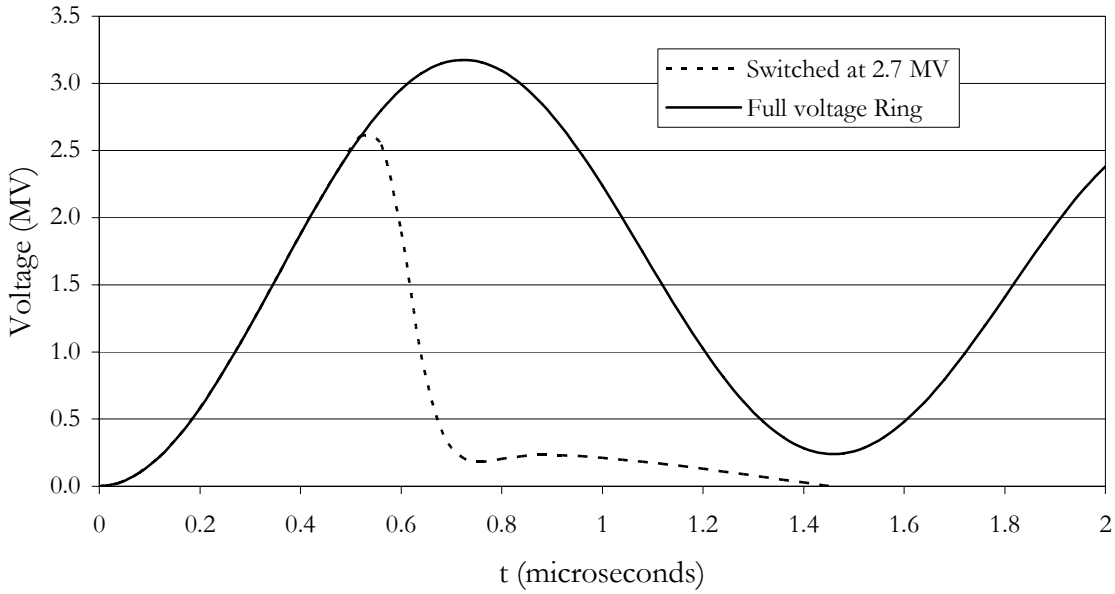

Fig. 3-3. Intermediate store charge voltage.

determined by investigating the pulsed breakdown of SF_6. The pulsed breakdown field of SF_6 is empirically determined to be related to the gas density and time to breakdown by,

$$\rho\tau = 97800\left(\frac{Epeak}{\rho}\right)^{-3.44} \qquad \text{Eq. 3-1}$$

where,

$$\rho = \frac{PM}{RT}. \qquad \text{Eq. 3-2}$$

ρ is the gas density in gm/cc, τ is the delay time to breakdown from the E_0 breakdown field in seconds, E_{peak} is the pulsed breakdown field in kV/cm, P is the pressure in atm, M is the molecular weight in gm/mol (145 for SF_6), R is the universal gas constant in $atm{\cdot}L{\cdot}K^{-1}{\cdot}mol^{-1}$ [22,23]. In order to solve Eq. 3-1 for E_{peak}, the E_0, or minimum breakdown field and time to breakdown must be known. The time to breakdown is extrapolated from the slope of the voltage rise from the time of E_0 breakdown to pulsed breakdown. E_0 breakdown and delay time are related to the pulsed peak field by,

$$Epeak = \frac{dV}{dt}\tau\frac{1}{d} + E_0 \qquad \text{Eq. 3-3}$$

where dv/dt is the change in voltage over the change in time from Fig. 3-3. From Eq. 3-1 and Eq. 3-3, an E_{peak} may be determined.

A controversial issue when dealing with SF_6 breakdown is the appropriate E_0 breakdown value to use in a non-uniform field calculation. Several experimental values were utilized in order to obtain a likely range of potential pulsed breakdown values. Fig. 3-4 shows relevant dc breakdown curves for SF_6 non-uniform breakdown. The three curves plotted are E_0 from Nitta, a J.C. Martin Air breakdown curve multiplied by 2.7 for SF_6, and a formula for E_{DC} breakdown that was empirically determined [24,25,22]. Nitta's E_0 curve is plotted as a reference and there is a discussion of this curve and its influence on pulsed breakdown in Chapter 6, Section D. Using the Nitta curve and the straightforward, albeit largely simplified design calculation for Eq. 3-3, the pulsed breakdown fields are found to be at odds with previous experimental breakdown fields [14,17]. This curve is rejected for this

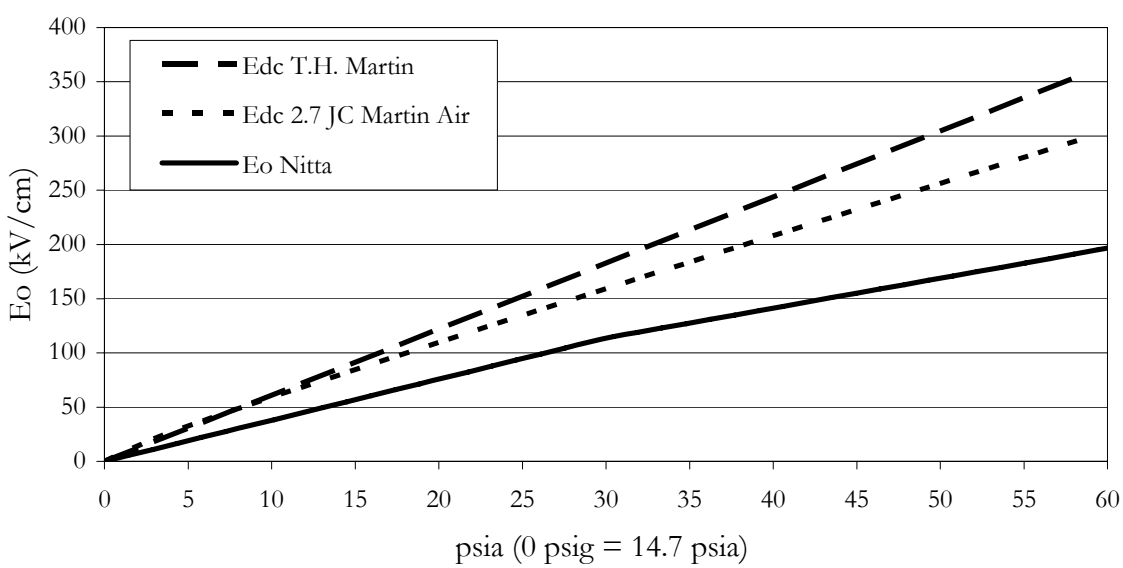

Fig. 3-4. SF_6 DC breakdown curves.

calculation and to error on the conservative side, the JC Martin air equation with a SF_6 correction is used in Eq. 3-1 and Eq. 3-3.

Looking at the system macroscopically, the voltage in each cascade gap will rise to 182 kV with a 10%-90% of 350 ns. Thus *dv/dt* for the cascade gaps is 414 E 9 V/s. The triggered gap will rise to 900 kV in 350 ns with a *dv/dt* of 2.057 E 12 V/s. Each *dv/dt* is subject to a delay time associated with the capacitance of each gap. This delay time is on the order of a few nanoseconds and is ignored in this calculation [7]. Using this information in Eq. 3-1 and with E_0 breakdown of the JC Martin type, the pulsed field at the time of breakdown of the switch for each type of gap is shown in Fig. 3-5. This plot really indicates what the field is at the time either the cascade or trigger gaps breakdown. For all pressures the trigger field is larger and therefore the trigger section dominates switch breakdown.

For 47 psig the cascade section has a pulsed breakdown of 255 kV/cm and the triggered section has a pulsed breakdown of 288 kV/cm. These are conservative numbers

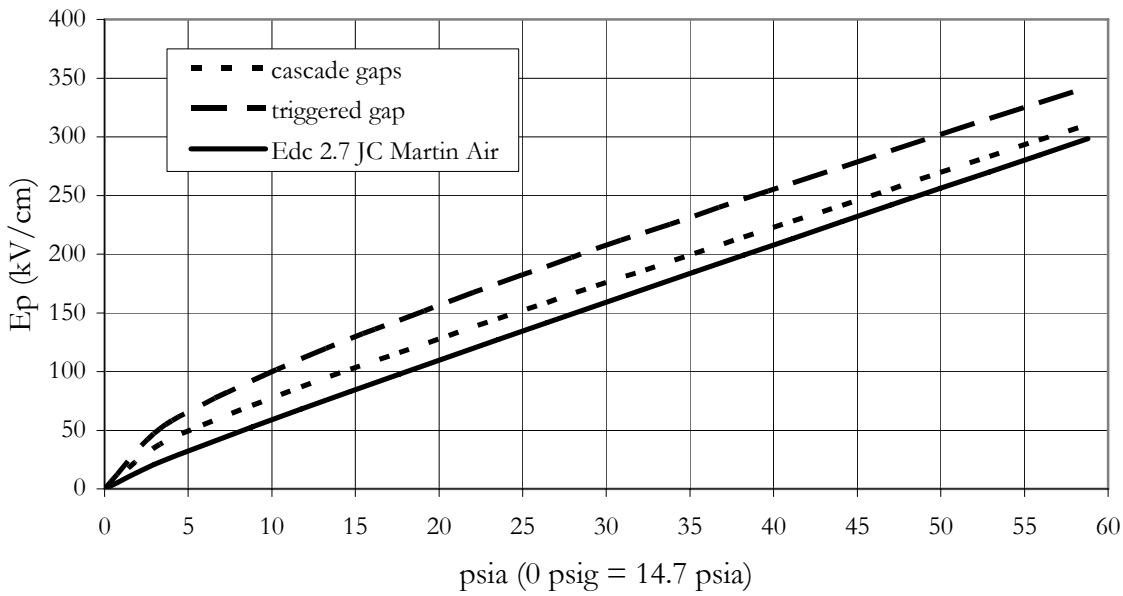

Fig. 3-5. Anticipated breakdown fields.

and are used in the field simulations for the switch. As a comparison, for the handbook dc data, the cascade gaps breakdown at 294 kV/cm and the triggered gap at 319 kV/cm. Using these values, the 2.7 MV Rimfire was implemented with 10 cascade gaps and a trigger gap spacing of 4.7 cm (1.852").

B. Switch Charging Phase

A complete picture of the intricacies of breakdown requires 3D electro-dynamic field solvers. These field solvers are unavailable, but a 2D electrostatic solver was used to simulate switch charging and conduction phases. This provided sufficient results for design purposes. For a 2.7 MV charge the field in the cascade region is roughly 210 kV/cm in the center of the gap with 180 kV in each gap. The highest field point in the gap is between the center of the gap and the edge of the ring. The fields at that location are roughly 225 kV/cm in all gaps as shown in Fig. 3-6. The gap length is 0.866 cm and the field enhancement

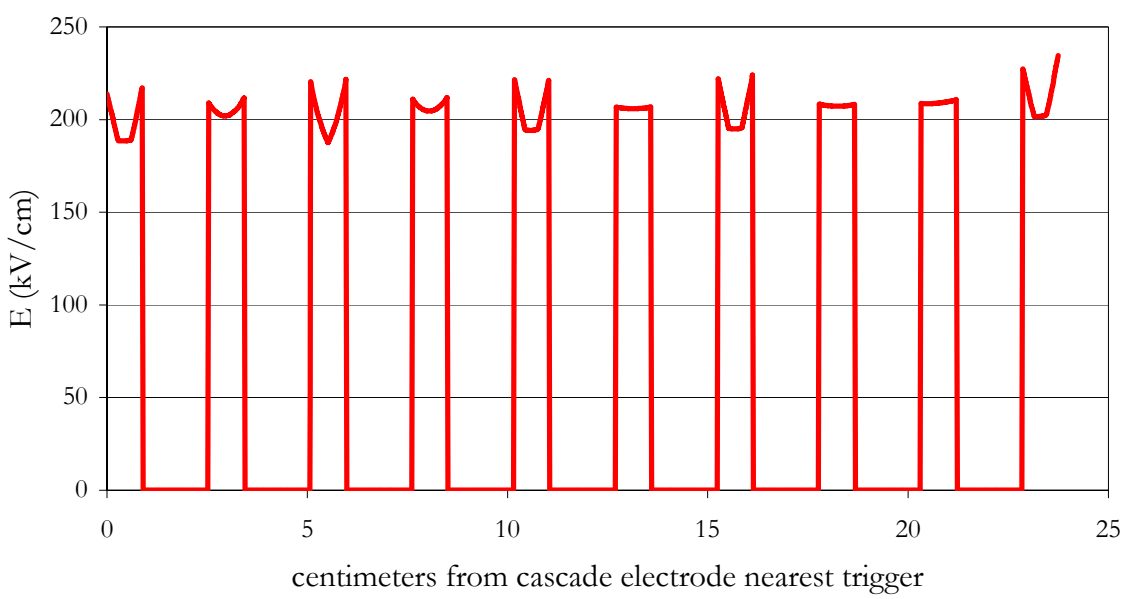

Fig. 3-6. Cascade gaps field at 2.7 MV.

factor is roughly1.1. The field is graded evenly via placement of the Proto II field shapers in the appropriate locations in all gaps of the cascade section. For a 2.7 MV charge there is 875 kV in the triggered gap resulting in a peak field of 255 kV/cm. A 4.7 cm (1.852") trigger gap with 8.89 cm hemispherical electrodes and a laser hole for laser propagation results in a field enhancement factor of 1.4. A field profile is displayed in Fig. 3-7. During charging, the peak field on the casing in both the trigger section and the cascade section does not exceed 80 kV/cm. The field on the disks separating each electrode is 83 kV/cm. The highest field in the oil occurs at the high voltage electrode and it is 351 kV/cm. With a –2.4 MV charge the peak field in the cascade section is 200 kV/cm and in the triggered section is 227 kV/cm.

C. Load Section and Switch Fields During the Conduction Phase

The load was designed to be 4 Ω and the conductivity of the liquid in the resistor must not exceed 50 mS/cm. Load plastics must not experience fields greater than 80 – 90

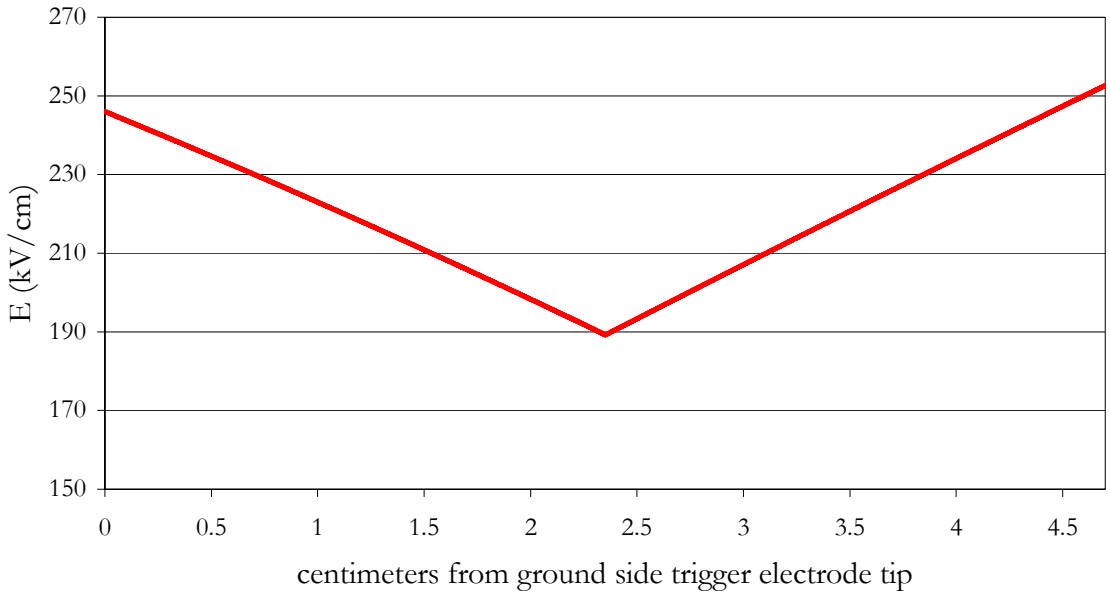

Fig. 3-7. Trigger field at 2.7 MV.

kV/cm despite sharp crimps on the load to hold it together. This results in the maximum length of the resistor liquid section to be 33 cm (13 in.) with a conductivity of 50.5 mS/cm. In the conduction phase, the load section of the system is stressed electrically. This results in adding additional field shapers to the load section to protect the sharp crimps and lower the fields at the triple points. Though the maximum I-Store voltage is 2.7 MV the load will never see this because the switch does have impedance. The purpose of experiments being conducted at MUTTS is to reduce this loss by increasing the symmetry of switch breakdown and develop low inductance designs. The switch's impedance will not be eliminated. The following design is for a system *if* 2.4 MV was the maximum voltage across the load leaving a drop of 300 kV across the switch. The peak fields during conduction are experienced on the grating ring on the switch side of the load. This field is 325 kV/cm. The peak field experienced across the load is 90 kV/cm at the electrode/water/Tygon triple point. This is below the absolute maximum 100 kV/cm level for –2.4 MV at the switch plate (see Fig. 3-8).

The field shaper at the high voltage side (bottom of Fig. 3-8) is that of the Proto II intermediate store connector. The field shaper on the load side is the Proto II trigger side

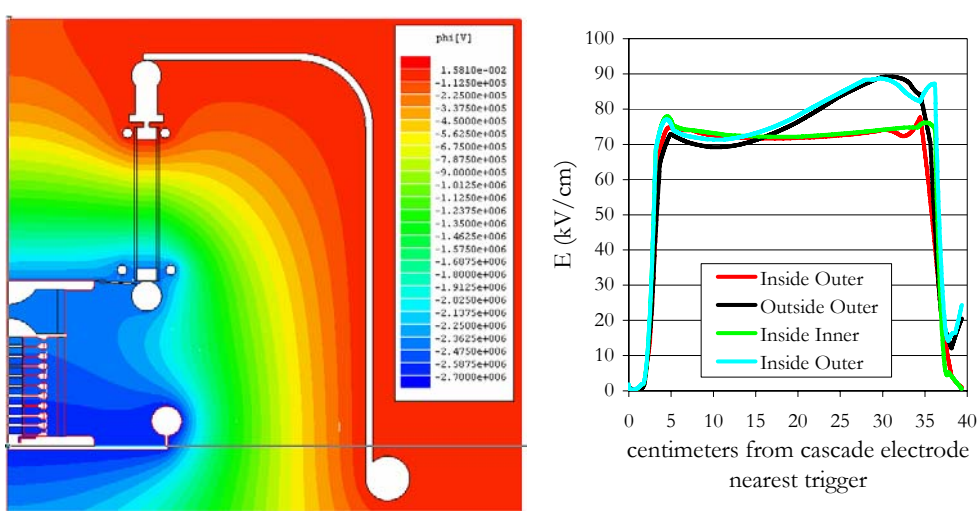

Fig. 3-8. Maximum theoretical load voltage gradient and load field.

field shaper. The field shaper on the load side is in a slightly lower plane than the ground plate of the switch. The load extends from this trigger field shaper to another field shaper ring that holds the load. Each end of the load is surrounded, on both sides, by copper pipe field shaping rings to alleviate high fields at triple points at the load electrodes. Current is returned from the load section to the I-Store by six 0.75" copper pipes. A macroscopic drawing of the switch and load section is depicted in Fig. 3-9.

D. Intermediate Store Considerations

All return conductors must stay at least 18" away from the switch support plate and bus bar to keep fields sufficiently low in the oil. The following two scenarios were possible. Each scenario includes a field profile for the water and oil sides of the intermediate store barrier. The straight feed is for the case where the feed will not naturally interfere with the

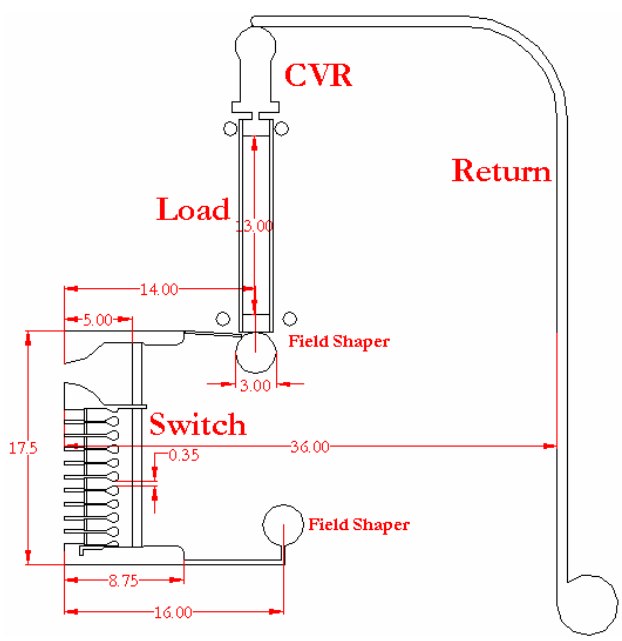

Fig. 3-9. Macroscopic drawing of load and switch (all dimensions in inches). The outer return conductor is listed here as 36". This was for simulation purposes only. It was really 51".

high voltage switch plate. The bowed scenario accounts for this interference. As shown in Fig. 3-11, the fields due to a straight feed exceed the maximum 100 kV/cm and are determined to be unacceptable. Fig. 3-11 indicates all fields stay below the 100 kV/cm theoretical maximum and thus bowed field shapers were implemented for the return conductors.

E. Output Section Inductance

The shortened 10 gap switch's inductance is dependant on the distribution of arcs in the cascade section. Inductance of the switch may be calculated from the electrode rings, plates, and trigger electrodes and, for non magnetic materials, it is based purely on the geometry. Six copper pipes are used to roughly approximate an outer conductor coaxial ground return for the intermediates stores (see Appendix Section A). Since not all outer conductors are perfectly symmetric, an average return radius was taken. Conductor radii and length are needed to determine the inductance. The outer conductor outer radius and inner

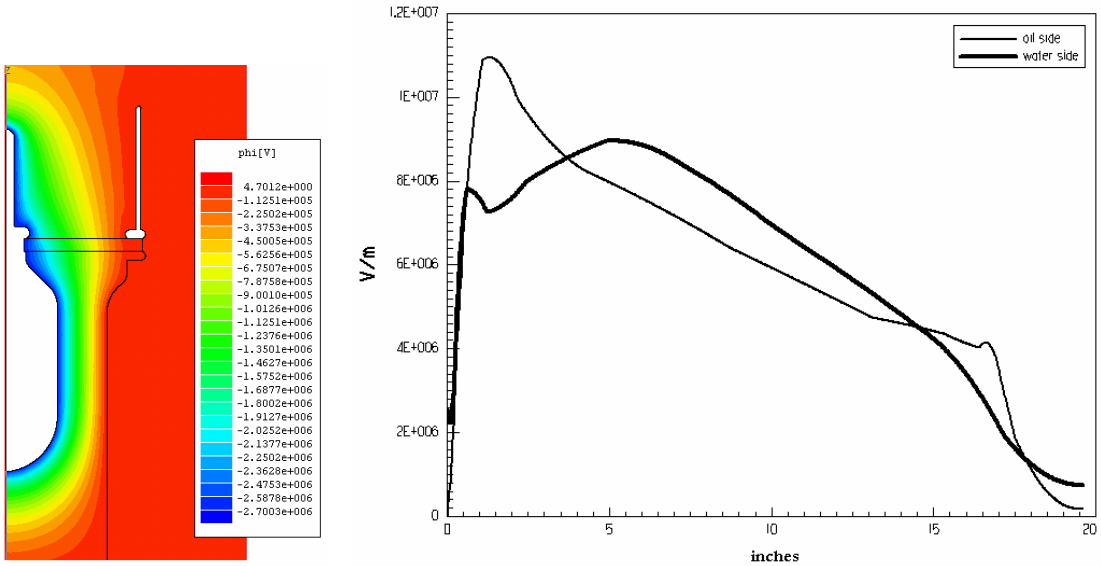

Fig. 3-10. (left) voltage potential lines for a straight return, (right) intermediate store surface electric field for straight coaxial returns.

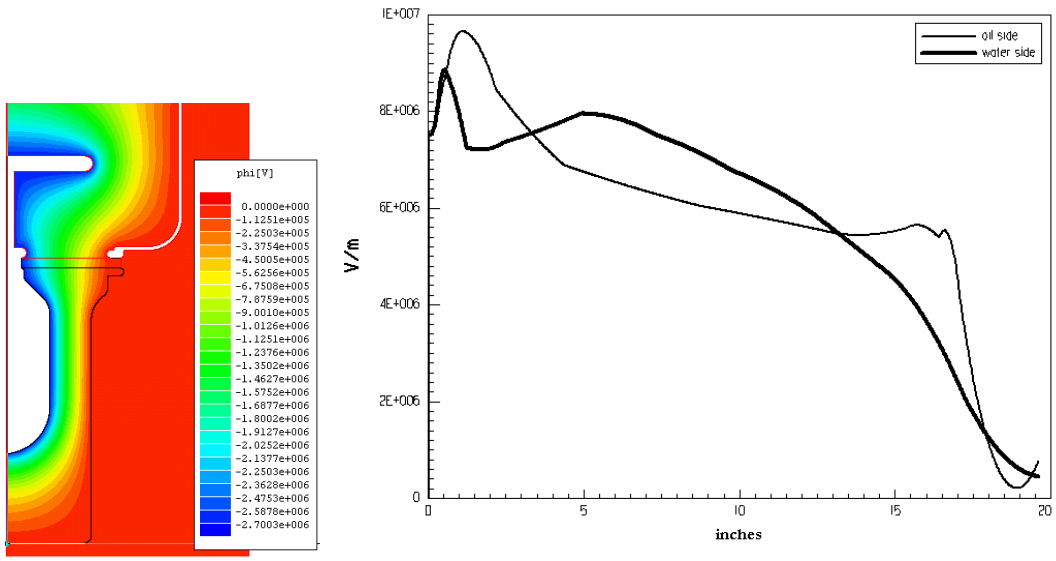

Fig. 3-11. (left) voltage potential lines for bowed returns, (right) intermediate store surface electric field for bowed coaxial returns.

radius are essentially the same since the ratio of the radii is very near unity. This radius, both inner (ρ_2) and outer (ρ_1), is 132 cm (51”). The radius of each return conductor is 1.27 cm (0.5”).

Eq. 9-3 in the Appendix was used to find the inductance for several portions of the switch. For the cascade electrodes, the radius, ρ_3, is 6.67 cm (2.625”) and the combined length, l, of all of the electrodes is 16.535 cm (6.51”). The $\ln\zeta$ term is 0.25 for all calculations (see Appendix). The inductance of the cascade electrodes is roughly 124 nH. For the switch end plates, the radius is 44.45 cm (17.5”) and their combined length, l, is 5.08 cm (2”). The inductance of the end plates is approximately 19 nH. For the trigger electrodes, the average radius is 3.81 cm (1.5”) and its length is 7.87 cm (3.1”). The inductance of the trigger electrodes is roughly 68 nH. For the trigger arc, arc radius is assumed to be 0.15 cm and have a length of 4.7 cm (1.85”). The inductance of the trigger arc is approximately 71 nH.

For cascade arcs, Eq. 9-2 was used to calculate the inductance. The arc array radius is 6 cm (2.375") and an arc radius of 0.1 cm is assumed. The arc array is assumed to be symmetric and all arcs are assumed to be equally spaced from each other. The combined length of the arcs is 8.86 cm. For a three arc per gap arrangement, the inductance is roughly 74 nH and for 10 arcs it is roughly 58 nH. This inductance is likely a slight underestimate considering the actual geometry.

Summing all contributions, the total inductance of the switch is 340 nH to 356 nH. The most significant ways to reduce this inductance is to shorten the switch, or decrease the ratio of the radii of the outer and inner conductors.

The calculation of inductance of the load carriage is similar to that of the arcs in the cascade section. There are eight parallel evenly spaced resistors each of radius 2.54 cm in an array of radius 33.8 cm and with a length, including connections and diagnostics of 53.34 cm (21"). The inductance of the load section is 155 nH. The total inductance of the output section including the switch is roughly 500 nH.

The inductance of the connection between the Marx and the switch is calculated using,

$$L = 2\,l\left[\ln\frac{2l}{r} - 0.75\right] nH \tag{4}$$

where l is 133 cm (52.5") and r is 2.9 cm (1.125") [26]. The inductance of the pipe is 1 μH. Using the same equation, the inductance of the I-Store connection to the switch may be determined. The shorter leg has an inductance of 210 nH and the longer has an inductance of 450 nH.

F. Diagnostics

Phase I had a diagnostic suite consisting of voltage, current and optical monitors for shots 1 through 141. The following is a description of the diagnostics installed except where the shot log states otherwise (see Appendix Table 9-3). Load current was measured by eight T&M Research Model 250-1 current viewing resistors (CVR's). Each had a risetime of 2 ns with a maximum dissipated energy of 250 J. Table 3-1 is a list of the resistance value of each CVR and where it was mounted during phase I. The maximum current theoretically possible for a ±30 kV Marx charge is roughly 200 kA. Thus each load resistor received was roughly 25 kA. The voltage at the output terminals of each CVR was nominally 500 V at this current level. Each load CVR and a Marx CVR had a 30 dB Weinschel Model 1 attenuator inline. This reduced the voltage at the scope by a factor of 31.62. The expected voltage representing load current at the scope (diagnostic lines labeled "1"-"8") was 16 V. The total cable length for each load CVR was 24.6 meters (80' 10", 121 ns) to the scope.

Marx current was measured by a single CVR with a value of 0.004995 Ω (diagnostic line labeled "9"). With a peak Marx current of 50 kA, the voltage at the Marx CVR was 1000 V. At the scope this attenuated to 8 V. There was 30.1 meters (98' 10", 148 ns) of cable for the Marx current CVR up to the scope

The load voltage was monitored with a voltage divider (labeled "A") and a 52.4 Ω

Table 3-1: CVR resistance values

CVR	Value (ohms)	Load R (ohms)
1-L	0.01967	32.71
2-L	0.02036	32.56
3-L	0.01979	33.09
4-L	0.01979	33.63
5-L	0.01981	33.03
6-L	0.01984	33.51
7-L	0.02047	33
8-L	0.01982	32.68

high voltage attenuator (labeled "A-52.4 input" and diagnostic line labeled "10"). The VM saw roughly 1.2 MV (could be less depending on energy required to drive the spark gaps). The output was 28 V with a voltage division ratio of 1220:1 and a HV attenuator division ratio of 17.7:1 and a 6 dB attenuator at 1.2 MV. The cable length for this monitor is 97' 4" (146 ns). Marx output voltage is monitored with voltage divider (labeled "B") and a 49.7 Ω high voltage attenuator (labeled "B-49.7Ω input" and diagnostic line labeled "11"). The maximum this voltage monitor theoretically saw was 900 kV peak at a Marx charge of ±30 kV. At 900 kV the output of the voltage monitor was 21 V. The intermediate store voltage was monitored with a voltage divider (labeled "C") and a 48 Ω high voltage attenuator (labeled "C-48 Ω input" and diagnostic line labeled "12"). The VM was 500 kV peak. At 500 kV the output of the voltage monitor was 12 V. This monitor has a cable length of 25.2 meters (82' 8", 124 ns).

G. Gas Operating Curves

The spark gaps in the Marx and mini-Marx (MTG) were each leak tested to 40 psig before installation. The operating curves for the TG-70, MTG and Marx are obtained from manufacturer data sheets and are depicted in Fig. 3-12 [27]. A similar set of curves were obtained using self break data for the Rimfire switch. These curves are plotted in Fig. 3-13.

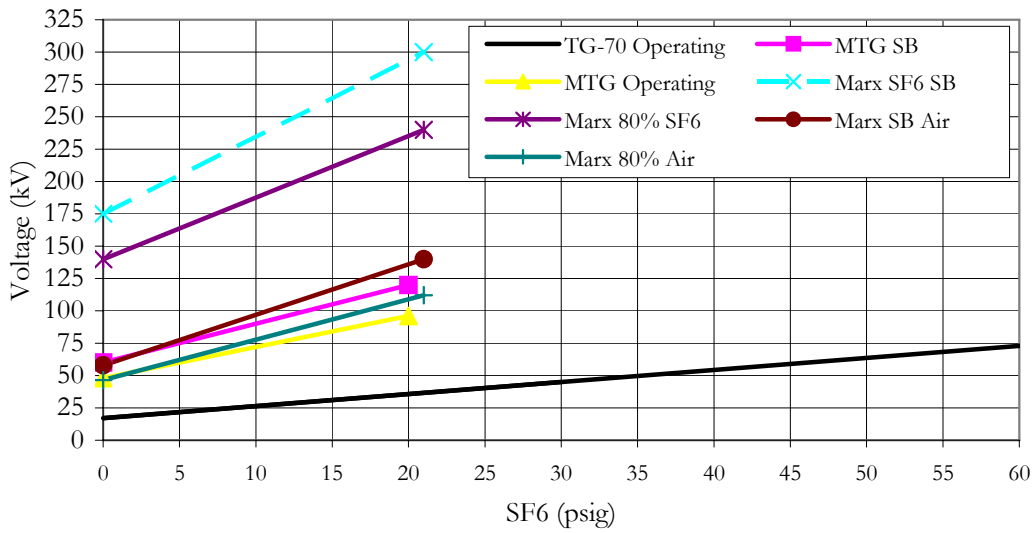

Fig. 3-12. Gas operating curves for the TG-70, MTG and Marx.

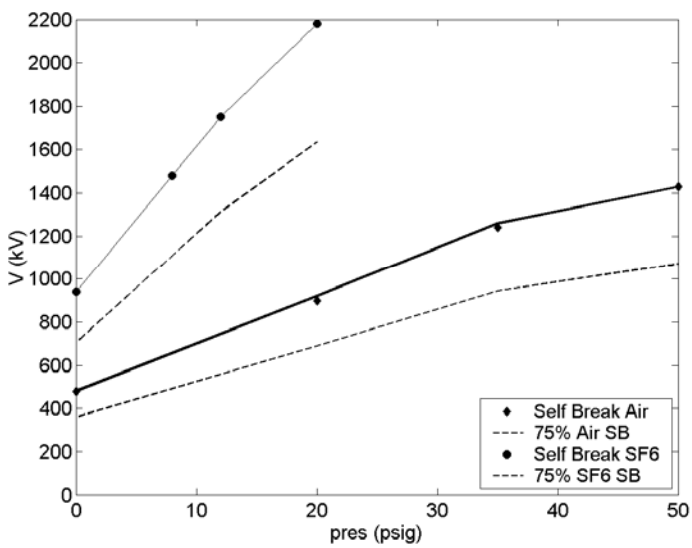

Fig. 3-13. Gas operating curves for the MUTTS Rimfire Switch.

H. Marx Equivalent Circuit

An equivalent circuit was derived for the Marx bank, interconnects to the I-Store, and load. It is depicted in Fig. 3-14 [28]. The circuit was derived from a previous equivalent

circuit for a Proto II Marx [8]. The values for each component were determined empirically using open circuit shots into the I-Store and the circuit served as a preliminary design resource. This caused voltage and current ringing that allowed a fit to simulated data. The parameters that provided a sufficient fit are listed in Table 3-1. The load inductance and capacitance were calculated to be 160 nH and 60 pF, respectively. The intermediate store impedance is 4.2 Ω and the load impedance is 105 Ω if the load is simulated as a transmission line. Z_0 was obtained by assuming the I-Store was an ideal transmission line with a transit time length of,

$$T_d = \Delta z \sqrt{LC}. \qquad \text{Eq. 3-4}$$

Knowing the length z (0.914 m), capacitance C (6.9 nF), and determining the transient time T_d by comparing simulations to data, Z_0 is obtained using,

$$Z_0 = \frac{T_d}{\Delta z\, C} = \sqrt{\frac{L}{C}}. \qquad \text{Eq. 3-5}$$

An example of the output waveforms at the load are plotted in Fig. 3-15. Both circuits were simulated and compared to data to evaluate the first order accuracy of the model. The simulated switch inductance was 490 nH (370 nH calculated) in the discrete case for shot 19 and 435 nH (335 nH calculated) for shot 101. A more thorough approach to circuit modeling was implemented in phase II of the program, but these models are presented here since they were used as design tools for phases I and II.

Discrete Elements

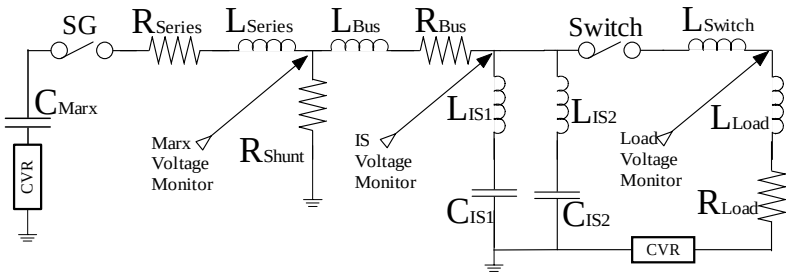

T-Line I-Stores

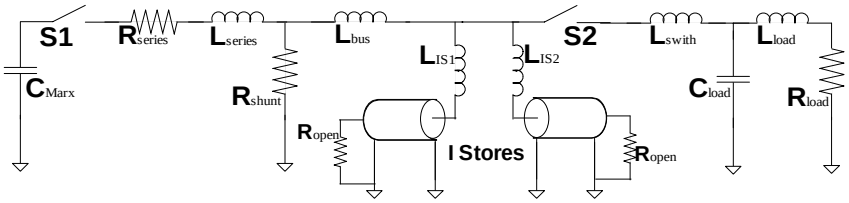

Fig. 3-14. Equivalent Circuits.

Table 3-2: Equivalent Circuit Parameters

R_{Series}	L_{Series}	R_{Shunt}	L_{Bus}	R_{Bus}	L_{IS1}	L_{IS2}
2.4 Ω	5.25 μH	730 Ω	1.4 μH	0.2 Ω	600 nH	450 nH

Zo	TD
4.2 Ω	27 ns

Zo	TD
105 Ω	5.5 ns

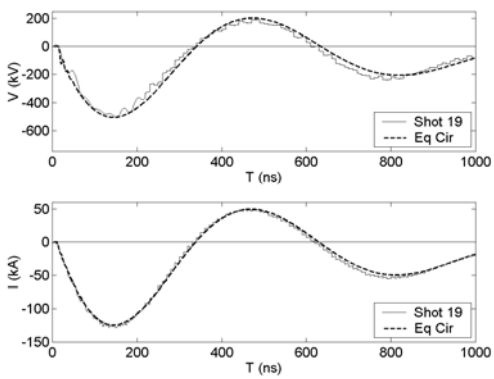

Discrete

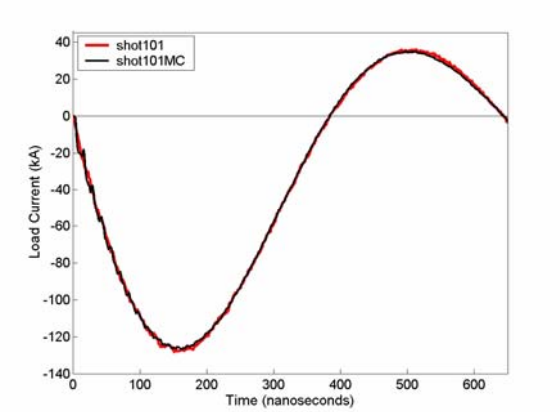

T-Line

Fig. 3-15: Circuit simulations.

Chapter 4
Self-Break Data

The following is a summary of self-break data obtained during phase I. There are three separate sets of electrode trials presented. Data were taken at either ±30 kV Marx charge (1MV peak at the I-Store) or ±40 kV Marx charge (1.4 MV peak at the I-Store). All data are self-break using air as the fill gas. Breakdown photos for these data are arranged in the Appendix in Fig. 9-8 to Fig. 9-17. The analysis presented here is an extension of work that has been reported elsewhere that was conducted concurrently and separately from the analysis presented in this chapter [29]. The analysis that follows was approached with an objective of obtaining proper experimental setup and parameter space for laser trigger data, which has not been reported elsewhere. Therefore, data are presented in a manner that was directed toward guiding the MUTTS program in the direction of laser triggered experiments.

Three electrode arrangements that were not designed by the author were tested under self-break conditions [30]. They are described here since they are referred to frequently throughout the chapter. They are:

1) Original 5.25" disc electrodes. These electrodes exhibited no obvious predictable multichanneling pattern, but have dense multichanneling in many gaps. The gaps nearest the trigger section frequently did not multichannel. These experiments are referred to as "original" electrode experiments.

2) Three discrete floating spherical conductors aligned in three columns throughout the cascade section. This arrangement frequently single channeled in all gaps. These experiments are referred to as "sphere" experiments.

3) Alternating sphere electrodes and disc electrodes. This arrangement improved multichanneling compared to the sphere case. There were three arrangements of alternating electrodes: two balls spaced uniformly and aligned in a column (referred to as "2-ball"), three balls spaced uniformly and aligned in a column (referred to as "3-ball"), and six balls spaced uniformly and aligned in a column (referred to as "6-ball").

An example of the alternating disc and floating ball electrodes is depicted in Fig. 4-1. The all ball experiments were similar except with the disc electrodes replaced with dielectric plates and floating conductors.

A. Data Analysis

Data were analyzed post hoc so that the results could be applied to phase II experiments. Post hoc analysis of the variance (ANOVA) allows a useful comparison of the means between different data sets. Two assumptions for relevant ANOVA analysis are that the data are normally distributed and that all data sets should have equal variance. The later

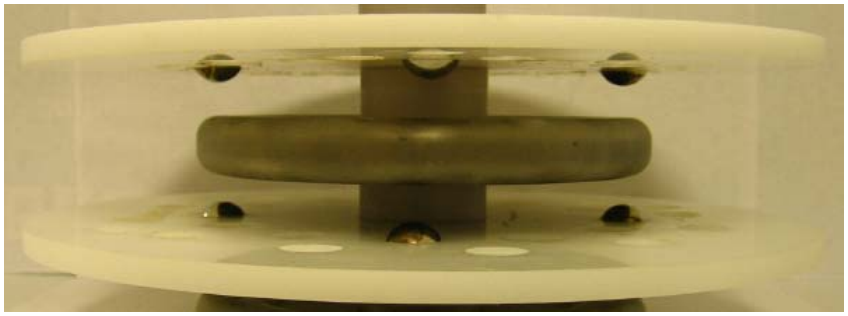

Fig. 4-1. Example of a 3-ball setup.

of the two, or homogeneity of variance, is more stringent of a requirement than the data adhering to a strict normal distribution. Homogeneity of variance was tested using Levene's method, which is less sensitive to violations of normality than other commonly used methods. Post hoc comparison of means was conducted using the Tukey-Kramer method, which is a conservative method when data sets to be compared are of unequal size. In this method, the difference in the mean between each paired combination of data is compared to the value in the studentized range distribution for a given confidence and number of data categories.

The null hypothesis in ANOVA analysis is that the means are the same. We seek to reject this claim. On all tests an α of 0.05 was used, providing a confidence interval of 95% for rejections of the null hypothesis. If a p value is obtained that exceeds 0.05, we fail to reject the null hypothesis. For a Levene test, the null hypothesis is that the variances are the same. If we fail to reject this, it is concluded that for a given confidence there is sufficient homogeneity of variance. For both ANOVA and Levene tests, the same α should be used. All statistical inferences throughout this report follow these standards. When a pair-wise comparison does not meet these criteria, additional methods are needed.

Nonparametric analysis is used when data do not represent a normal distribution. Normality is determined using the Shapiro-Wilk test in which the null hypothesis is that the data are normal. If $p > \alpha$, we fail to reject the null hypothesis. If data are non-normal a nonparametric t-test, called a Wilcoxon test, is used to pair-wise compared means between data sets. The appropriate test, either ANOVA or Wilcoxon was used depending on the homogeneity of the variance and the distribution of the data.

Analysis of covariance (ANCOVA) is used in situations in which there are several groups (independent variable 1) that vary along some parameter (dependant variable), and

that are thought to be directly affected by some other parameter (independent variable 2, the covariate) [31]. One critical factor that must be considered before relevant statistical analysis is attempted is that, ideally, compared data should only vary because of the identifiable dependant variables that are subject to random error. This is the purpose of trying to eliminate variables that are difficult to categorize when monitoring the influence of one in particular. When looking at the effects of multichanneling by itself, it would be ideal to subject all electrode experiments to the same conditions (charge voltage range, trigger method, gas pressure for a given charge voltage, same circuit, etc). It should be noted that the interpretation of results of ANOVA analysis must be conducted in the context of the number of data that are present. All data were analyzed using sophisticated statistical software [32].

B. Multichanneling

Self-break data were analyzed with an emphasis on determining if there was a statistically significant difference in the electrical effects of multichanneling between electrode configurations. At the outset of analysis, it was unknown exactly how electrode arrangement would affect the number of channels other than that each arrangement had a cap on the maximum number of channels that could form. It was assumed, however, that there would be a detectable difference in the electrical performance if a range of multichanneling was experienced. Differences in electrical performance were monitored as differences in current rise time, di/dt, ringing frequency, etc. If there was not a detectable difference in these parameters as a function of multichanneling, the results would be informative in that it would be known that differences in multichanneling would either have some or no measurable effect on the electrical performance of the switch.

Fig. 4-2 depicts a plot of the number of channels visible in seven cascade gaps (out of ten) for each electrode configuration and at each charge voltage (30 kV means ±30 kV Marx charge). Breakdown photographs are depicted in Fig. 9-8 to Fig. 9-17. It appears from Fig. 4-2 that the number of channels increases with voltage when a given configuration is compared, although statistically this is not certain. When grouping each set of data by electrode configuration there is a statistically significant difference in the number of channels between the 2-ball and 3-ball experiments. There is generally, though not necessarily statistically, more channels that form in the original case and more channels form as channel locations are increased. From this it may be concluded that adding field enhancement points will encourage more channels in each gap in an air filled environment and that adding more points will add arc locations. Increasing charge voltage by only 1.25 will not necessarily encourage more channels for a given electrode configuration. With these multichanneling conclusions obtained, an investigation was launched into the effect of multichanneling on

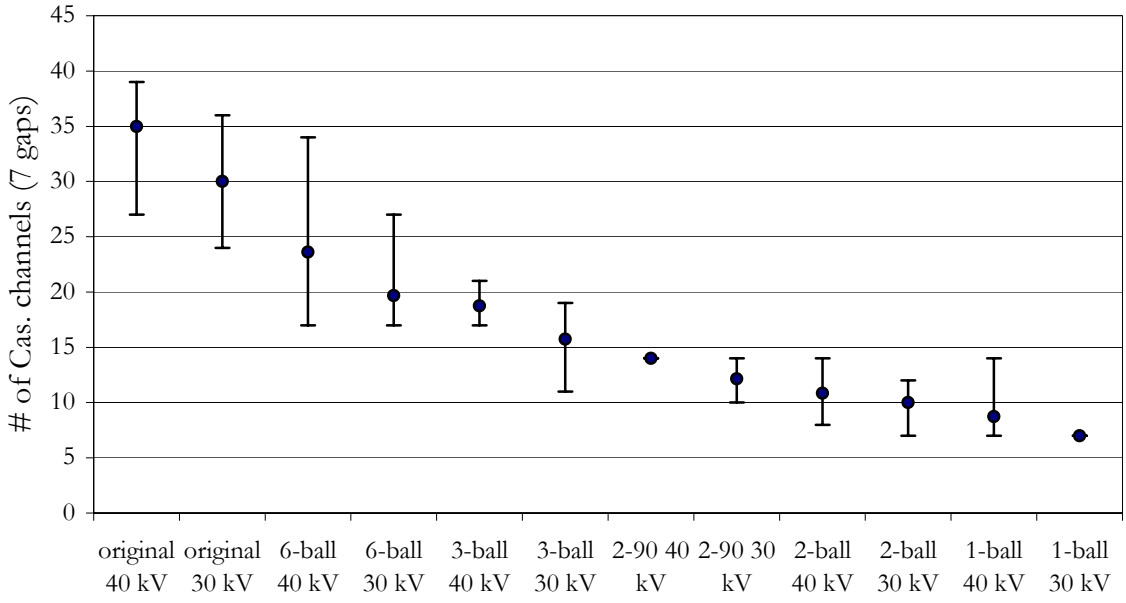

Fig. 4-2. Breakdown voltage versus di/dt.

calculated switch inductance.

A set of experiments was conducted in which the 2-ball configuration was altered. Every other electrode was oriented 90 degrees out of phase with respect to the next ball electrode (referred to as "2-90"). This arrangement was attempted to elongate the current conduction path through the electrodes and to provide a larger inductance separation between each channel location. By doing this, there should be a larger number of channels for the larger inductive case since the voltage fall between locations would be more inductively isolated. There was an average of 13.1 channels that formed in seven cascade gaps for the 2-90 case and 10.5 in the 2-ball case indicating that in fact the inductive path affects the number of channels that formed. It is worth noting for the ±40 kV charge, the 2-90 case multichanneled for every shot.

C. Multichanneling Effect on Period, di/dt and Rise Time

In the phase I configuration the output is a damped sinusoid. If the resistance is assumed constant an approximation to the circuit ringing frequency may be made. For a damped sinusoid the ringing frequency is given by [33],

$$\omega = \sqrt{\frac{1}{LC} - \frac{R^2}{4L^2}}. \qquad \text{Eq. 4-1}$$

Using a constant combined resistance of the load and switch of 4.8 Ω, the inductance may be found for each shot based on its ringing frequency. A plot of this is depicted in Fig. 4-3. An analysis of inductance using a more complex method yielded similar results [34].

Multichanneling was investigated using a combination of ANOVA and ANCOVA analysis. In Fig. 4-4, di/dt (dependant variable) for a given electrode configuration

(independent variable 1) is plotted against breakdown voltage (independent variable 2). It was of interest to determine how di/dt differs between each of the configurations since if a configuration facilitates more multichanneling it should have a larger di/dt (this same premise is used when comparing risetimes). To determine if this hypothesis is correct, the null hypothesis for statistical analysis is that all groups have the same di/dt. It was sought to determine this was false.

A coefficient of determination of 0.87 in Fig. 4-4 indicates that di/dt data clearly depend on the voltage at which the switch breaks down. Since we suspect the inductance, and thus the risetime, to be affected by the number of channels, we want to limit the effects of breakdown voltage on the statistical analysis of the data. Although some sets had discernable statistical differences between them, the normalized di/dt (di/dt divided by the breakdown voltage) did not statistically improve as the number of channels was increased. The same was found analyzing rise time versus electrode configuration. It should be noted

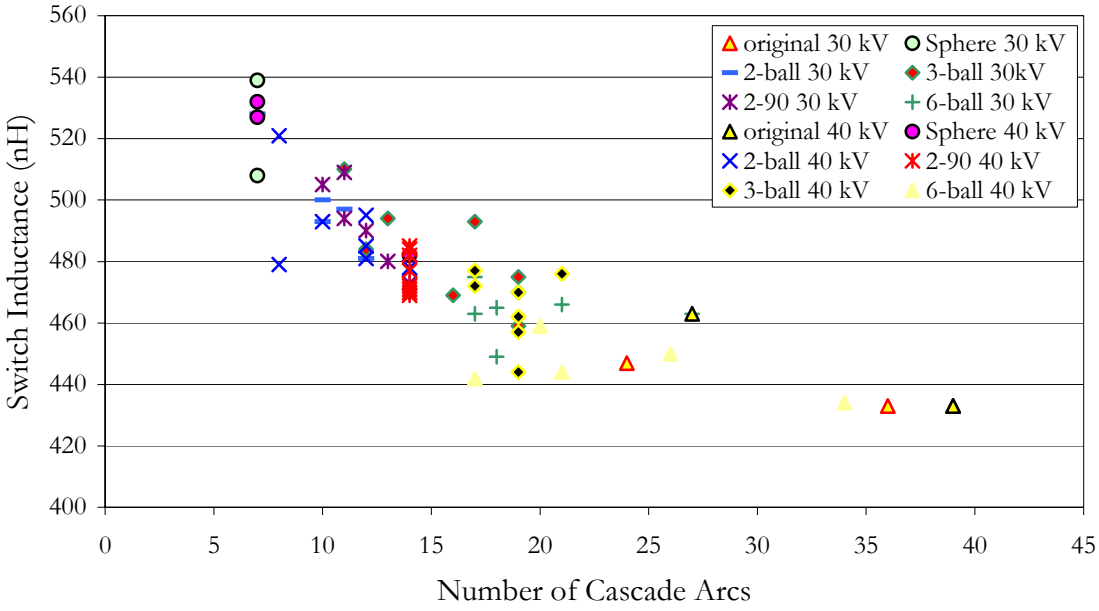

Fig. 4-3. Inductances obtained from ringing frequency.

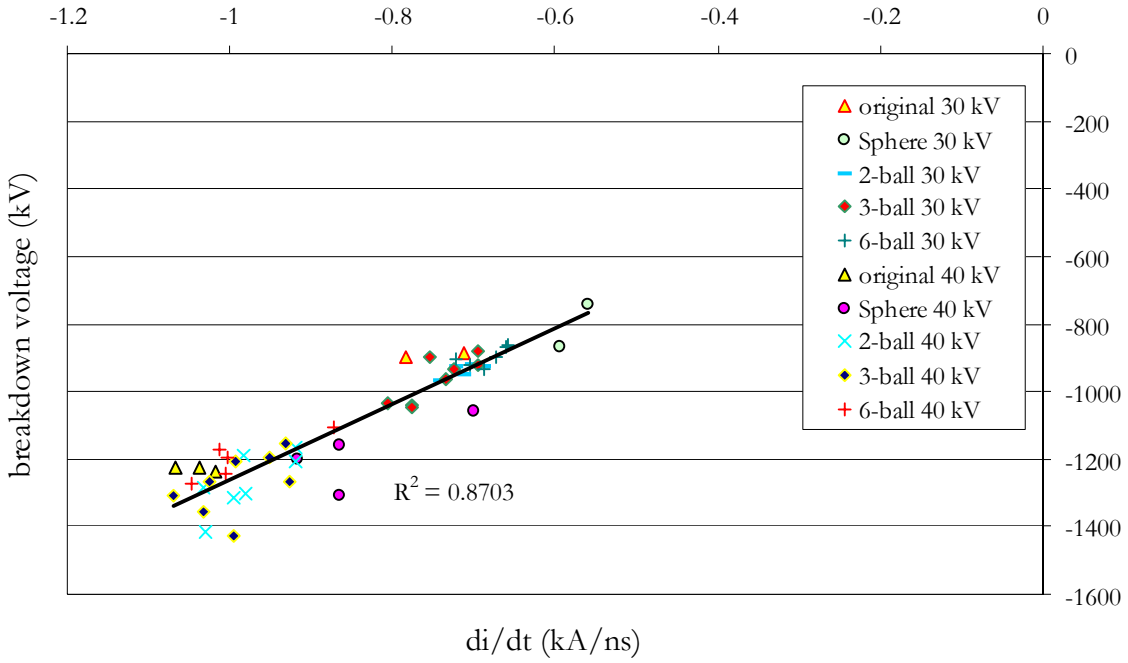

Fig. 4-4. Breakdown voltage versus di/dt.

that risetimes were roughly 10-15% larger in the single channeling 1-ball experiments when compared to other configurations, though there were five total 1-ball shots conducted.

The self-break data, perhaps most importantly, provided some insight into the expectation of laser testing and allowed a determination of number of shots necessary to obtain statistically different sets on phase II. Before conducting such calculations, a maximum acceptable number of shots must be defined. This was defined as 15 shots per electrode configuration. Therefore, using the untriggered data, power analysis was used to calculate how many shots were needed to see statistically different data for a given fidelity of confidence. Any comparison that requires the number of data points to be above the critical level is considered too large, and therefore any difference in risetime or di/dt will not be considered improving operation of the switch.

For the four electrode configurations analyzed the maximum number of data points acceptable is 60. Power analysis was conducted with a power of 0.8 and a variable correlation between the risetime and voltage was set to 0.9 and 0.98 (quite large). The standard deviation of the set is 1.87 E11. All comparisons of electrode pairings are out of the acceptable shot number range except those between sphere and all others, 3-ball and all others, and 3-ball and 6-ball. To obtain a statistically different comparison of di/dt between the other combinations would require hundreds of shots per electrode configuration. This number of shots is not practical. Simply put, determining a statistical difference in di/dt (rise time has a similar effect) between different electrode configurations is not practical. Or in other words, there is not an improved di/dt (risetime) for increasing the number of channels beyond two channels per gap that is detectable for a reasonable number of self-break shots. Therefore, in phase II, the electrodes that were tested addressed both multichanneling issues and other inductance lowering techniques, such as, a reduced ratio of the radius of inner conductor to outer conductor in the coaxial arrangement. If a difference in inductance is not observed within the defined shot count maxima, the electrode configuration will be deemed to have no improvement over the original cascade electrodes.

Several things must be considered when interpreting the statistical results. Since it is important to look at consistency of multichanneling, the data were compared by electrode configuration. Comparing the risetime and di/dt for a given electrode configuration assumes that each configuration multichanneled in a consistent manner and does not include the actual sporadic nature of multichanneling other than it being absorbed into error. In reality, actual breakdown patterns or number of channels for any electrode configuration must be compared. Therefore, it is important to look at the breakdown configuration for a given electrode configuration to truly analyze improved electrical characteristics.

The plot of risetime versus channel factor appears in Fig. 4-5. Channel factor is a value that was computed by multiplying the number of arcs in a gap by the number of arcs in the subsequent gap and doing so for each adjacent gap. Then for all pairs of gaps that were multiplied together the values were summed. The sum of these values was then divided by the total number of visible arcs (seven gaps are visible). For example, in an arbitrary three gap system if gap 1 contains one arc, gap 2 has two, and gap 3 has three, the channel factor would be the sum of the number of arcs in gap 1 multiplied by that of gap 2 (which is 1 * 2) plus the number of arcs in gap 2 multiplied by that of gap 3 (which is 2 * 3). This is then divided by six, or the total number of arcs present, giving a channel factor of 1.33. This allows for some measure of the density or clustering of channels from one gap to the next rather than just a total number of arcs. Fig. 4-5 indicates there is no strong correlation between the channel factor and the rise time. Fig. 4-6, however, shows that the period is a stronger function of channel factor. This indicates the ringing period is more

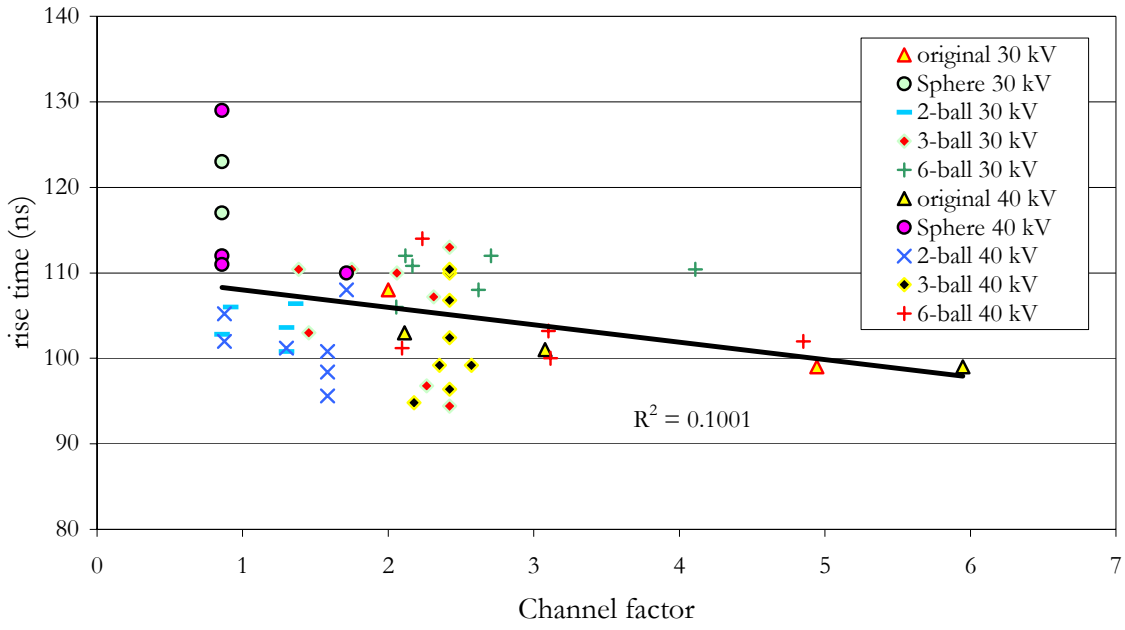

Fig. 4-5. Risetime versus channel factor.

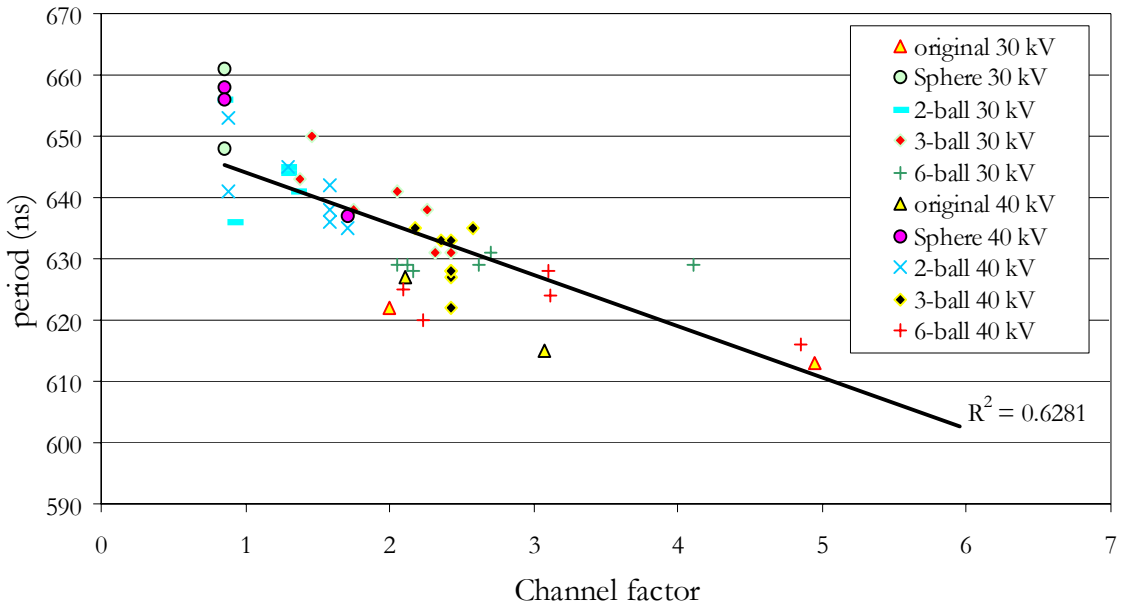

Fig. 4-6. Period versus channel factor.

susceptible to the number of channels, or that inductance due to different channel arrangements is more pronounced in late time than in early time. Comparing Fig. 4-5 and Fig. 4-6 and the statistical analysis of the electrode groups, questions arise on the detection of small rise time changes in the phase I setup. Both the fact that the number of channels does not seem to effect the rise time drastically beyond two channels per gap and that the small difference in inductance between different multichanneling arrangements may lend to this lack of detection. This was the driving force for a test stand redesign for phase II.

D. Transitioning from Phase I to Phase II

Phase I allowed a period of familiarization with the control of the machine as well as time to address problems and correct issues in the Marx and intermediate store. Operating the switch with a laser trigger is more applicable to the environment that the switches are

normally operated in on Z. Moving from phase I to phase II, several lessons that were learned in phase I were applied to the framework of the phase II experiments. Since the purpose of phase II experiments was to investigate multichanneling under the influence of a laser trigger, all sphere electrodes were not utilized since that arrangement frequently single channeled. A hybrid electrode configuration consisting of field enhancement points and holes that allow optical line of sight to subsequent gaps was attempted along with original style electrodes of varying radius. Pressure effects on multichanneling and impedance were investigated. The impedance was considered for laser data by observing characteristics of the entire waveform to ensure accuracy in calculations.

Chapter 5
Laser Triggered Data

This chapter covers phase II of MUTTS beginning with the redesign of the test stand. It includes all laser data taken for shots #A1 to #A216 as described in the phase II shot log in Table 9-4.

A. Phase II: Test Stand Redesign

The output section was redesigned for vertical orientation by splitting the two intermediate stores into two separate testing "towers". There were six main reasons driving this redesign. The redesign:

1) Has a substantially simpler laser propagation path.
2) Provides two test stands for two experimental setups simultaneously.
3) Drastically simplifies technician operations when removing the switch.
4) Lowers output section inductance and increases the percentage of switch inductance contribution to the total output section inductance.
5) Allows lower Marx charge because of higher intermediate store ring up.
6) Has a more coaxial geometry, which is of interest for future research.

The phase II redesign consisted of four major changes (See Fig. 5-1) to the phase I setup. The new load that is one concentric water resistor with four CVR's is much smaller and much less awkward to remove and maintain (Fig. 5-1, item 1). This drastically improves the ability of a single technician to work on the switch inside the tank. Reduction to four

CVR's instead of eight simplifies data acquisition. Fields along the Lexan and acrylic load envelopes remain below 80 kV/cm on all surfaces for a 1 MV load voltage. The load was replaced with a magnesium sulfate/DI water mixture with a resistance of 2.5 Ω. The radius of the return outer conductor was reduced from 132 cm to 76 cm (Fig. 5-1, item 2). These modifications decreased the inductance, resulting in the reduction of the output section inductance by 10% to 15%. This system decrease assists in measuring the switch inductance contribution. A field shaper was added to I-Store side of the switch (item 3, Fig. 5-1). This decreased the fields from near breakdown levels to under 300 kV/cm everywhere for a –2.7 MV charge. The conductor connecting the I-Store to the switch was shortened (item 4, Fig. 5-1), reducing the inductance contribution while maintaining acceptable fields in the oil. This reduction coupled with the more coaxial design reduced inductance significantly for the I-Store, switch and load section. Fields in the cascade and trigger section remained as in phase I.

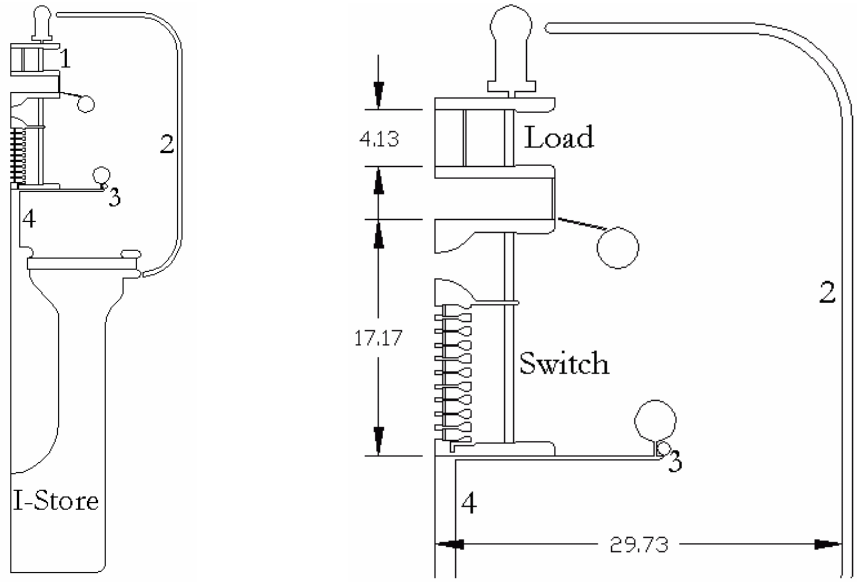

Fig. 5-1. Test stand redesign (dimensions in inches).

B. Output Section Inductance

The inductance for phase II was calculated using the same techniques as in phase I (see to Chapter 3, Section E). The major difference between the phase I and phase II geometry is the return conductor radius. Both inner ($\rho 2$) and outer ($\rho 1$) radius are taken to be 76 cm since the actual ratio is very near unity (within 1% for an individual conductor diameter of 1.27 cm (0.5")).

Eq. 9-3 was used to find the inductance for several switch portions. For the cascade electrodes, the radius, ρ_3, is 6.67 cm (2.625") and the combined length, l, of all of the electrodes is 16.535 cm (6.51"). The $\ln \zeta$ term is 0.25 for all calculations. The inductance of the electrode rings is roughly 100 nH. For the switch end plates, the radius is 44.45 cm (17.5") and their combined length, l, is 5.08 cm (2"). The inductance of the end plates is roughly 11 nH. For the trigger electrodes, the average radius is 3.81 cm (1.5") and its length is 7.87 cm (3.1"). The inductance of the trigger electrodes is roughly 56 nH. For the trigger arc, arc radius is assumed to be 0.15 cm and has a length of 4.7 cm (1.85"). The inductance of the trigger arc is approximately 64 nH.

For cascade arcs, Eq. 9-1 was used to calculate the inductance. The arc array radius is 6 cm (2.375") and an arc radius of 0.1 cm was assumed. The arc array was assumed to be symmetric and all arcs were assumed to be equally spaced from each other. The combined length of the arcs is 8.86 cm. For a three arc per gap arrangement, the inductance is approximately 64 nH and for 10 arcs it is approximately 48 nH. This inductance is likely a slight underestimate considering the actual geometry in Fig. 9-2. This is because the equations assume a continuous return conductor sheath and it is only approximated using discrete return conductors. The calculated is likely 10 to 15% lower than the actual

inductance given its arrangement. Summing all contributions, the total inductance of the switch is 278 nH to 295 nH.

The calculation of inductance of the load carriage is similar to the cascade electrodes. It has a radius of 25.4 cm and a length, including connections and diagnostics, of 46 cm (18"). The inductance of the load section is 156 nH. The total inductance of the output section including the switch is approximately 440 nH. This is 12% reduction in inductance from phase I.

C. Experimental Setup

The number of current viewing resistors was reduced from eight to four for phase II. They had values of R_1 = 0.01979 Ω, R_2 = 0.01967 Ω, R_3 = 0.02047 Ω, and R_4 = 0.01982 Ω. All pre-shot settings were based on the self-break switch curve depicted in Fig. 3-13. Data were collected via two Tektronix TDS2024 oscilloscopes and one Tektronix TDS224. All three are capable of connecting via serial port to a common data acquisition computer. A Canon PowerShot A75 camera is used with neutral density filters to capture all breakdown photographs as in phase I. All images were remote captured to a data acquisition computer.

The laser timing system consists of a combination of triggering from data acquisition lines and delay generators. When the fire button is pushed, a Tektronix Type 114 pulse generator supplies a 100 μs wide, 5 V pulse immediately to the flash lamp input on the laser and to the first delay generator called RoxBox. RoxBox provides a delay time for the application of the Marx trigger signal. The optimum delay time between the flash lamp input signal and application of the Q switch signal at the laser is 180 μs [35]. The delay between the time the fire button is pushed and the Marx begins to conduct current is 2 μs. Therefore, a trigger signal for the flash lamp is needed approximately 178 μs for the flash

lamp prior to triggering the Marx. The time delay on a second delay generator (HP 222A Pulse Generator) is set to trigger the Q switch depending on the delay required for the desired breakdown voltage. The voltage on the I-Store rises at approximately -2.11 kV/ns so the desired laser application voltage is determined using the timing delays for all the connections in Table 9-2. Laser light detection via a photodiode and Q-switch engagement (items R and S in Table 9-2) are monitored at oscilloscope 3 in the screen box and are subject to a specific shot settings and pre-firing caused by noise. Noise issues plagued laser trigger controls and a discussion of the solutions to these issues is described in the Appendix Section D.

The laser used for triggering is a 30 mJ, 5 nanosecond, frequency quadrupled Nd:YAG made by New Wave Research (custom made Tempest model at 1 Hz). The laser delivery system consisted of a CVI Laser 3X beam expander with a UV coating to expand the beam to 1.5 cm. This beam expander was required to have a convergence angle at the output of a CVI Laser plano-convex lens with a focal length of 31 cm so that a visible laser spark at the focal point would result. This spark was approximately 1 cm in both pressurized air and SF_6. The laser beam exited the laser, propagated through the beam expander and was reflected 45 degrees via an 5.08 cm aluminum coated dielectric mirror. The beam then propagated through a 5.08 cm UV coated laser window that isolated the switch volume from the ambient air. The beam continued through the lens and into the middle of the trigger section. Losses for the total laser propagation system were approximately 15%. The laser tube that housed the window and lens was pressurized to the switch volume. A configuration that was attempted in which the tube was not pressurized to the switch pressure and was left open to the ambient air resulted in catastrophic disassembly.

D. Electrode Radius and Field Perturbations in SF_6

Four sets of cascade electrode configurations were tested, all of similar cross section as in Fig. 5-2. Three configurations were implemented to study the radial dependence of multichanneling in a multigap switch. These radii included 6.67 cm (2.625”), 8.26 cm (3.25”), and 10.16 cm (4”) electrodes with a radially uniform field enhancement factor of 1.1. A fourth set was implemented using a 6.67 cm radius electrode with four 0.318 cm (0.125”) holes drilled through the electrodes aligned with the cascade stack axis (see Fig. 1-1). Electrodes were oriented so as to align the holes in all gaps throughout the stack. Holes were located uniformly about the perimeter at a radius of 5.86 cm, the radius at which arcs usually form. The holes served as both field enhancement locations and provided an optical line of sight to subsequent gaps. This was to encourage uniform channeling in all gaps via the localized presence of UV photons by the irradiation of one gap to the next as the switch was over volted. Shots were conducted at a nominal 1.5 MV and at a switch pressure of 18 psig of SF_6. All shots were triggered at 65-70% self break to allow maximum over voltage and dv/dt in the cascade gaps to study their multichanneling characteristics.

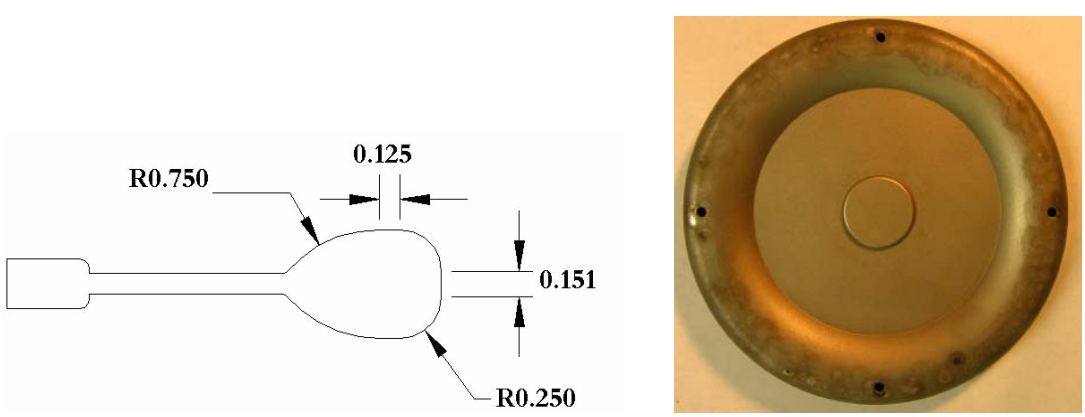

Fig. 5-2. Electrode cross section and a picture of a 6.67 cm electrode with holes (dimensions in inches).

Fig. 5-3 depicts a synopsis of the total number of channels in the cascade section for each configuration. There were seven shots taken at 6.67 cm both with and without holes, fifteen shots taken at 8.26 cm, and thirteen taken at 10.16 cm. Fig. 5-4 depicts a summary of the breakdown pattern per cascade gap. Gap one is the cascade gap closest to the trigger gap with gap ten located nearest the intermediate store (I-Store). A general pattern is evident with fewer channels present at the trigger gap end (gap one) and more channels present toward the IS end. All gaps single channeled on at least one occasion for each electrode configuration, though not necessarily all at once and with no consistent pattern from shot to shot.

Fig. 9-18 through Fig. 9-28 depicts breakdown photographs that were obtained using a commercial off-the-shelf digital camera in open shutter mode equipped with a neutral density filter. Although there was no consistent pattern from shot to shot, gaps 4-10 frequently channeled in some nearly aligned manner for up to eight gaps without the

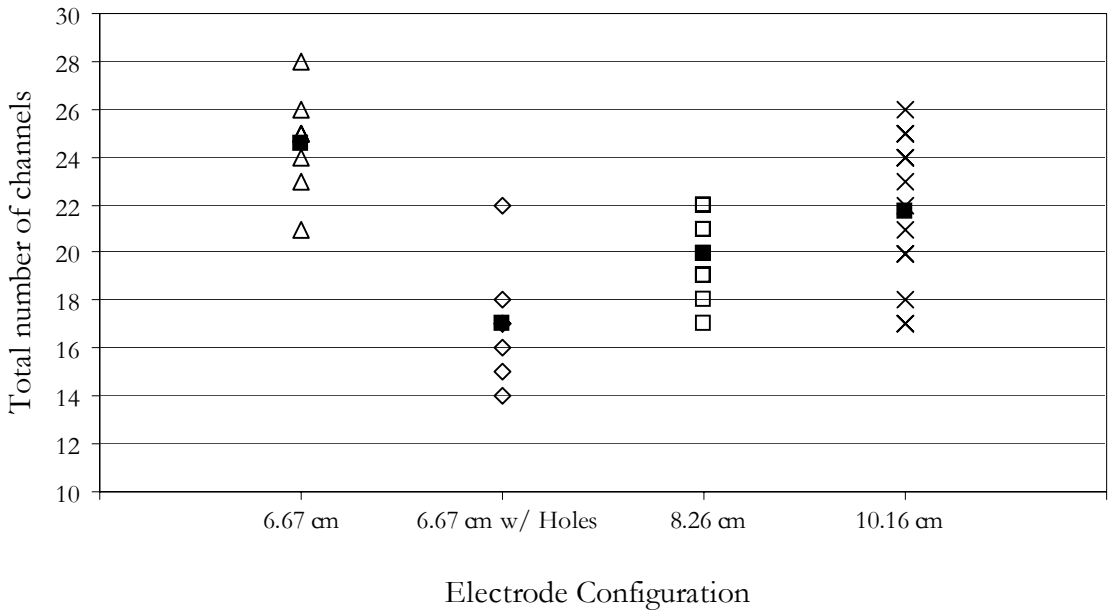

Fig. 5-3. Total cascade channels. Box denotes channel average.

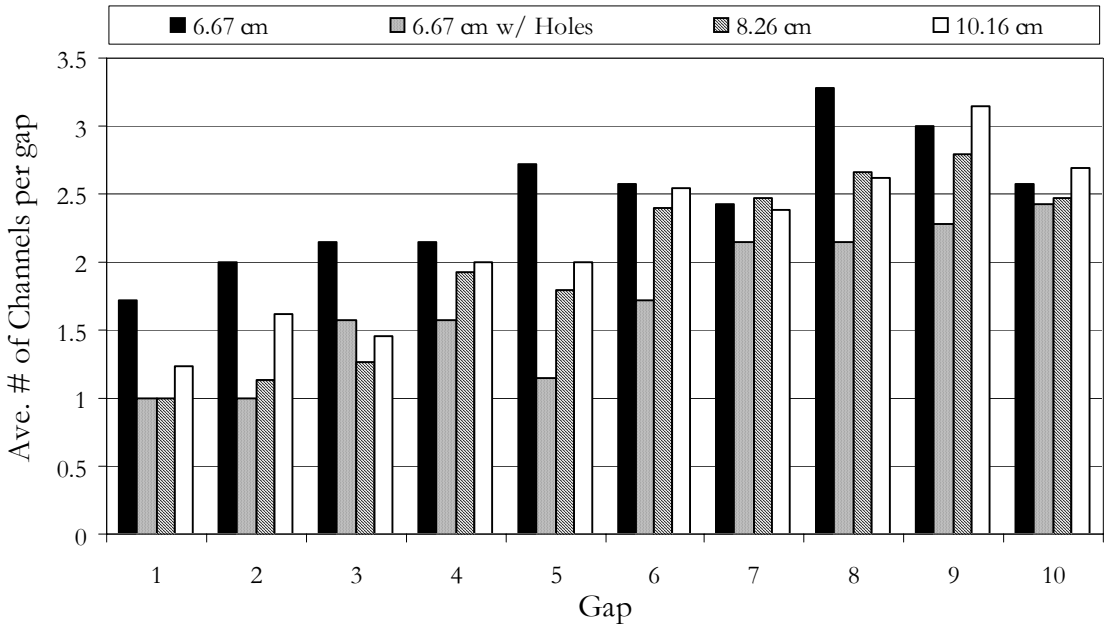

Fig. 5-4. Multichannel breakdown synopsis.

presence of field perturbations. The field enhancement holes reduced and effectively capped the maximum number of channels that formed when compared to the 6.67 cm case with no holes. Ideal uniform channeling (four channels in all gaps at each hole position) was never achieved using the hole scheme for an SF_6 environment. In many cases there were consecutive gaps that formed arcs at aligned hole positions. Frequently this would result in no more than two consecutive arcing gaps at the same location and never occurred for more than seven consecutive gaps. Only one shot formed an arc at a non-hole location. Data suggest that using field enhancement locations susceptible to only self irradiation does not improve uniform multichannel performance in an SF_6 laser triggered environment and, in fact, worsens multichannel performance. This is contrary to results observed in an air filled environment where the presence of holes more uniformly aligned channels, although still with a capping effect on the total number of arcs per gap [36]. The number of channels, therefore, may not be predetermined by assuming a localized number of field enhancement

points for SF_6. There is no statistical difference in the average number of channels that formed between the 6.67 cm case and the 10.16 cm case. There is also no difference between the 8.26 cm and the 10.16 cm case. Therefore it is concluded that an increased electrode radius will not attribute to worsened multichanneling performance.

A comprehensive circuit simulation was implemented that included all capacitances (obtained from Maxwell 2D static solver), calculated inductances, and calculated resistances to analyze the switch at the time of breakdown (see the Appendix for a brief description of the software packages utilized) [26,37]. A capacitance matrix was implemented that includes the capacitance between each conductor and each conductor and ground. The capacitance between adjacent electrodes in the 6.67 cm case is 11 pF, for the 8.26 cm case it is 18 pF and at 10.16 cm it is 21 pF. The matrix, consisting of nearly 80 elements, creates a voltage distribution throughout the switch that does not scale by a simple factor as radius increases. This matrix will influence the breakdown characteristics of the specific switch studied.

A breakdown field of 200 kV/cm at 18 psig was determined from self-break data

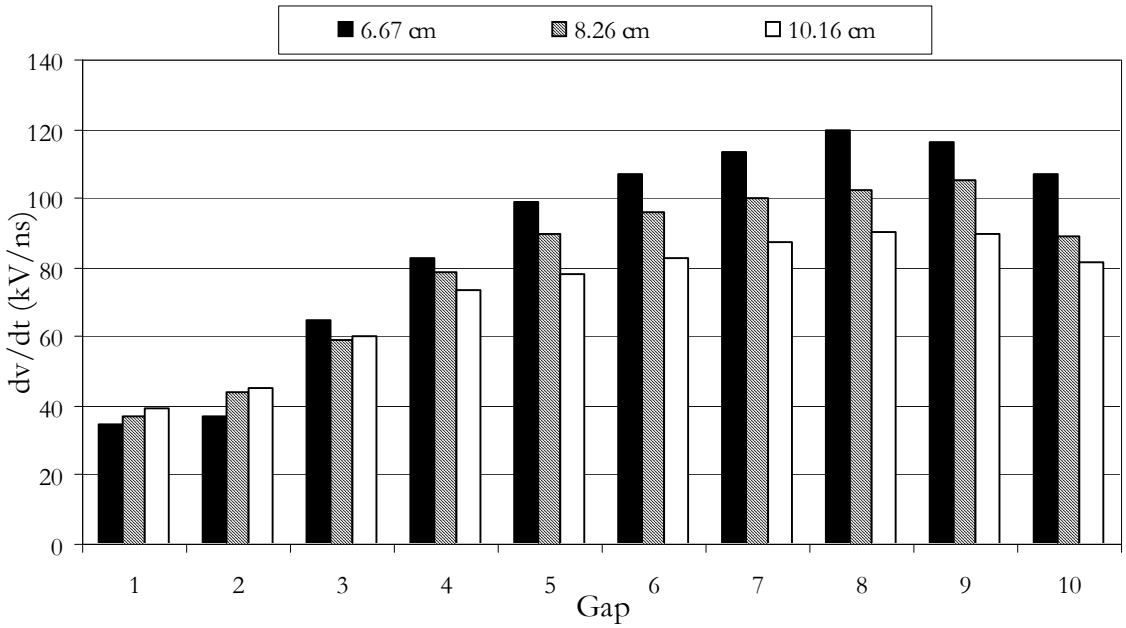

Fig. 5-5. Simulated rise rate of voltage across each gap at time of breakdown.

and was applied to all gaps [7]. Fig. 5-5 depicts the difference in simulated dv/dt at the time of breakdown for each configuration assuming a breakdown voltage of 1.55 MV (67% of self-break). The differences in dv/dt between each case are due to the slight difference in the capacitance distribution as the electrode size increases. A dv/dt of >60 kV/ns is required to ensure multichanneling for electrodes without field perturbations as occurs in gaps 4 through 10.

The switch appears to breakdown sequentially from trigger end to I-Store end as depicted in Fig. 5-6. A similar result was observed on a 6 MV Rimfire where the runtime from trigger closure to the 7th gap breaking down was 3.4 ns. That agrees quite well with 3.6 ns depicted in Fig. 5-6 [7]. Comparing Fig. 5-4, Fig. 5-5, and Fig. 5-6 a parallel may be drawn between experimentally observed breakdown and simulated breakdown. As breakdown time increases a larger dv/dt results as depicted in Fig. 5-5. A larger number of channels are observed in these gaps as depicted in Fig. 5-4 [2,38].

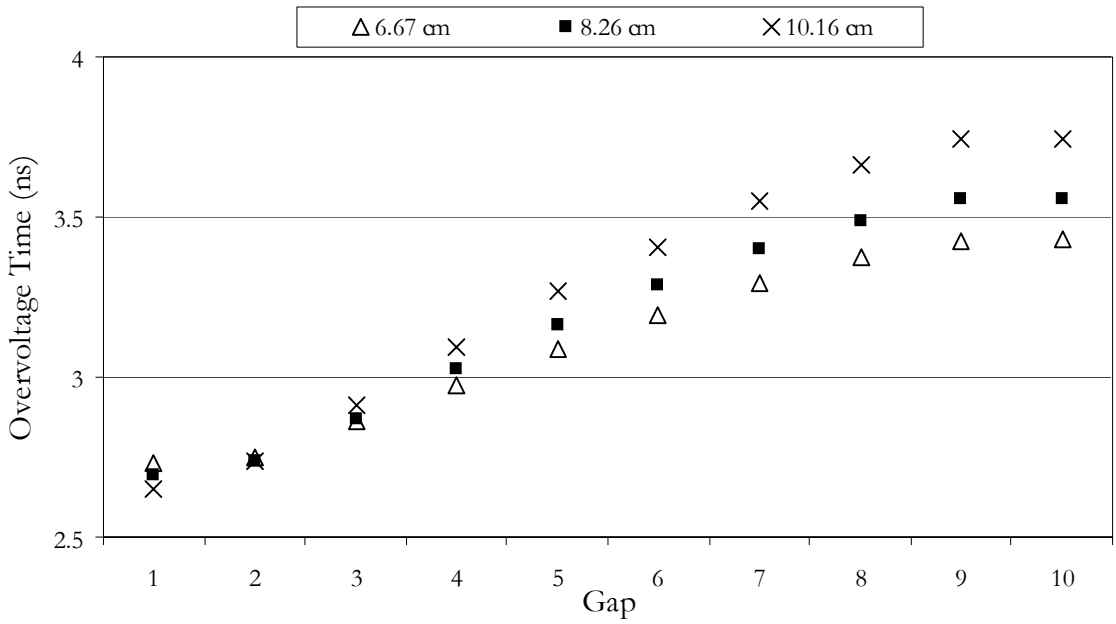

Fig. 5-6. Simulated breakdown sequence after presence of laser trigger at t=0 ns.

E. Impedance Calculations

Intermediate store voltage (V_{IS}), load voltage (V_L) and load current (I_L) were obtained for the switch and load section using monitors positioned as in Fig. 5-7. The voltage across the switch is related to the switch current via,

$$V_{SW}(t) = L_{sw} \cdot \frac{d}{dt} i(t)_{sw} + R(t)_{sw} \cdot i(t)_{sw} \quad V \qquad \text{Eq. 5-1}$$

$$V_{SW}(t) = V_{IS}(t) - V_L(t) \quad V. \qquad \text{Eq. 5-2}$$

Switch inductance (L_{SW}), is comprised of the total arc inductance and the inductance of the conductors within the switch. L_{SW} is assumed constant and calculable and is based on a specific shot's breakdown pattern that is obtained from a photograph. A time varying switch resistance ($R(t)_{SW}$) is comprised of a varying arc resistance and a constant resistive drop element. $R(t)_{SW}$ is obtained from Eq. 5-1 and this assumption of constant L_{SW}. Resistance may then be solved for a time varying arc radius, if the conductivity is assumed constant and

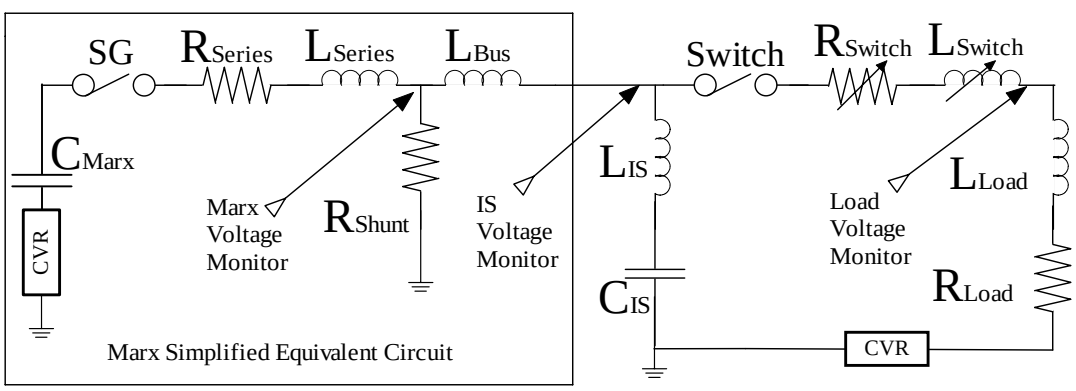

C_{Marx}	R_{Series}	L_{Series}	R_{Shunt}	L_{Bus}	L_{IS}	C_{IS}
22 nF	3 Ω	6.3 mH	1000 Ω	1.4 mH	600 nH	6.9 nF

Fig. 5-7. System equivalent circuit.

known, since the time varying nature of resistance is typically attributed only to arc radius [39,40]. In order to apply this time varying arc radius to each gap, an additional assumption of the relationship of arc radius to arc current must be made [44]. Once a time varying arc radius is obtained, it may be substituted into the geometrical equations for calculated switch inductance and the assumption of a constant switch inductance may then be evaluated. Then, the obtained time varying inductance and resistance may be substituted back into Eq. 5-1 for quality of fit analysis. This process is conducted one time, though slightly more adequate fit parameters (less than 5% different) may be found through multiple stable iterations.

A 6.67 cm shot was sampled at random to illustrate this commonly used method. The time scale of interest is during current rise or the first 150 ns after switch breakdown. The total switch inductance for this example is 290 nH when the specific breakdown pattern is considered with a 140 nH contribution from the electrode rings and switch end plates.

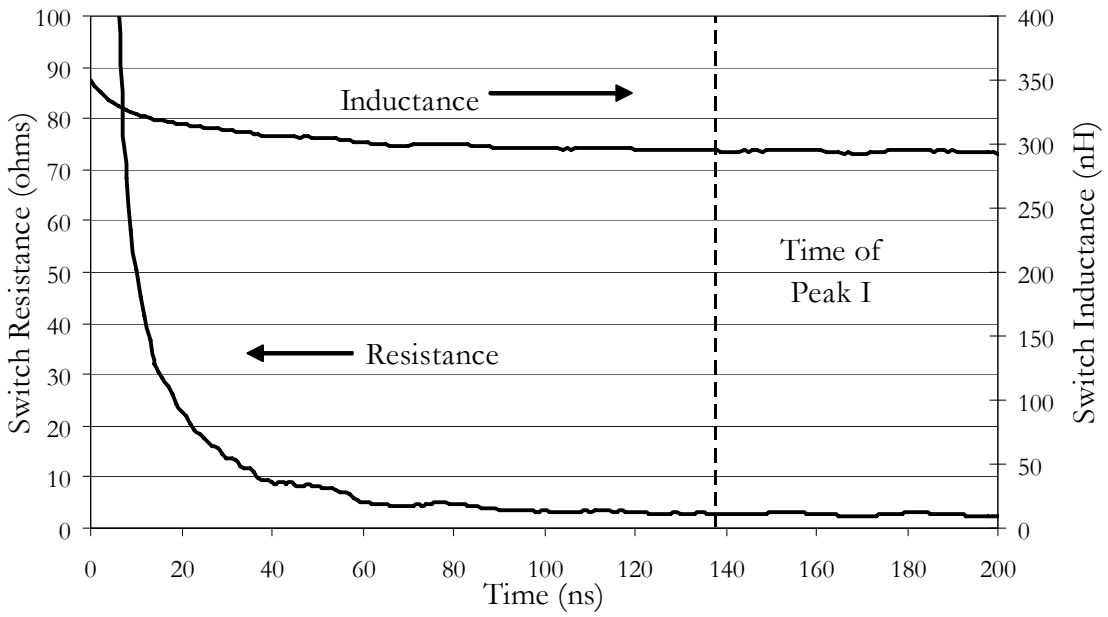

Fig. 5-8. Switch impedance for a 6.67 cm electrode example.

Using this value, the resistance may be solved using Eq. 5-1, and an assumed conductivity of 160 Ω^{-1} cm^{-1} [39,40]. This resistance is plotted in Fig. 5-8 with peak switch current occurring at 140 ns. The resistance falls several orders of magnitude in approximately 40 ns (30% of the time to peak current). A conduction value of 2.8 Ω is reached in another 50 ns. Kushner observed a similar time to plateau resistance of 50 ns, with a time to peak current of 80 ns [41]. Akiyama observed a resistive fall to below 0.5 Ω in 50 ns, with a time to peak current of 680 ns [42]. Resistance remaining large for a significant portion of the risetime indicates the resistive phase will contribute substantially to overall switch impedance during this time. All shots conducted at MUTTS illustrated similar behavior. There is no notable difference in switching resistance between untriggered and laser triggered data [36]. This is because only 20% of the gap is shorted by the focused laser beam and the ionized channel created by the laser is not wide enough to dramatically affect the radius of the trigger section arc.

Time varying inductance is solved by obtaining a time varying arc radius from the resistance plotted in Fig. 5-8 and the breakdown geometry. The inductance, also plotted in Fig. 5-8, has a conducting value of 290 nH. The inductance varies by 20% over all time, not several orders of magnitude as for the resistance. It is therefore acceptable to consider the inductance constant as was assumed at the outset of analysis.

Both the time varying resistance and inductance are used to determine voltage and current waveforms from Eq. 5-1 and compared to the original data. L_{SW}, R_{SW} and I_{SW} are used in Eq. 5-1 to find V_{SW}. L_{SW}, R_{SW} and V_{SW} are substituted into Eq. 5-1 to find I_{SW}. Calculated voltage and current solutions to Eq. 5-1 are plotted in Fig. 5-9 with the measured voltage and current waveforms. The closeness of fit indicates that the time varying

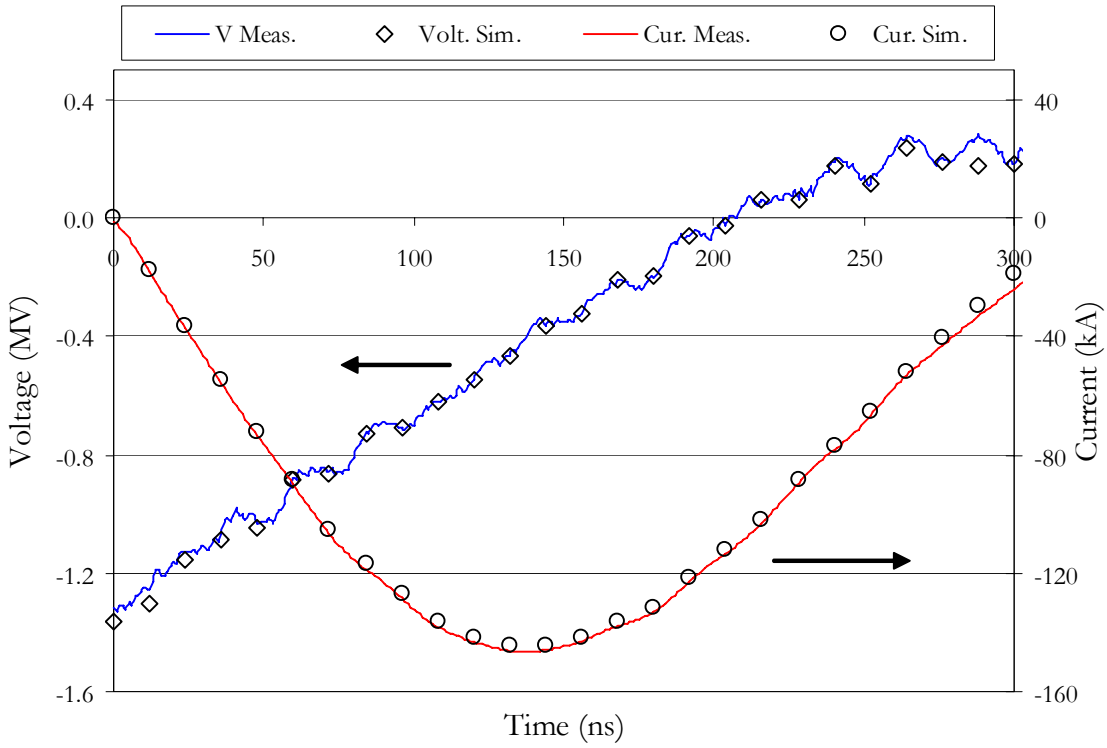

Fig. 5-9. Measured voltage and current plotted with solved voltage and current using the time varying parameters in Fig. 5-8.

resistance and inductance plotted in Fig. 5-8 are sufficient fit parameters to the original differential equation.

The aforementioned method was applied to each electrode configuration for all data. Conduction, or final value on state inductances and resistances were determined by averaging the time varying values about the peak current, or from 100 to 200 ns. The spread in the total channels for all data is fourteen, giving a range of 1.4 to 2.8 channels per gap in the ten gap system. The inductance, depicted in Fig. 5-10, is quite linear with an R^2 of 0.85. There is a statistically significant difference in inductance with 95% confidence between the 6.67 cm with holes tests and all other configurations. There is no difference in inductance between the 6.67 cm without the holes and 10.16 cm tests. This echoes the data for the total number of cascade channels indicting that the holes experiments had a significantly larger

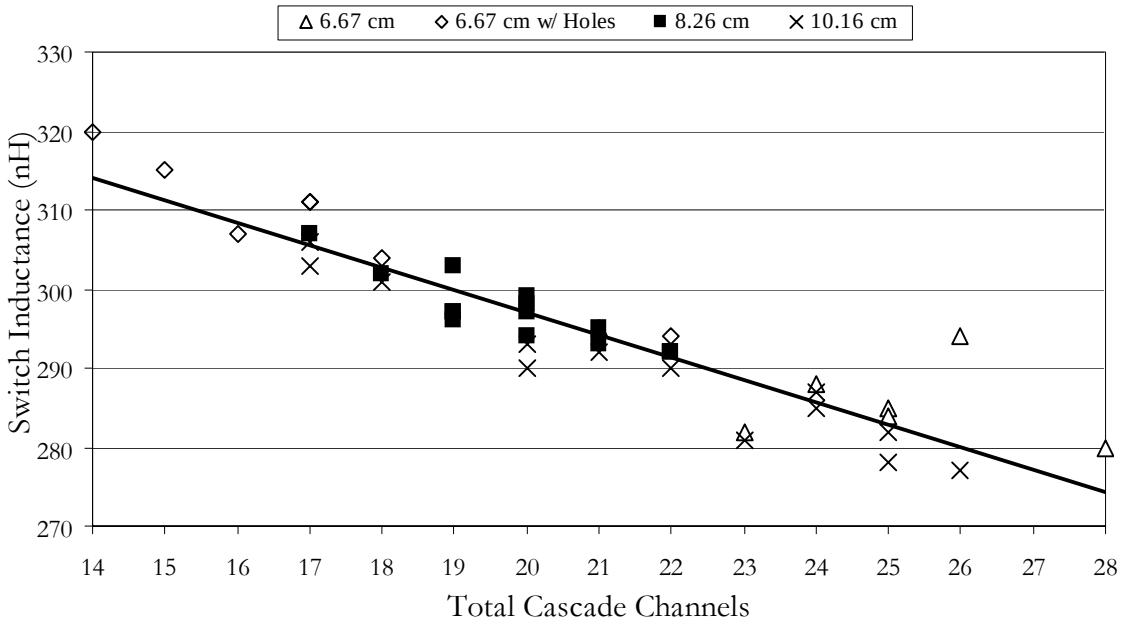

Fig. 5-10. Total switch inductance.

inductance than all others and for the arrangements tested. A lowering of inductance due to increased electrode radius was not observed. It can be concluded that arrangements that experience denser multichanneling will have lower inductances and that number of channels dominates inductance over electrode radius for these experiments.

A summary of total arc inductance arranged by electrode configuration is depicted in Fig. 5-11. A spread in inductance increased slightly from 6.67 cm to 10.16 cm indicating that perhaps the arc distribution pattern had an influence on measured inductance outside of the number of channels, since there was no discernable difference in the number of channels between the two. A general increase in normalized risetime (rise time divided peak current) as a function of inductance was observed within each electrode configuration and is depicted in Fig. 5-12.

The total switch conduction resistance, plotted in Fig. 5-13 is more loosely dependent on the number of channels than inductance. When the cascade section resistance

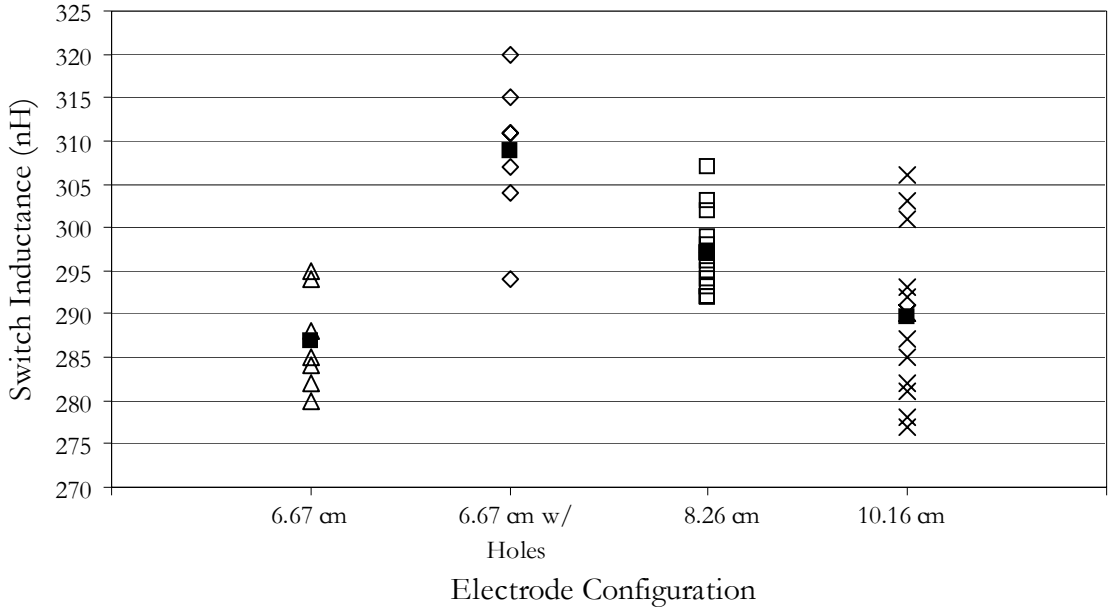

Fig. 5-11. Switch inductance by electrode configuration.

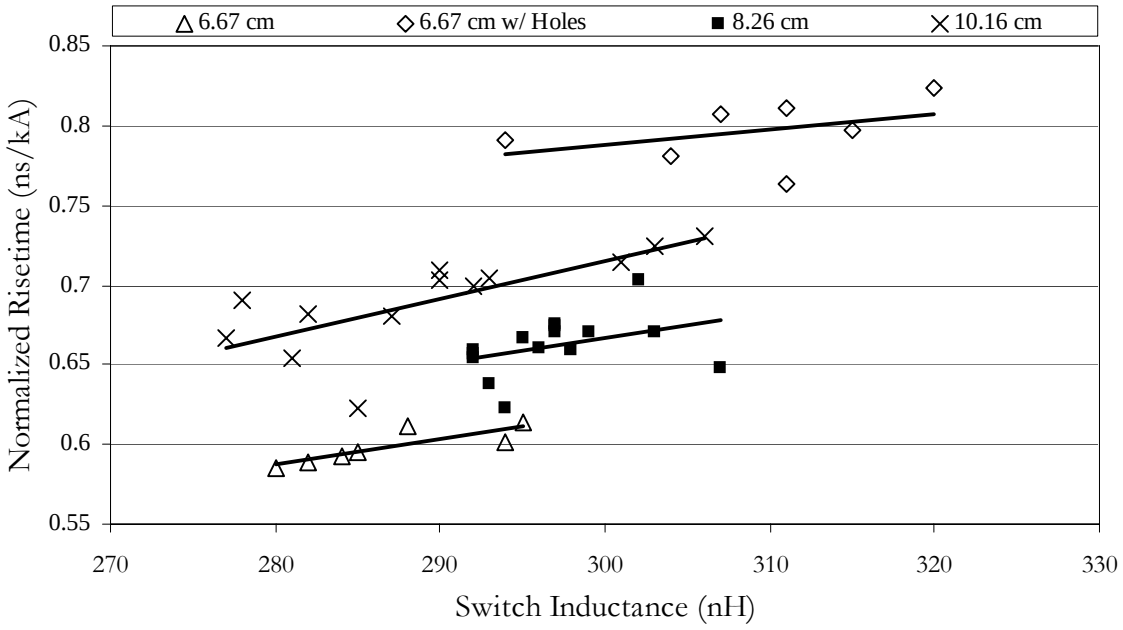

Fig. 5-12. Rise time versus inductance.

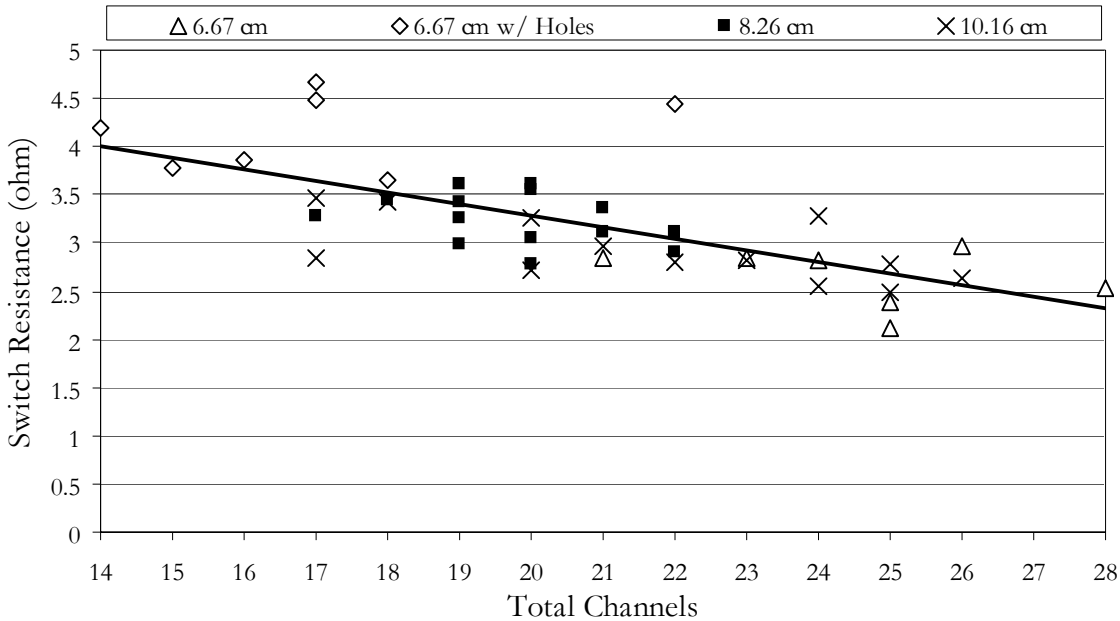

Fig. 5-13. Total switch conduction resistance.

is plotted versus the inverse of the average number of channels per gap, n_g^{-1}, a positive linear relationship is evident as in Fig. 5-14 to within 10%. For a total cascade switching length of 8.86 cm, assuming a constant conductivity of 160 Ω^{-1} cm^{-1} and an assumed arc diameter of 0.15 cm, the cascade conduction resistance R_C may be related to n_g^{-1} by,

$$R_C = \frac{l}{\sigma A} \cdot n_g^{-1} = 3.13 \cdot n_g^{-1} \quad \Omega. \qquad \text{Eq. 5-3}$$

This line is plotted with measured cascade conduction resistance in Fig. 5-14. A shift of approximately 0.3 mΩ more closely matches the data that is due to other switch losses. Kushner found a 1.2 cm SF_6 laser triggered arc to have a conduction resistance of 0.25 Ω at a peak current of 18 kA [41,43]. Applying this resistance per unit length to the Rimfire geometry and considering a multichanneling arrangement for an average per arc current of

18 kA, the fit line in Fig. 5-14 suggests a total cascade resistance of 0.42 Ω that is within a factor of 1.4 of Kushner's extrapolated value of 0.3 Ω.

The trigger gap is a long, single channel gap contributing approximately 35% of overall switching length. Experiments were conducted in which the cascade section was shorted and only the triggered gap was allowed to conduct. The measured trigger resistance contributes >50% to the overall switching resistance for the first 70 ns. After this, its contribution is 25 to 40% depending on the number of channels and typically has a conduction resistance of 1.1 Ω. The calculated inductance contribution of the trigger section is 40 to 50% of the total switch inductance depending on the channel arrangement, with a typical value of approximately 65 nH. This indicates the single channeling trigger gap must be the focus to improving switching performance for both inductance and resistance. Hybrid trigger schemes have been utilized to address the large inductance of a single channeling gap but the designs tested to date have provided no conclusive solution [3].

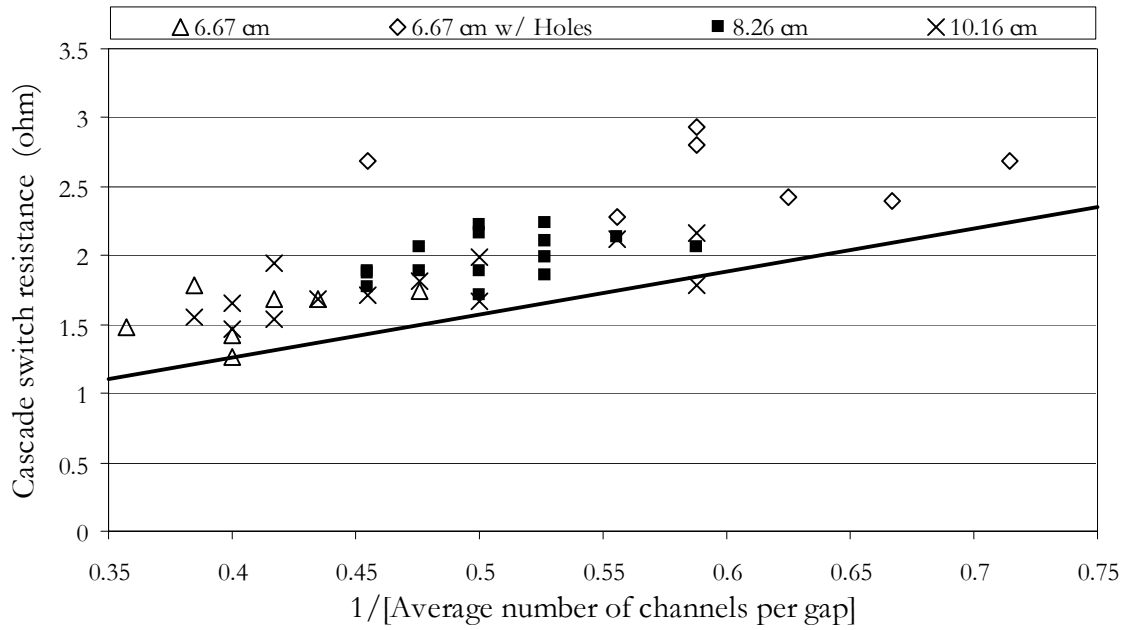

Fig. 5-14. Cascade conduction resistance with Eq. 5-3 line.

Switch resistance is highly influenced by both the drive circuit impedance and switch inductance. If the driving circuit or switch inductive impedance is large, the current will rise more slowly as is generally seen in Fig. 5-12. This alone causes slower arc expansion, but aside from this, voltage fall in a typical application of a large multigap switch may be dictated by impedances external to the switch that it is driving [44]. High driving impedance will lead to a slower resistive voltage fall, thus producing the effect of a higher measured resistance at the time of peak current. In air experiments conducted by Akiyama, the conduction resistance for a 1 cm gap at 20 kA was 50 mΩ while Kalstrom measured a 0.4 cm gap with a peak current of 25 kA to have a conduction resistance of 7.5 mΩ [42,45]. These measurements differ by a factor of 2.85 when scaled to the same length and they are both nearly an order of magnitude different from Kushner and the results presented in this work. Each experiment used different driving circuit impedances that affect measured conduction values and how the voltage is distributed at the time of peak current. For example a 6.67 cm shot with a cascade conduction resistance of 1.42 Ω, at the time of peak current (t_p), falls to 0.78 Ω at three times t_p, which is much closer to observed values by Akiyama and Kalstrom.

The long resistive fall time has significant implications for the design of fast switches. Reducing the resistive fall time will extend the ceiling to which a reduction in inductance provides improvement to rise time for a given switch. For example, in a simulation using the circuit in Fig. 5-7, a 6.67 cm shot was simulated for two cases: 1) with a reduced inductance by a factor of two, and 2) with a reduced inductance by a factor of two and a rapid transitioning resistance to the conduction state (essentially instantaneously). The rise time of switch current for case 1 decreased by 20% while the peak current increased by 6%, and for case 2 the rise time was reduced by 37% and peak current increased by 20%. For fast switching, geometrical changes must be implemented that reduce inductance and trigger

methods or gas types must be chosen to reduce resistive effects for a truly optimized switching scheme. This is discussed in more detail in Section G.

F. Switch Gas Type and Pressure

The scaled Rimfire is designed for use with a fill gas of SF_6 at roughly 20 psig (referred to as the baseline Rimfire test case), but multichanneling experiments were also conducted using air in a pressure range from 25 to 35 psig. Electrode configurations tested included 6.67 cm disc electrodes of the cross section in Fig. 5-2 and the 6.67 cm electrodes with holes. Experiments were also conducted utilizing SF_6 in elevated pressures of 35 and 50 psig. High pressure SF_6 shots required the trigger gap to be shortened from 4.7 cm to 2.45 cm and gaps 1, 5, and 10 to be electrically shorted due to voltage limitations of the Marx and I-Store. The voltage distribution between the trigger and cascade section remained at roughly 30%, while the fields increased 32%. The fields are uniform in the cascade section within ± 10% as in the baseline scaled Rimfire case. A self-break curve is depicted with the scaled Rimfire self-break curves for all shot configurations in Fig. 5-15. All shots were

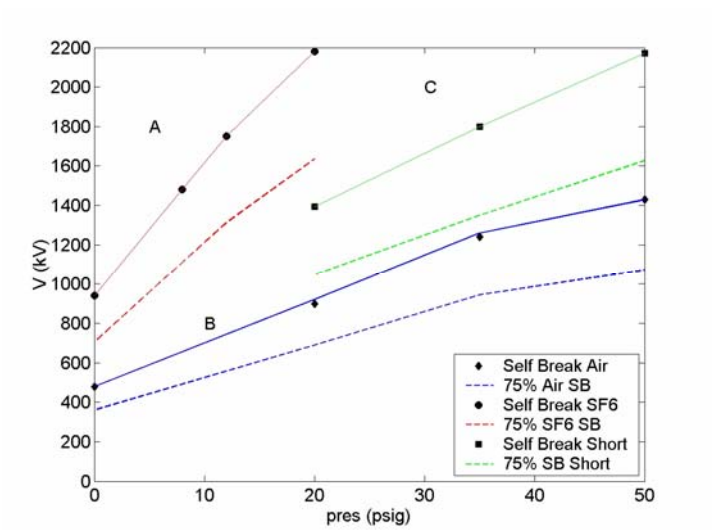

Fig. 5-15. Self-break curves for all Rimfire variations tested.

conducted in a voltage range from 820 kV to 2.1 MV at a varying percentage of self-break.

Fig. 5-16 gives a synopsis of the breakdown pattern for the both air and SF_6 shots. Air shots were triggered between 75-85% self break (SB). SF_6 laser shots at 18 psig were conducted between 65-70% of SB. The 25 psig shots were conducted between 75 and 90% of SB. Breakdown photographs are depicted in Fig. 9-18, Fig. 9-19, and Fig. 9-23 to Fig. 9-27. In gaps in which there are six or more channels, referred to as "dense" channeling, the number of channels assigned to that gap were six. This was to curb erroneously high total channel numbers where dense channeling occurs. It is evident by the time evolved photos that when dense channeling occurred, some arcs carried substantially lower current, hence the need to define a maximum (six). Dense channeling was observed in the air filled gaps and is consistent with previous experiments [2]. Dense channeling occurs in the first few gaps for untriggered air experiments and throughout the entire cascade section when a laser trigger is implemented. There are a higher number of channels for air for any given

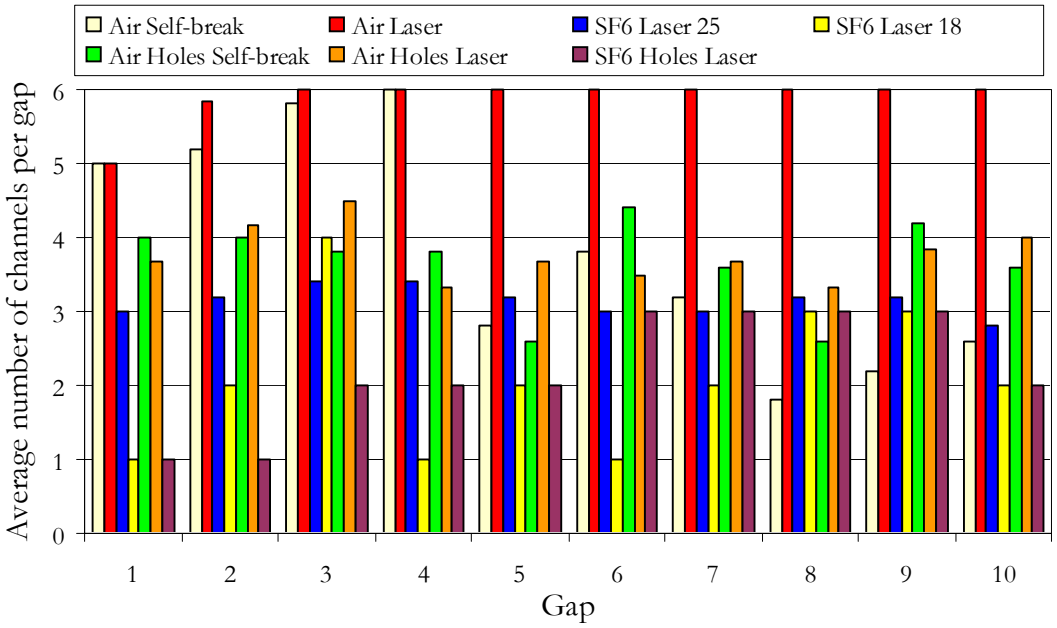

Fig. 5-16. Breakdown synopsis for the air and SF_6 experiments.

setup in Fig. 5-16, even though the pressures and breakdown voltages vary widely. This pattern is not observed in the SF_6 case and in fact multichanneling exhibits much different behavior between gases.

There is a dramatic difference in the multichanneling ability between the two gases as is depicted in Fig. 5-17. Sulphur hexafluoride is a highly electronegative gas. Fluorine, with an electron affinity of 3.45 eV and an electronegativity of 3.98 on the Pauling scale, is the highest of all atoms. A high electronegativity means the SF_6 molecule is exceptionally willing to absorb free electrons into its' outer most shell because of its relatively large electron attachment and electron scattering cross sections coupled with high electric breakdown strength. These factors hinder free electrons from accelerating in the applied field and this hindrance prevents avalanche breakdown. This absorption is primarily governed by resonance capture ($SF_6 + e \rightarrow SF_6^-$) or through dissociation ($SF_6 + e \rightarrow SF_5^- + F$) [46,47]. These properties are what make SF_6 an ideal high voltage insulating gas [48].

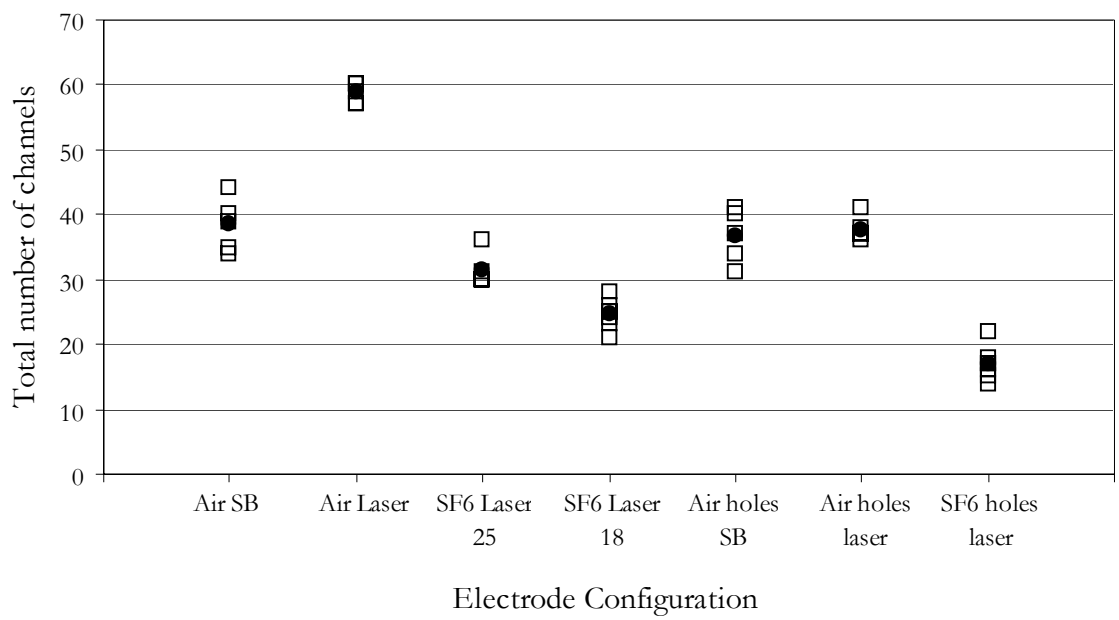

Fig. 5-17. Total channels breakdown synopsis.

These properties also contribute to the relative inability of pure SF_6 to multichannel when it is compared to inhomogeneous gas mixtures that primarily contain components that are not electronegative. Many of the most recently studied multichanneling gas mixtures seem to exhibit a relationship between low proportions of gases with high electron affinity and high multichanneling ability. SF_6 has a relatively large electron affinity (3.45 eV for fluorine, 15.32 eV ionization energy, relative breakdown voltage of 2.5), and multichannels relatively poorly [49]. Air, containing 78% nitrogen and 19% oxygen, exhibits dramatically better multichanneling characteristics when compared to SF_6 (nitrogen electron affinity 0.072 eV, ionization energy 14.53 eV, relative breakdown voltage of 1, oxygen electron affinity 1.46 eV, ionization energy of 13.62 eV). SF_6 – Argon mixtures (argon has an electron affinity of 0, ionization energy of 15.76 eV, relative breakdown voltage of 0.15) with low (<10%) SF_6 content are known to multichannel better than air [50]. Although the lower breakdown strength of the buffer gases in this mixture will increase the relative production of ions as the breakdown strength is exceeded, it is unlikely that the combination of a highly electronegative gas and the buffer gas increases the multichanneling ability of the buffer gas compared to it by itself. The SF_6 merely increases the breakdown strength of the buffer gas [38]. For example, argon is known to multichannel well by itself and the addition of SF_6 does not improve its' ability to multichannel, but rather the breakdown strength of the bulk gas. Experiments using SF_6 – Argon mixtures were not conducted, however, because of the impractically low breakdown strength caused by the high argon content needed in such a mixture for multichanneling.

There were fewer channels that formed in the holes experiments then in the original electrode configuration. In addition, field enhancement holes forced a more aligned breakdown pattern for the air filled case and effectively capped the maximum number of

channels that formed at four per gap. There was no increase in the total number of channels formed using a laser trigger in this arrangement compared to SB experiments. The spread in the total number of channels decreased from nine total channels in the SB case to only four in the laser triggered case. Data suggest that using field enhancement locations susceptible to only self irradiation, limits the number of channels that form in a gap, but improves their uniformity. This was seen in an air laser triggered environment, but not in an SF_6 environment as described earlier. This is consistent with experiments conducted by Sandstrom and Furuya using the bombardment of ionizing radiation into an air or nitrogen filled gap [51,38].

A comprehensive circuit simulation was implemented in a similar manner as for the electrode radius tests described in the previous section. For these simulations the transition time for switching from off to on in a given gap was simulated as a rapidly decreasing resistance as in Fig. 5-8. Fig. 5-18 depicts the difference in dv/dt at the time of breakdown

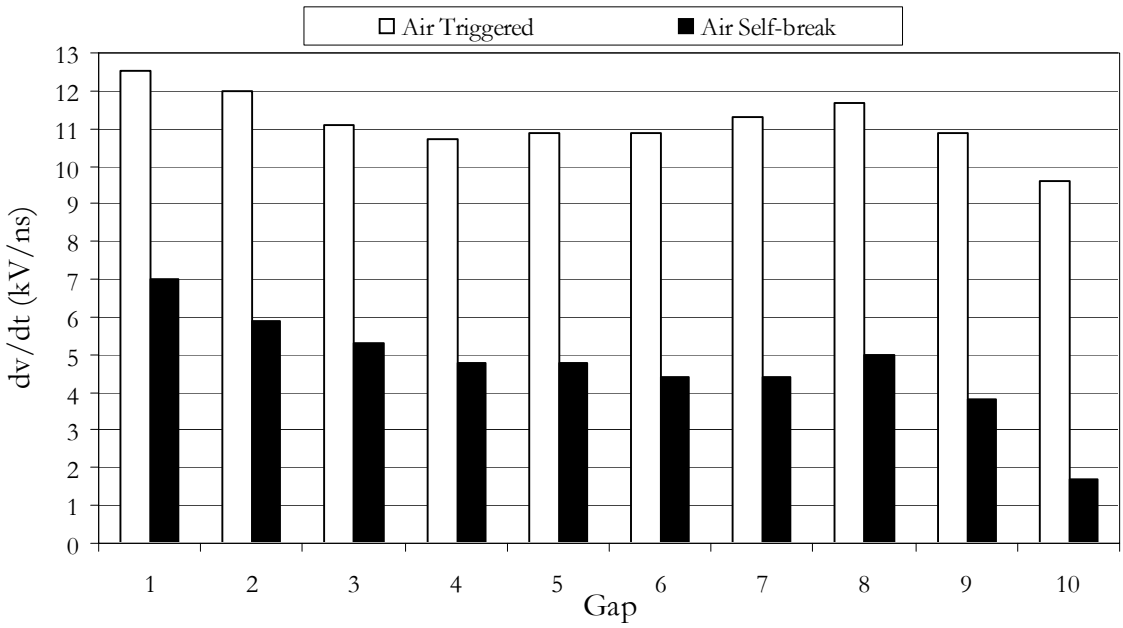

Fig. 5-18. dv/dt at the time of trigger for all cascade gaps for air filled Rimfire. Gap 1 is nearest trigger gap.

for a triggered and untriggered shot for air. For triggered experiments (at 85% of SB) the average breakdown voltage is 0.942 MV (E_{sb} = 108 kV/cm at 35 psig) and the breakdown voltage for the SB case is 1 MV (E_{sb} = 90 kV/cm at 26 psig). dv/dt is larger for the triggered case in all gaps and in the SB case there is a declining trend in dv/dt from gap 1 to gap 10. This explains the observed increase in number of channels between untriggered and triggered experiments in gaps five through ten without holes since multichanneling likelihood is affected by voltage rise rate [38]. The larger dv/dt in the first three gaps agrees with the results in Fig. 5-16 in which the switch multichanneled more readily in these gaps where the dv/dt exceeds 5 kV/ns. This is consistent with work conducted by Neil and similar trends of increased multichanneling were observed by Bergmann as dv/dt increased [52,53].

Similar analysis was for SF_6. Fig. 5-19 depicts the difference in dv/dt at the time of breakdown for a triggered and untriggered shot for SF_6. For triggered experiments (at 70%

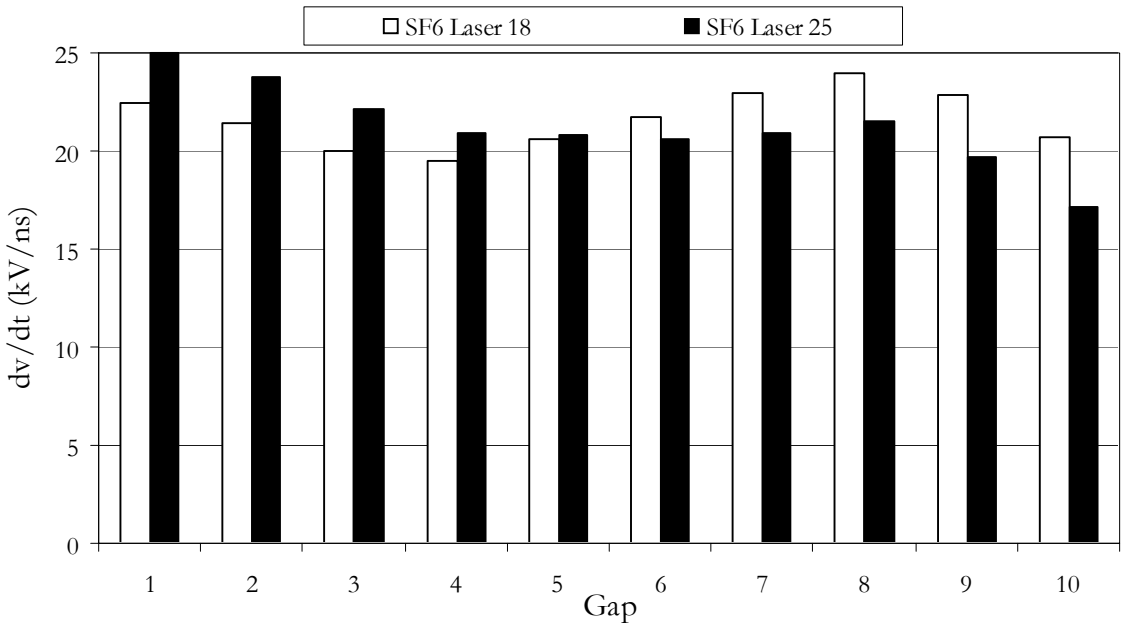

Fig. 5-19. dv/dt at the time of trigger for all cascade gaps for SF_6 filled Rimfire. Gap 1 is nearest trigger gap.

of SB) at 18 psig the average breakdown voltage is 1.55 MV (E_{sb} = 200 kV/cm at 18 psig with a SB voltage of 2.2 MV) and the average breakdown voltage for laser experiments (at 83% of SB) at 25 psig was 2 MV (E_{sb} = 216 kV/cm at 25 psig with a SB voltage of 2.4 MV). dv/dt is quite similar between the two cases which coincide with the observed result in Fig. 5-16 in which there was no observed difference between the two cases indicating that percentage of SB did not influence multichanneling substantially.

dv/dt in Fig. 5-19 is rather similar from gap to gap and does not explain, by itself, the breakdown pattern observed both in Fig. 5-16 and Fig. 5-4. This is because in addition to dv/dt there is the concept of a multichanneling window that will affect the number of channels that form. This window is described by the period of time in which the voltage that is imparted across a gap exceeds the breakdown voltage of that gap before the resistance falls. Since the resistance does not fall instantaneously, there is a finite time, of several nanoseconds in which the gap could potentially multichannel because breakdown voltage is exceeded in this interval. If dv/dt is increased, or this time is increased, multichanneling should increase. In Fig. 5-20, an over voltage value is presented in which dv/dt is multiplied by the multichannel window time. This voltage value is really a combined measure of each factor in which a large value corresponds to a gap in which multichanneling is more likely. It is interesting to note the similarity between Fig. 5-20 and Fig. 5-5 in which dv/dt was obtained by assuming an instantaneous transition from off to on. The over voltage value explains the breakdown pattern for SF_6 much more thoroughly than purely looking at dv/dt. For an over voltage value of 60 kV, increased multichanneling is seen in a given gap. Similarities may be drawn between the breakdown patterns and the over voltage value for air, although they are not as strong.

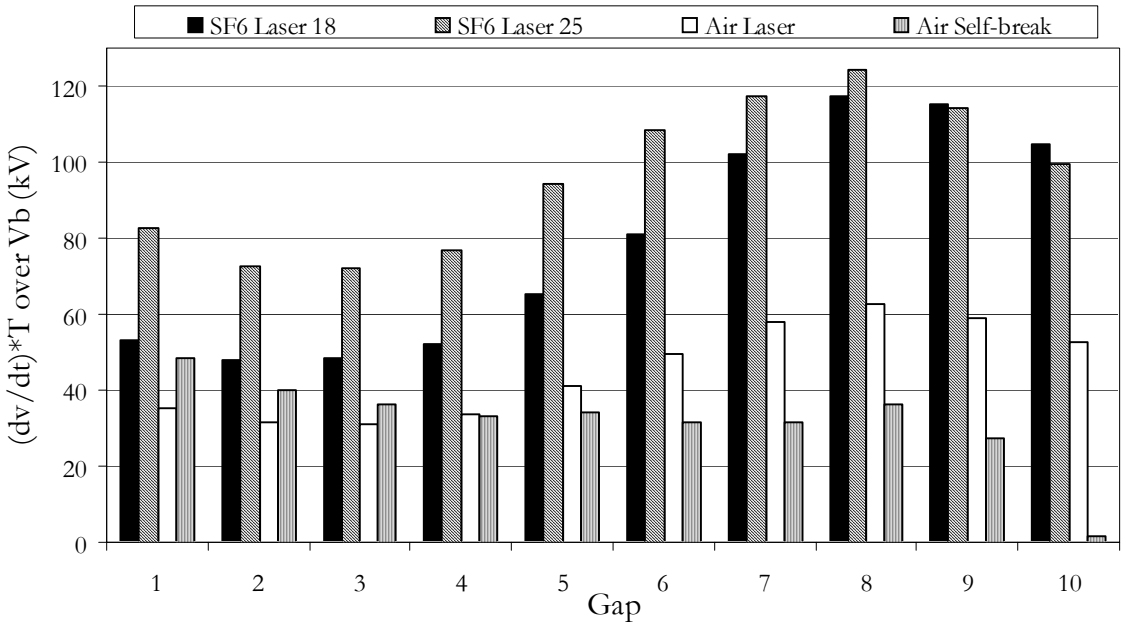

Fig. 5-20. Over voltage for a theoretical instantaneous switch transition.

Experiments were conducted at elevated pressures to determine if channeling would decrease as pressure increased for the electrically negative SF_6 as others had observed with oxygen [38]. There were eleven experiments conducted at 80% of SB for 35 psig and five experiments conducted at 50 psig in a shortened Rimfire. There was statistically no observed decrease in the number of channels as pressure increased. These experiments, with a channel breakdown synopsis depicted in Fig. 5-21, were conducted at approximately twice the dv/dt per gap as in Fig. 5-19, but did not form more channels than SF_6 laser shots as depicted Fig. 5-16.

Cascade gaps are overvolted differently depending on the percent of SB and whether or not the laser trigger is present. In the laser trigger mode the switch breaks down nearly sequentially from trigger end to IS end as depicted in Fig. 5-22. In the untriggered mode, cascade breakdown is nearly instantaneous and does not breakdown in a sequential order as in the laser triggered case. The runtime and breakdown sequence will affect both dv/dt and

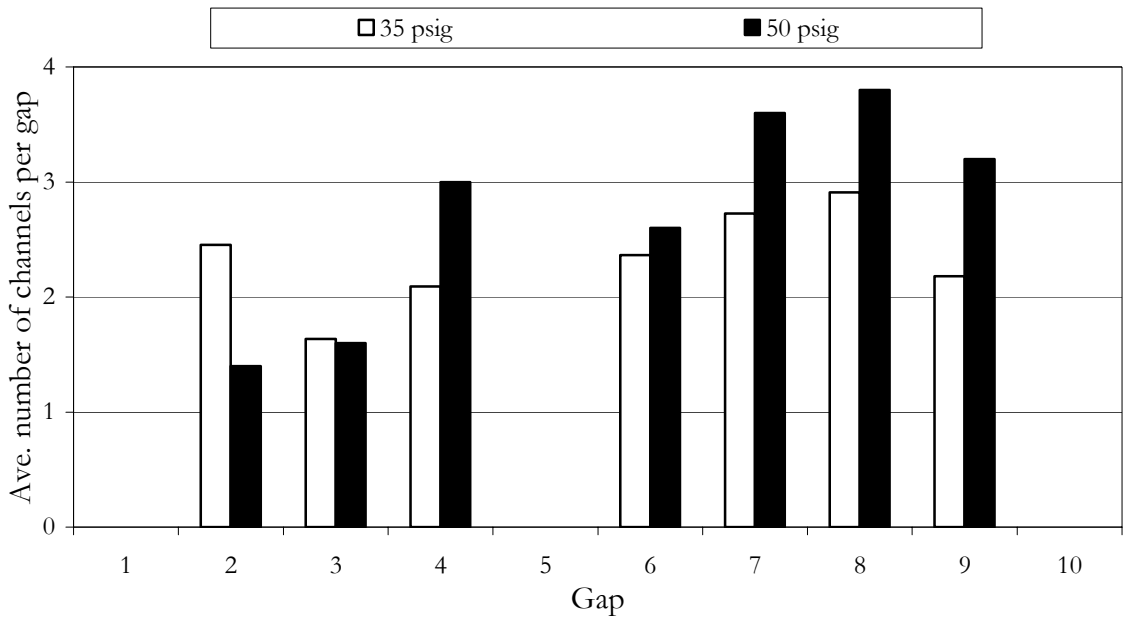

Fig. 5-21. Breakdown synopsis for shortened switch. Gap 1 is closest to triggered gap. Zero time is when the first cascade gap breaks down. Gaps 1, 5 and 10 are electrically shorted.

the time over which the voltage exceeds the breakdown voltage, whereby a longer time between gaps breaking down will increase both factors.

The impedance was calculated using a similar method as in Section D for all data. The spread in the total channels for all data is 46, giving a range of an average 1.4 to 6 channels per gap in the ten gap system. The measured inductance, depicted in Fig. 5-23 exhibits a generally decreasing behavior over the channel range. Inductance was plotted as a function of one over the number of channels since the calculated inductance in Eq. 9-1 depends on this term. Fig. 5-24 depicts a rather linear fit to the data indicating the strong influence of the inverse of the number of channels and the relatively lesser influence of the natural log term. A summary of total arc inductance arranged by electrode configuration is depicted in Fig. 5-25. The single channeling trigger gap has a similar influence on the inductance and resistance as was stated in Section D.

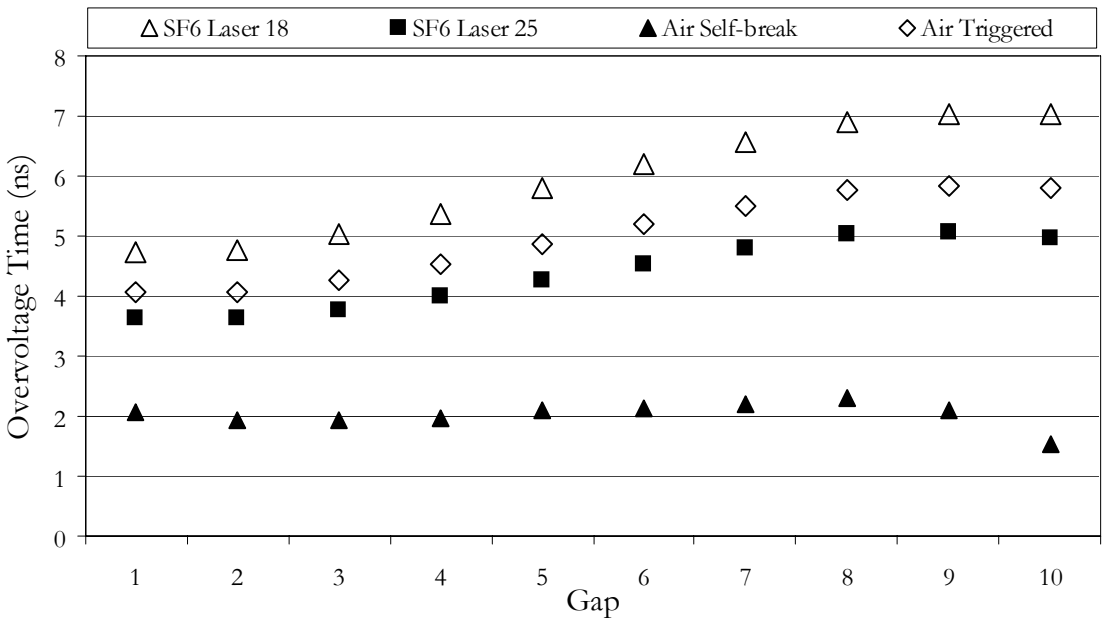

Fig. 5-22. Breakdown sequence. Laser gap closes at t = 0.

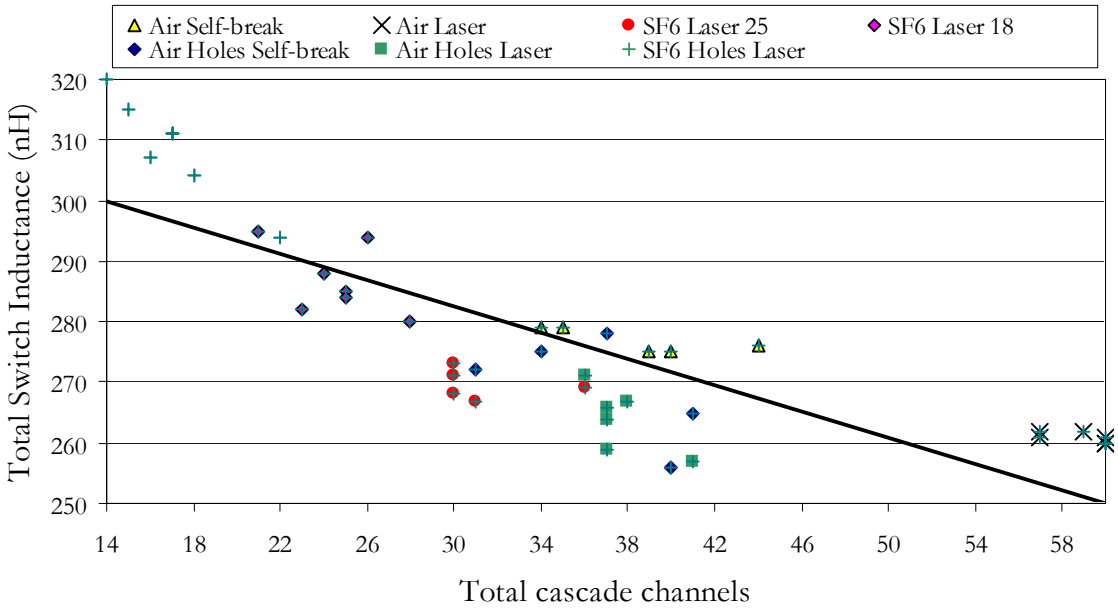

Fig. 5-23. Total arc inductance by electrode configuration.

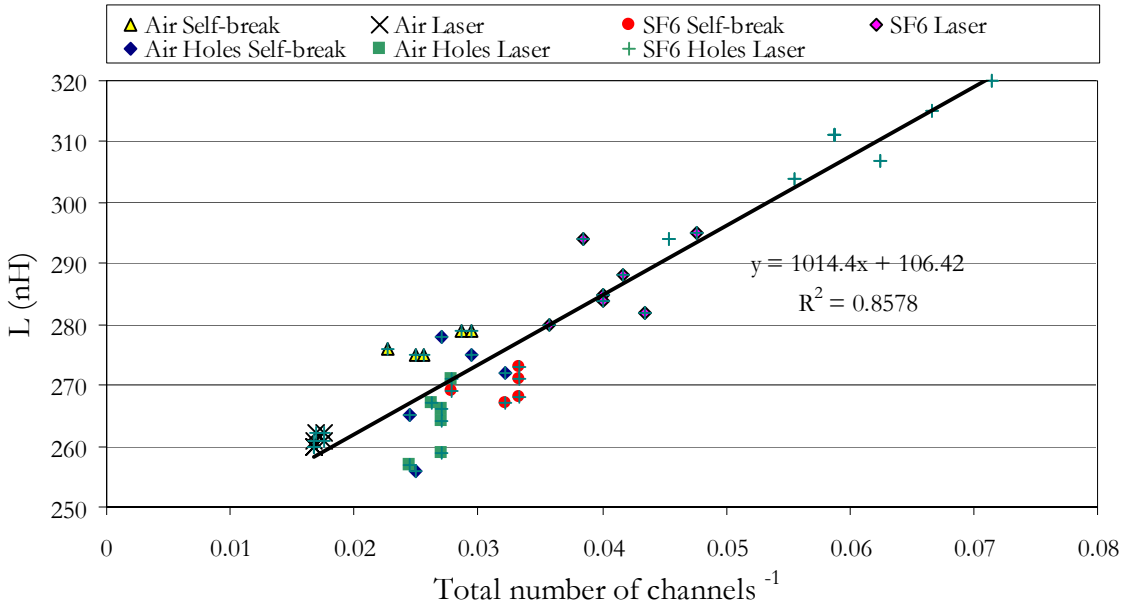

Fig. 5-24. Total arc inductance versus 1/n.

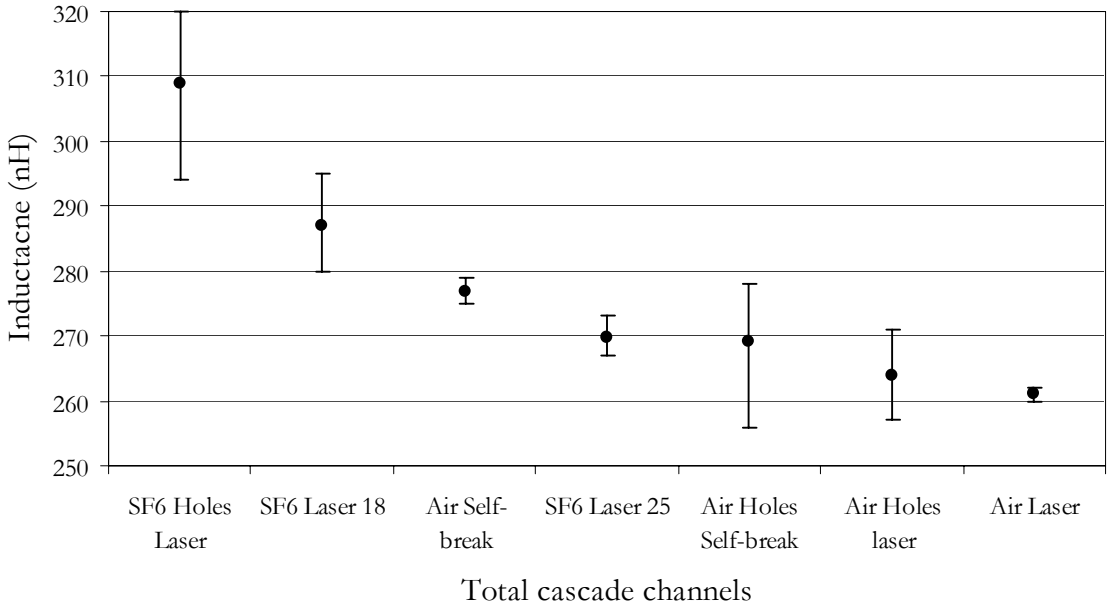

Fig. 5-25. Arc inductance by electrode configuration.

There is a statistically significant difference (with 95% confidence) in the inductance between the SF_6 laser shots at 18 psig and all other data. There is a difference between the air laser and the SF_6 laser experiments, which is due to dense multichanneling in the air case. The SF_6 laser shots at 18 psig have a larger inductance than the shots at 25 psig likely due to the larger number of single channeling occurrences at 18 psig. There is no difference between the inductance for the air SB shots and the SF_6 25 psig shots indicating that above four channels per gap there is no advantage for inductance.

Total conduction resistance exhibits a similar relationship to the number of channels than the inductance as depicted in Fig. 5-26. Data indicate a 1/n dependence of switching resistance on the number of channels. Above 26 total channels in the cascade this relationship deteriorates to a value that is not dependant on the number of channels. This is consistent with the data presented in Section D. Eq. 5-3, the resistance as a function of the number of channels, is plotted with cascade section resistance in Fig. 5-27. Resistance was found to have no dependence on breakdown voltage, peak current, or any other identifiable variable other than the number of channels up to 26 total channels. There is a statistically significant difference in the resistance between the SF_6 Hole experiments and all other sets. This indicates resistive losses in the switch are not purely a function of the number of channels and may not be expected to decrease necessarily as channel number increases to large gap densities. This is because as the number of channels increase, the current any one channel carries is reduced, thereby reducing the radius it will expand to. Thus each arc will become more resistive and there will be increased losses per arc.

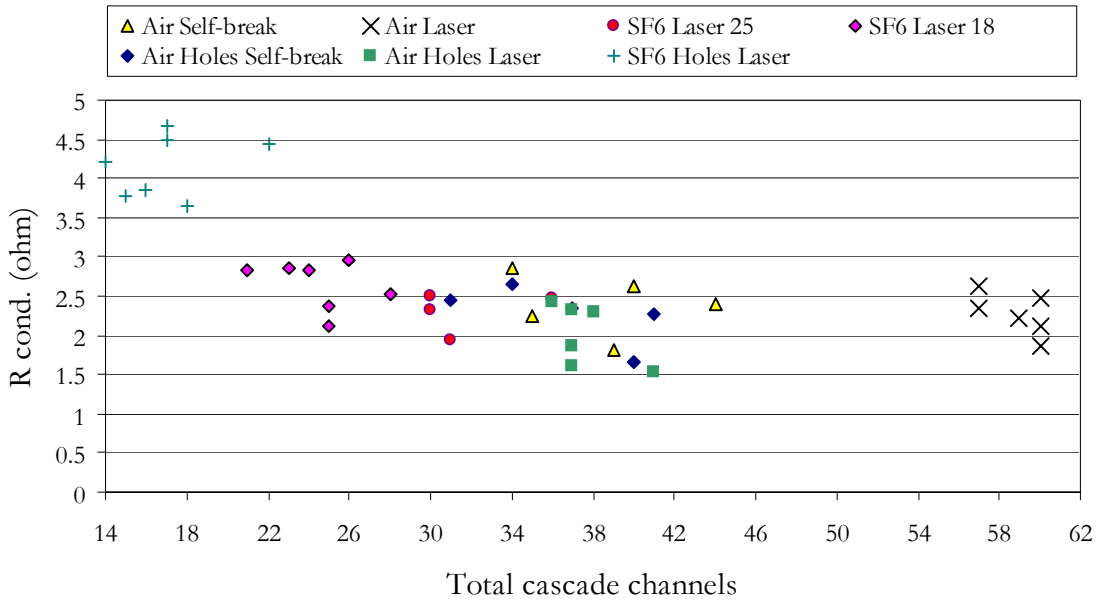

Fig. 5-26. Conduction resistance.

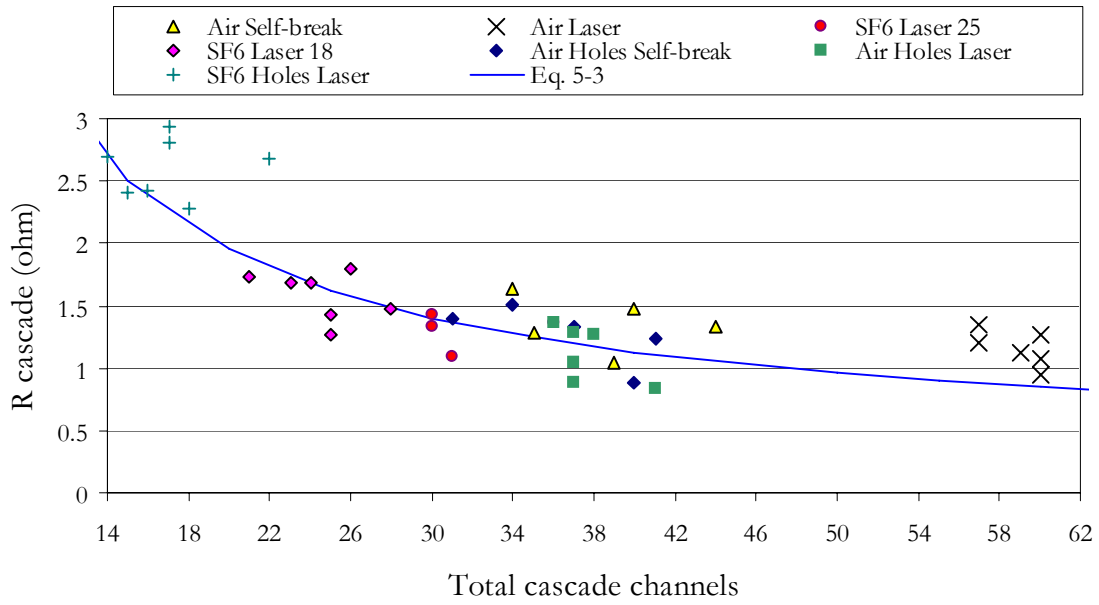

Fig. 5-27. Cascade conduction resistance and Eq. 5-3 line with a 0.3 Ω shift.

G. Impedance Discussion for Laser Data

An assumption must be made, either with resistance or inductance, in order to solve Eq. 5-1 since both time varying parameters are unknown. There is no direct way to measure either parameter, so both must be inferred from switch voltage and current. There is one general approach to this problem: assume one is known, or has aspects of it that are arguably known, then solve for the other parameter. In the previous sections, the inductance was assumed to be calculable using established inductance calculations that are based on the known geometry of the system. The inductance was also assumed constant because the only geometrically changing parameter is the radius of the arcs. This radial dependence of the inductance is natural logarithmic. The radius is known to grow from some initial value (10's of micrometers) to no more than a few millimeters [39]. Therefore the total arc inductance can vary by no more than a factor of two and is often assumed constant when spark gap switches are analyzed [25]. The inductance assumptions made in the previous section are consistent with physical processes and with previous researchers' work [41,42].

The time varying resistance that results from the previous section has a final conduction value that is consistent with other researchers work on SF_6 conductivity. In addition, the time varying resistance in this model will produce exactly the voltage and current waveforms, when combined with the assumed inductance. Solutions obtained will not be unique in that a change in the inductance assumption will change the resistance result. This emphasizes the importance of proper assumptions that were used in the previous sections.

Time variance in the resistance and inductance will only be a function of time variance in arc radius if the conductivity is assumed constant, or relatively constant on the time scales of interest [7]. It is clear that as the switch transitions from off to on, the largest

change that will take place in either parameter is during early time through peak current. Although in reality both parameters will change to some degree during this time, they both will reach some relatively constant or conducting state, at least until current changes directions. According to commonly used arc physics techniques, a conduction radius is reached within a 15% or less by the time of peak current [44]. It is therefore reasonable to believe that a time varying impedance would have more immediate and direct effects on switching current and voltage during this transition phase (early time) and that the conduction value will more directly effect things like peak current, ringing frequency, and other late time characteristics. Under this framework it is clear that assuming a time varying resistance and a constant and calculable inductance is appropriate.

A large early time resistance has significant implications on the design of fast switches. If when optimizing a switch the inductance is reduced, and not the resistance, such as by reducing the ratio of inner to outer conductors, the resistive contribution to rise time will begin to approach the rise time contribution due to inductance. Since this limiting factor will be reached for any lower inductance design, it is advantageous to address the reduction of switching resistance along with switching inductance. A reduction of resistance alone will not decrease switch rise time significantly and will have less of an effect as the reduction of inductance alone. Reducing the resistive rise time, however, will extend the ceiling to which a reduction in inductance provides improvement to rise time for a given switch. For example, in a simulation using the circuit in Fig. 5-7, a 6.67 cm shot was simulated for two cases: 1) with a reduced inductance by a factor of two, and 2) with a reduced inductance by a factor of two and a rapid transitioning resistance to the conduction state (essentially instantaneously). The rise time of switch current for case 1 decreased by 20% while the peak current increased by 6%, and for case 2 the rise time was reduced by

37% and peak current increased by 20%. There is dramatic improvement by removing this long transition, that is gas, pressure, and trigger method dependant.

Theoretically, reducing the inductance may be accomplished by increasing number of channels, reducing the ratio of outer to inner conductor radius in a coaxial system, and reducing length. Most SF_6 experiments exhibited between one and three channels with only 30% of shots experiencing over three channels in any one gap, eliminating this as the primary inductance reducer for SF_6 switching. The outer to inner conductor ratio is limited by the hold off distance between the two at high voltages. For a dramatically reduced inductance, a ratio of less than two would be required, that is physically impossible using any known gas dielectric. One way to reduce both inductance and resistance is to reduce switching length. This is the best option for dramatically reducing switching impedance, but likely has the most challenging design hurdles. These hurdles are addressed in Chapter 7.

Chapter 6
SF_6 Breakdown – Experimental Study

This chapter presents a collection of work regarding high pressure SF_6 and SF_6 – Argon break down. These subjects have been studied for decades, but little data exists for high pressure (>50 psig). Experimental work was conducted to determine how viable these mixtures would be to the development of a new switch. There are three parts to this chapter; 1) a brief discussion of impulse gas breakdown, 2) experimental data collected on the breakdown of SF_6 – Argon gas mixtures at elevated pressures, and 3) a summary of very high pressure gas switching and how the previous research relates to the experimental data collected. There is also discussion on very high pressure SF_6 switching. This section served as a guide for the design of a new switch presented in Chapter 7. In the end, a new switch using high pressure SF_6 was not pursued because the program funding the research was redirected post data collection and analysis.

A. Impulse Gas Breakdown

A wide array of data exists on gas breakdown of mixtures of SF_6 and argon [54,55,56,57]. There is, however, very little data available for pressures above 40 psia. In most previous works, data are usually presented in Paschen breakdown form, or plotting breakdown voltage versus the product of gap distance and gas pressure. There are several parameters that will effect an obtained Paschen curve outside of gap distance and gas pressure. They are pulsed versus static conditions, percent argon in the SF_6 mixture, and uniform field versus non-uniform conditions.

Generalizing voltage gradients into "uniform" and "non-uniform" categories can be misleading because of the wide variety of conditions these terms are used to describe. Paschen form is inconvenient because it forgoes field enhancement effects and invites broad comparisons between data collected in dramatically different conditions. In some cases non-uniform field can mean point-plane geometries. In others it may mean point-sphere geometries and yet in others it may mean sphere-plane. In all conditions the field enhancement factors may be very different and therefore comparing breakdown voltage is less useful than comparing breakdown field. Determining breakdown field from a Paschen curve takes some effort, but enough information is usually available to do so.

The condition under which electrodes are pulsed is another factor that affects not only the pulsed breakdown voltage, but also the field at the time breakdown is observed. The rate of rise of the applied voltage will dramatically affect the pulsed breakdown strength of a gas. As voltage is pulsed with increasing risetime, the breakdown field will increase with the increasing voltage. In fact, pulse rate is the only variable that for a given electrode shape and spacing will lead to a higher breakdown voltage and thus breakdown field. In other words, the breakdown voltage has a variable and it is the rate of rise of the applied pulse.

The effect of rate of rise on breakdown voltage is evident when considering corona stabilization. For the appropriate rising pulse rate, space charge will form at the tip of a corona discharge that will create a localized shielding of the discharge from the applied field across the gap. The result of corona stabilization is that a larger pulsed voltage is needed to overcome this shielding effect. For voltage applications > 350 kV/μs, however, corona stabilization does not take place in SF_6 [58]. Rate of rise and its effect on perceived breakdown voltage is discussed following a brief discussion of relevant breakdown processes.

There are several complex processes that lead to avalanche breakdown that are caused by the application of an electric field across a gas filled gap. They are [59]:

1) Number of initial electrons produced from the external source (dictated by electrode material, geometry and applied field).
2) Gas ionization characteristics by electrons accelerated in the applied field (dictated by the electron drift velocity (on the order of 10^7 cm/s) and gas type).
3) Photoionization caused by the radiation of the accelerating discharge (dictated by the speed of light in the media and gas type).
4) Secondary emission of electrons from the cathode caused by impacting ions (dictated by the ion drift velocity (on the order of 10^5 cm/s), and cathode material).
5) Gas ionization due to ion-gas collisions on their way to cathode (dictated by ion drift speed and gas type).
6) Photoelectric effect due to impacting ions on the cathode (dictated by cathode material).

Townsend breakdown theory is generally used to describe static voltage breakdown of a gas filled gap. In this theory, items 1, 3, 4, and 5 weigh in heavily in determining the number of electrons present in the avalanching process. Impulse breakdown, however, is commonly described by the streamer to avalanche transition theory. This theory was developed as a result of differences between breakdown delay time observed experimentally and those predicted using the Townsend breakdown theory.

Streamer theory describes pulsed breakdown as being primarily dependant on the initial electron avalanche and photoionization due to the radiation of the accelerating discharge (items 2 and 3). In Raethers' model for streamer formation, an initial electron avalanche is accelerated from the cathode toward the anode and photoionization just ahead

of this avalanche begins creating secondary electrons [59]. This creates a high localized electric field and high energy electrons efficiently collide with the background gas. The electrons created by the photoionization process are referred to as space charge and allow the secondary electron front to grow to the size of the original avalanche but more closely to the anode. Once the anode is reached, a similar process occurs just behind the initial avalanche and extends back toward the cathode. Once the space charge region reaches the cathode, the gap is bridged and a highly conductive arc channel allows the conduction of current and the fall of voltage.

There is a statistical delay time between the onset of the initial avalanche and bridging the gap of the space charge region. The delay time consists of a statistical lag time (from the application of voltage to the appearance of the breakdown initiating electron) and the formative lag time (the time it takes space charge to grow to allow voltage collapse). This delay is dependant on the velocity of the electrons in the inter-electrode region and the local velocity of light. Velocity of the electrons is dependant on the applied field. Therefore it is intuitive that if there are two scenarios, one in which the breakdown voltage of the gap is pulsed slowly and another in which the gap is rapidly pulsed, the fields at which breakdown will be observed to occur will be different because of the breakdown time delay. An example of these phenomena is depicted in Fig. 6-1. The breakdown delay time will be lessened for a larger applied voltage, but for tens of nanoseconds rate of rise, this delay will not be reduced substantially.

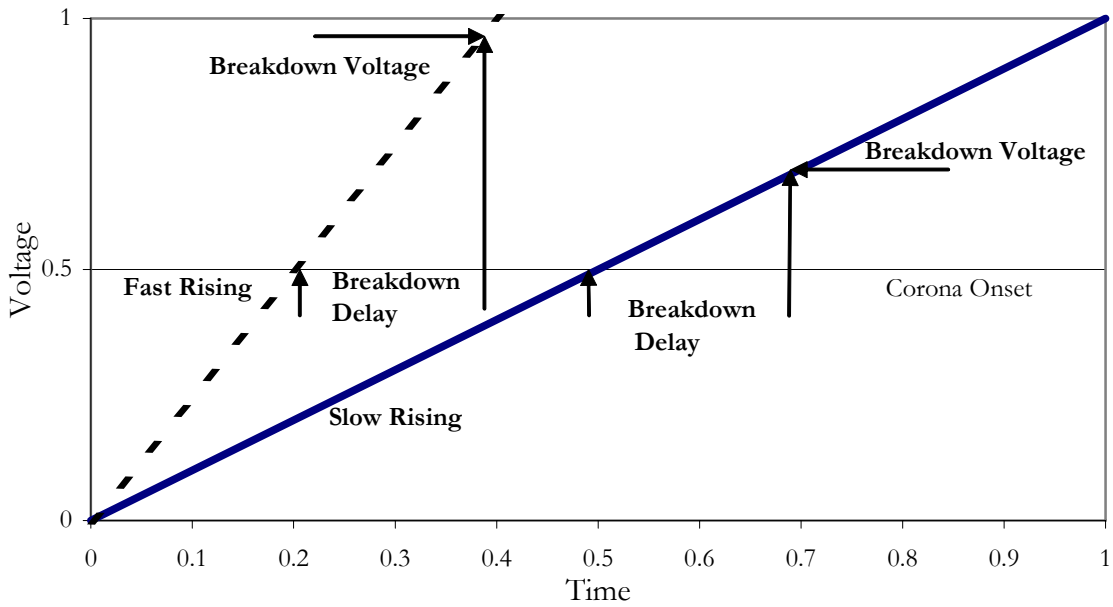

Fig. 6-1. Influence of rise rate on breakdown voltage.

B. SF_6 – Argon High Pressure Breakdown Experiments

A gas chamber consisting of a modified Physics International 760 spark gap was used as the test chamber for high pressure SF_6 – Argon pulsed breakdown experiments at MUTTS. The electrodes were 2.54 cm in diameter, with a 1.31 cm flat surface and a quarter-radiused edge to the outer diameter. Gas ports were fixed 90° apart to insure a complete purging of the inter electrode region between shots. The volume of the chamber was roughly 400 cm^3.

The chamber was pulsed with a four stage Marx bank that consists of 8, 150 nF, 50 kV capacitors that are fitted with four Physics International 760 spark gaps. The gaps are overvolted with a Physics International TG-70, 70 kV pulser. The Marx bank was pulsed into a 2 kΩ load that was in parallel with the test chamber. The 10-90% rate of voltage rise on the test chamber was 1 kV/ns for all shots.

The first set of experiments was conducted with an inter electrode spacing of 0.768 cm. Data were collected for pressures up to and including 100 psig. The second set of experiments was conducted with a spacing of 0.305 cm. Data were collected on three shots for each pressure and for a pressures range from 100 – 190 psig. For a breakdown field of 300 kV/cm at a pressure of 100 psig (an E/p (V/cm/torr) of 60), the drift velocity of SF_6 is 0.015 cm/ns, allowing an electron transit time of 50 ns for the first case and 20 ns for the second [60].

The percentage of SF_6 mixed into the argon was set using a gas proportioner. The proportioner uses two flow tubes, one for SF_6 and one for argon that are calibrated for the individual gas. Gas was flowed into the proportioner with a specified and constant inlet pressure. The individual gases were mixed in a third mixing tube. Pressure was monitored at the output of the mixing tube. The inlet pressure was set higher than all output pressures to be tested for a given experiment. The test chamber was slowly purged with at least two times the chamber volume after each shot with the desired gas mixture. After the purging process was complete the output end of the switch was sealed and gas was allowed to build pressure until the desired pressure was achieved.

Breakdown voltage for the first and second experiments versus fill pressure is depicted in Fig. 6-2 and Fig. 6-3, respectively. As in previous experiments, as the percentage of SF_6 is increased the breakdown voltage increases. The spread at any given data point is ± 5%. Fig. 6-4 depicts the pulsed breakdown field for both cases. This is a combination of both cases, corrected for electrode spacing and field enhancement correction factors due to non-uniformities. In this case, the field enhancement factor (FEF) is defined as the ratio of the peak field in the gap to the theoretical uniform field (mean field). This factor was determined through simulations of the electrode geometry in Maxwell [61]. For the 0.768

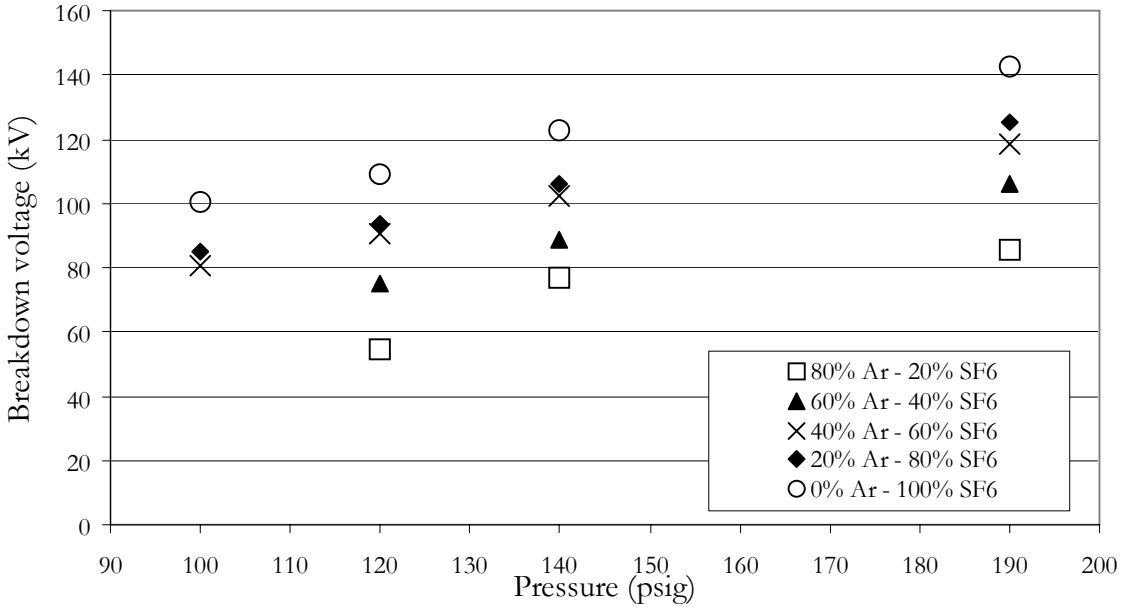

Fig. 6-2. Trial 1: 0.768 cm spacing, FEF=1.14.

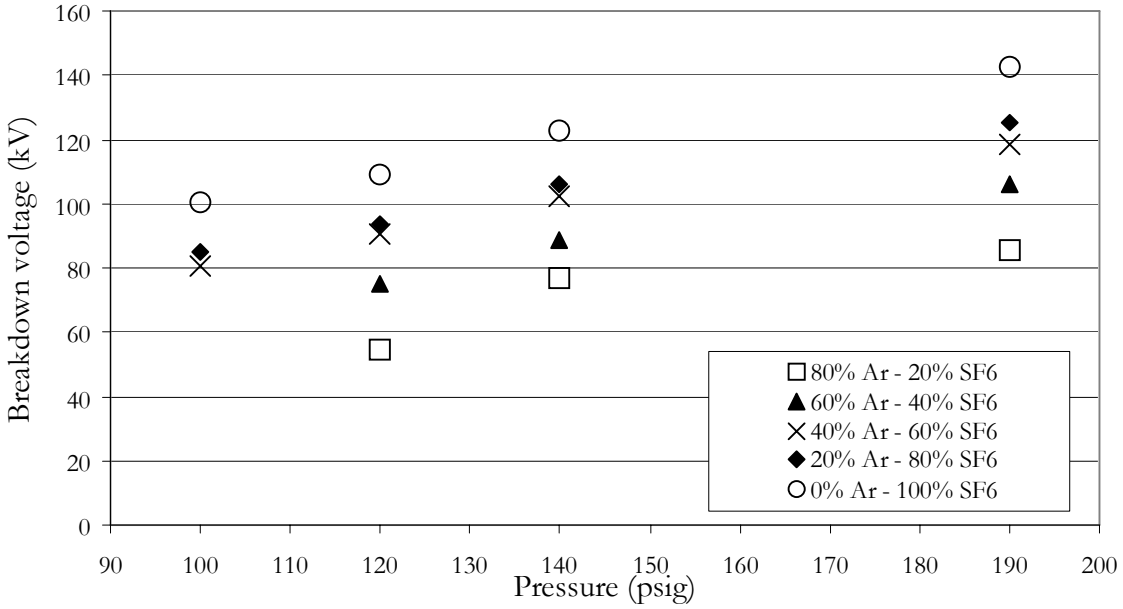

Fig. 6-3. Trial 2: 0.305 cm spacing, FEF=1.

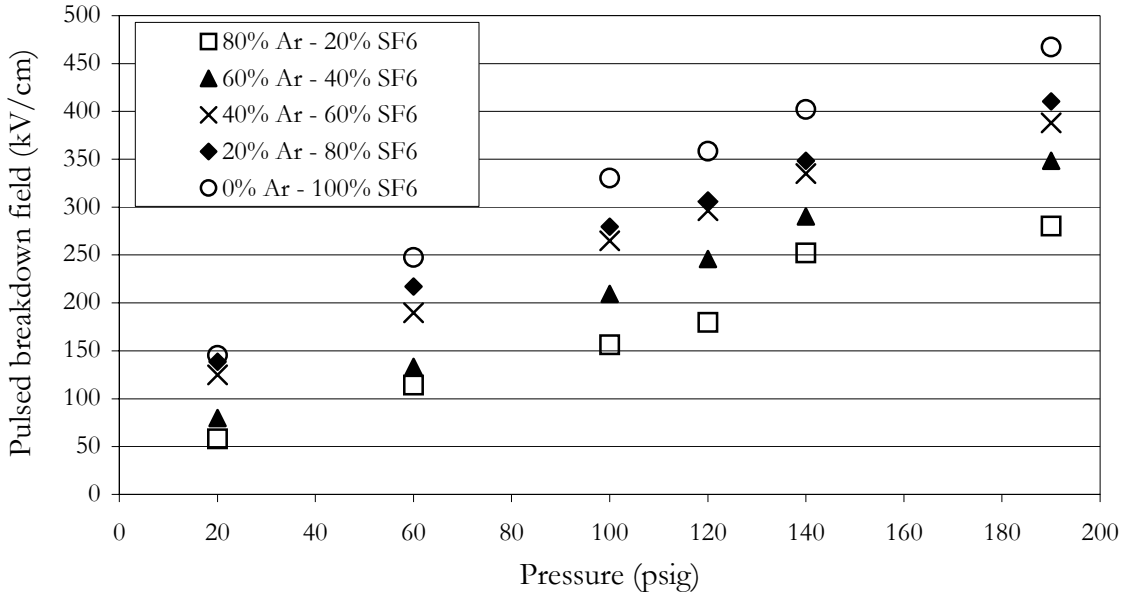

Fig. 6-4. Pulsed breakdown field for a rise rate of 0.863 kV/ns at the time of breakdown. Electrode area is 1.34 cm^2.

cm electrode spacing, this factor is 1.14. The field is uniform for trial 2 where the spacing is 0.305 cm. Breakdown voltage is affected by dv/dt since there is some delay time between corona onset and streamer propagation across the gap.

Pulsed breakdown field plotted in Fig. 6-4 increases very linearly with pressure for all mixtures. Fig. 6-5 depicts the reduced field E/p (kV/cm-bar), an important quantity to consider when designing low jitter laser gas switches. For Rimfire, E/p should stay above 46 kV/cm-bar for acceptable jitter [15]. The pulsed breakdown field of 100% SF_6 displayed in Fig. 6-4 was retested for large area electrodes, namely the 6.67 cm radius Rimfire cascade electrodes with an active area of roughly 13 cm^2. The electrodes were spaced 0.886 cm and have a FEF of 1.1. The maximum working pressure was 100 psig and the rise rate of applied voltage was 5.3 kV/ns for these experiments. Pulsed breakdown field for this experiment was consistent with the results obtained in Fig. 6-4.

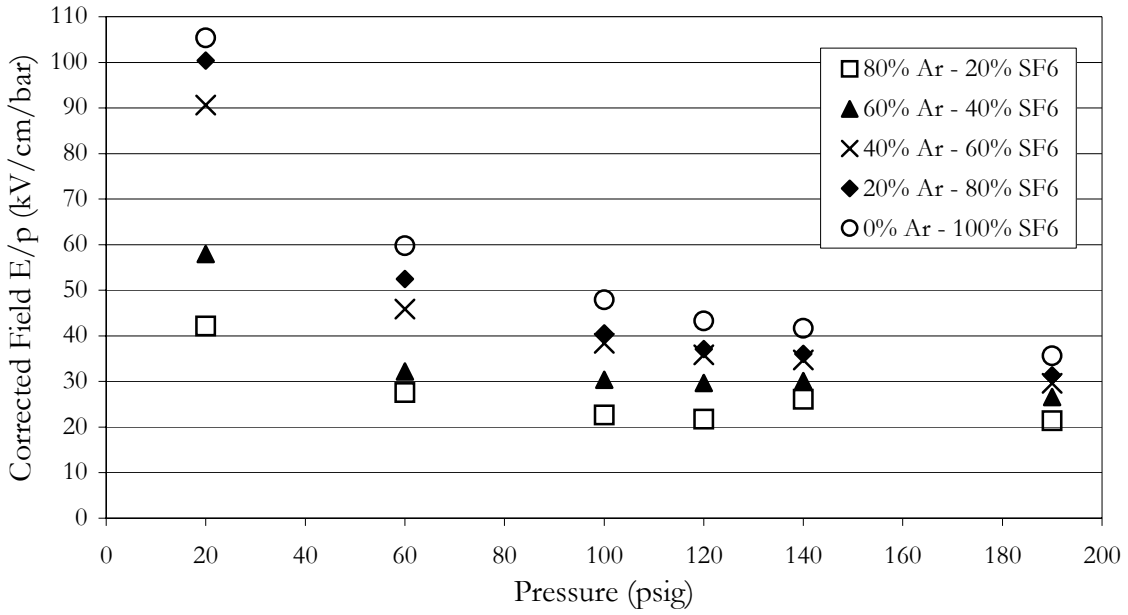

Fig. 6-5. Corrected field versus pressure.

An experiment was constructed to observe the pulsed flashover voltage of Lexan. A 1.26 cm (0.498") spacer (called a "hockey puck" spacer) from the Proto II switches was used under uniform field conditions to test surface flashover. The same Marx setup was used to test the flashover as was used to test SF_6 – Argon breakdown except the pulsed voltage rate of rise was 5.3 kV/ns. Flashover field increased slightly for the first three shots, than dramatically decreased as shots continued as depicted in Fig. 6-6. At first, a relationship seemed apparent between increasing pressure and decreasing flashover voltage since the pressure was increased to accommodate larger charge voltages. The final shot was at 50 psig, like the first few shots, thus suggesting this claim to be false. A decrease in flashover field as the shot number increased is attributable to a 1 cm wide carbon deposit on the surface that appeared after the third shot. A safe operating flashover field for the "hockey puck" spacers is 150 kV/cm at 5.3 kV/ns.

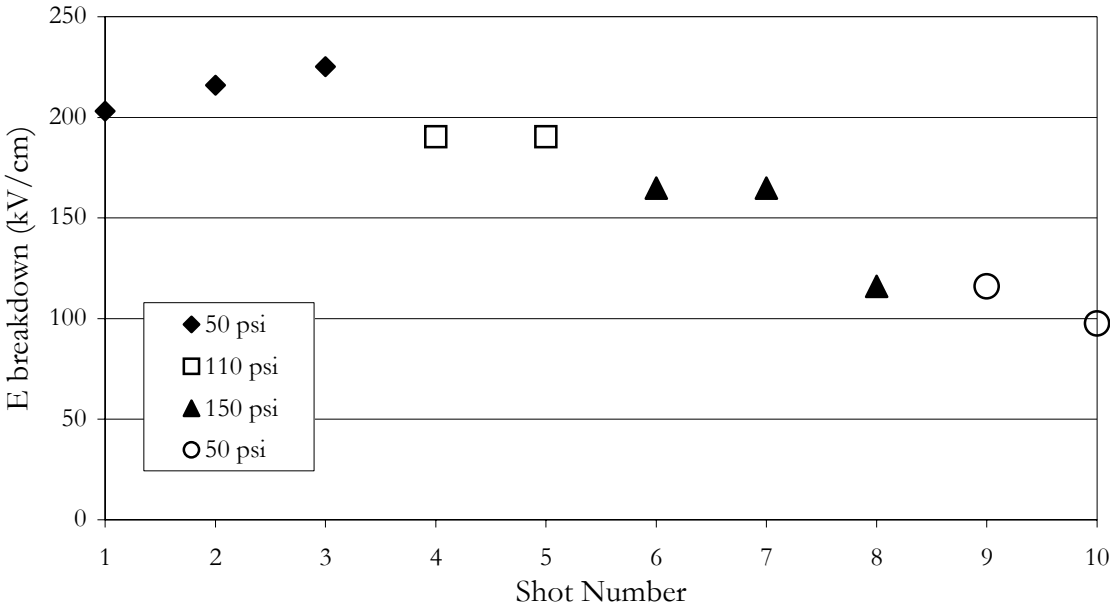

Fig. 6-6. Hockey puck flashover field.

C. SF_6 Microsecond Pulsed Breakdown

The focus of this section is to develop the background for high pressure SF_6 switching for the design of a 2 MV, 250 psig switch. It was originally pursued for the design of a shortened Rimfire. This shortened design is investigated as an option to reduce inductance and resistance during switch conduction. Fabrication of such a device did not come to fruition, but research in high pressure, pulsed SF_6 switching is presented here. Others' work is presented and compared to high pressure data collected at MUTTS.

The backbone of pulsed high pressure SF_6 switching in the pulsed power community is the E_0 curve published by Nitta [24]. This curve describes the minimum breakdown field strength, for very large electrodes, at which streamers would be initiated under pulsed conditions. His curves were obtained for 60 Hz pulses. Others have published similar curves at 50 Hz and under microsecond pulsed conditions [46,48]. These curves are plotted

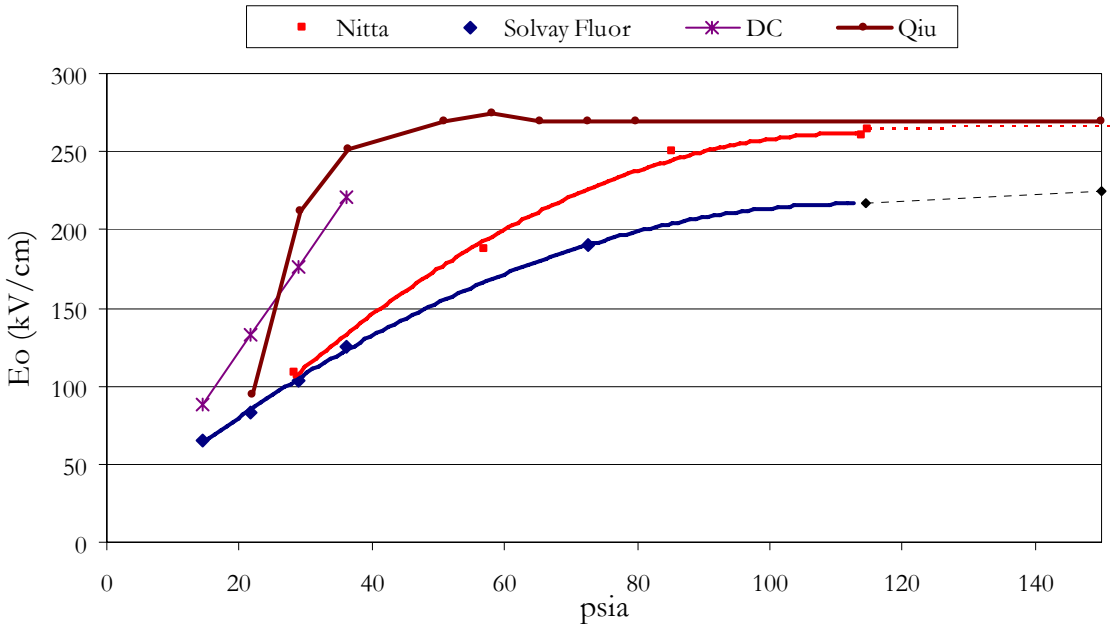

Fig. 6-7. SF_6 E_0 lines. Low probability breakdown lines exhibit roll-over.

in Fig. 6-7. Qiu describes a 2% breakdown probability for a highly non-uniform electrode arrangement under 1.25 μs positive pulsed conditions. Similar trends are observed for corona onset [62]. Martin's paper on pulsed gas switching thoroughly describes the relationship between E_0 and the anticipated pulsed breakdown field and will not be described here [22]. What will be discussed here is a further analysis of a section of that paper regarding higher-pressure gaps under pulsed conditions and the concept of "roll over".

As with the E_0 curves, the pulsed breakdown of gas switches at high pressure is said to roll over, at a pressure near 90 psig [22]. This means the pulsed breakdown field is no longer well defined as an increasing function of pressure, but rather a range of breakdown voltages spanning a breakdown probability from 0 to 100 %. Roll-over is caused by micro-protrusions on electrode surfaces that look more electrically rough at higher pressures than at lesser ones [63]. Any SF_6 switch with roughened electrodes will exhibit roll-over under

pulsed conditions for high pressure. Although a high pressure switch will exhibit roll-over, higher breakdown fields may be achieved when considering very fast switching. This is true where the pulse voltage rise rate is on the order of the electron transit time and the appropriate trigger method is used. Even though roll-over is present, it is possible to obtain benefits in breakdown strength at the risk of decreased reliability in the form of prefires. This issue is addressed in Chapter 7.

The concept of operating at high pressure has far reaching consequence when specific systems are considered. Published work in this area is scarce for pressures larger than 4 bar. It is assumed that at common operating charge transfer levels (10's to 100's of milli-coulombs) the electrodes of any such system will no doubt become severely worn. Severe wear generates a larger number of more pronounced micro-protrusions thus making a system more susceptible to roll-over at very fast pulsed voltages. The use high pressure SF_6 is not common practice, but should not necessarily be ignored as is described in the following sections.

D. SF_6 Sub-Microsecond Pulsed Breakdown

A tradeoff arises between prefire likelihood and increasing the operating pulsed field. Once the field is larger than E_0,there is a finite probability that a streamer has been initiated. Therefore, when triggering a gap above E_0 there is a chance that the gap has already begun to breakdown before application of the trigger. As long as the trigger level is set appropriately, it is possible to trigger above E_0 and still operate with an acceptable prefire rate. Switch jitter, however, increases as the application of trigger field is delayed further and further beyond E_0 [22]. If trigger application is allowed to delay beyond the time the E_0 field is surpassed, the cumulative probability of streamer initiation increases until the likelihood is

so great that the trigger field would statistically be applied at temporally different locations from shot to shot, thus increasing jitter. It is possible to mitigate this jitter when using a laser trigger, due to localized preionization just ahead of streamer formation for a laser focused in the center of the switch [64].

The probability of breakdown has been studied by many authors and is often expressed using Weibull statistics. When Nitta first relayed his data, he expressed the probability of breakdown using the Weibull function,

$$F(E) = 1 - \exp\left[-\lambda \cdot A \cdot (E - E_0)^m\right] \qquad \text{Eq. 6-1}$$

where $F(E)$ is the probability of breakdown at field E, A is the electrode area, E_0 was from his data in Fig. 6-7, and λ was a pressure dependant term [24]. Further analysis of his data yielded,

$$F(E) = 1 - \exp\left[-K \cdot A \cdot \left(\frac{E - E_0}{p}\right)^m\right] \qquad \text{Eq. 6-2}$$

where K was some constant, and p was the working pressure and replaced λ [15]. Upon applying Nitta's work to the Rimfire switch, the unknown's m and K in Eq. 6-2 were found using curve fitting techniques and the method was applied to a Rimfire switch resulting in [15],

$$F(E) = 1 - \exp\left[-2\,x10^{-18} \cdot A \cdot \left(\frac{E - E_0}{p}\right)^{10}\right]. \qquad \text{Eq. 6-3}$$

From this equation, a plot is possible for breakdown voltage as a function of breakdown probability, pressure and field. Fig. 6-8 shows several breakdown lines that were plotted in

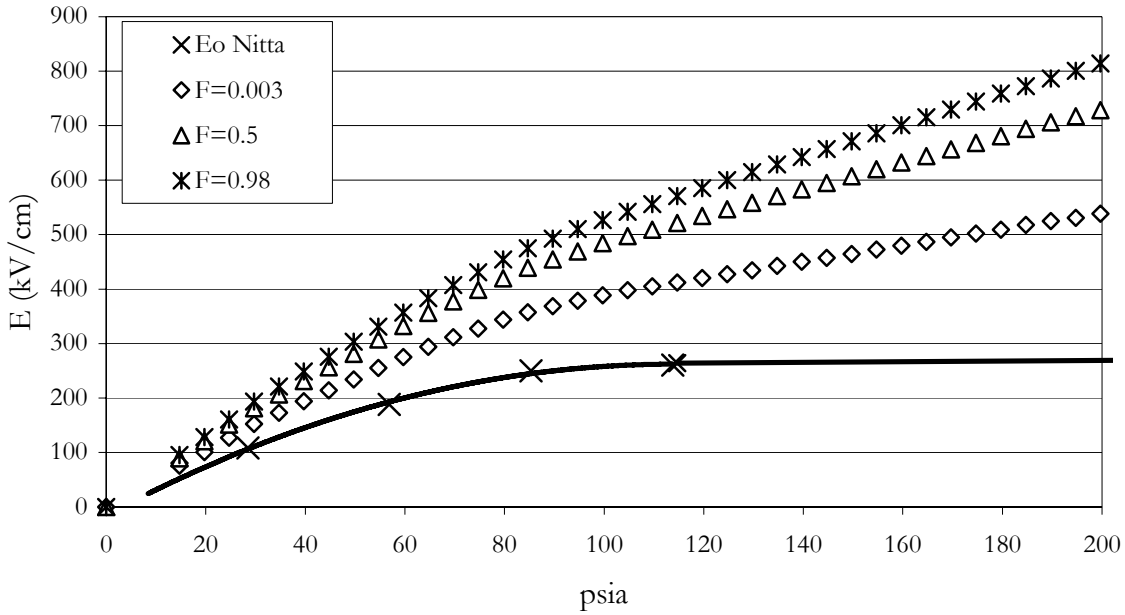

Fig. 6-8. Rimfire pulsed breakdown curves from Turman expanded to 300 psia [6]. Note the pulsed field at 250 psia is double from that at 50 psia for F=0.003. Even larger increases are noted for larger probabilities.

reference Turman up to 50 psig [15]. Expanding these results to larger pressures it is clear that the breakdown voltage increases with pressure.

The Weibull method was applied to the 100% SF_6 breakdown data of Fig. 6-4. Data in Fig. 6-9 fall between the 0.1 and 0.5 Solvay probability lines, indicating the electrode roughness is larger than 200 μm. This means a lower E_0 line would more appropriately describe these data. Nonetheless, an increase in self-break breakdown field with increasing pressure is noted for this experiment. The larger recorded breakdown voltages despite a non increasing E_0 are explainable when considering the relationship between pressure and the physical motion of electrons and the transit time in a gas gap under applied field.

Transit time is defined as the time it takes the leading edge of a streamer to traverse the distance of a gap. This time is pressure, field and gap length dependant. Runtime is typically defined as the delay time between the application of a trigger source and the flow of

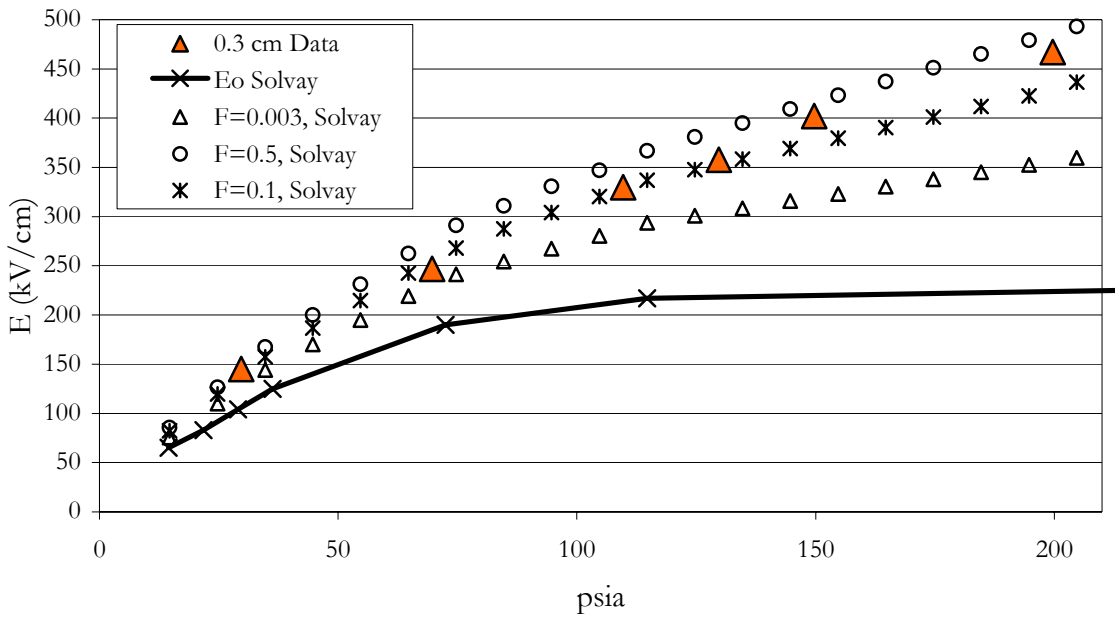

Fig. 6-9. MUTTS pulsed breakdown curves from [60].

current through a switch. Typically switches are fired at some high percentage of self-break (80-90%) to ensure a short run time and reduce the prefire probability rate. Therefore the appropriate trigger field may be established from Weibull breakdown probabilities for acceptable switch reliabilities.

The delay time, in the case of a laser triggered gap, is the time it takes the voltage to rise from the application of the trigger pulse to the self break voltage for the remaining portion of the gap that is not shorted with the trigger pulse. In many sub-microsecond pulsed cases, the delay time may account for as much as 50% of the perceived breakdown voltage [22]. The delay time has been empirically related to the field, gap distance, and pressure by,

$$E \cdot d^{1/6} \cdot t^{1/6} = K \qquad \text{Eq. 6-4}$$

where E is the applied field in units of 10 kV/cm, d is gap distance in cm, t is the time above 67% of peak voltage until the peak is reached and K is an empirical constant that is gas dependant [25]. Others have modified this formula to increase the contribution of the pressure term to account for underestimated values at higher pressures [22]. Neither Eq. 6-4 nor other equations presented in Martin have been able to predict reasonable transit times for the MUTTS experiments presented earlier. This is because the voltage of the MUTTS experiments is an order of magnitude lower than Eq. 6-4 is intended to be used for.

Many studies discussing the relationship between switch runtime and pulsed conditions relate the reduced electric field, E/p, and the percentage of self-break V_{op}/V_{SB}, as parameters that will effect run time. The smaller the E/p or $V_{op}/V_{SB,}$ the longer the runtime. A large E/p shortens voltage collapse time [65]. Therefore, increasing pressure above a few bars will begin to reduce substantially the E/p, since the rate of increase in electric field is reduced at elevated pressures. This emphasizes the importance of an appropriate trigger mechanism to reduce the effects of decreased E/p.

E. Electrode Roughness

A relationship exists between surface roughness and its' effect on E_0. An electrode roughness, R_{max}, will have no ill effect on dc operating field of Fig. 6-7,

$$p\,R_{\max} < 43 \quad bar \cdot \mu m \qquad \text{Eq. 6-5}$$

where p is operating pressure. Otherwise, breakdown field is related to the surface roughness by the plot depicted in Fig. 6-10 [66]. In any realizable system, there is some degree of surface roughness leading to the E_o curves of Fig. 6-7. Applying this method, Nitta's data indicate a surface roughness of 150 μm and the Solvay data correspond to a surface roughness of approximately 200 μm [66]. The Qiu data exhibits a much faster rising E_0 line because of highly non-uniform electrode conditions that equate to a very rough surface, but it also levels off with the Nitta E_0 line. Highly roughened electrodes are known to reach a point in which roughening them more will have little effect on the E_0 curve [67]. Therefore, electrode wear and material selection are paramount to operating at pressures greater than six bar (approximately 90 psia). Slight electrode roughness (bead blasted rough), as opposed to very smoothly polished electrodes, will exhibit substantially reduced jitter at the expense of a reduced electric field hold off for a given pressure [68]. Heat-treated 10W3

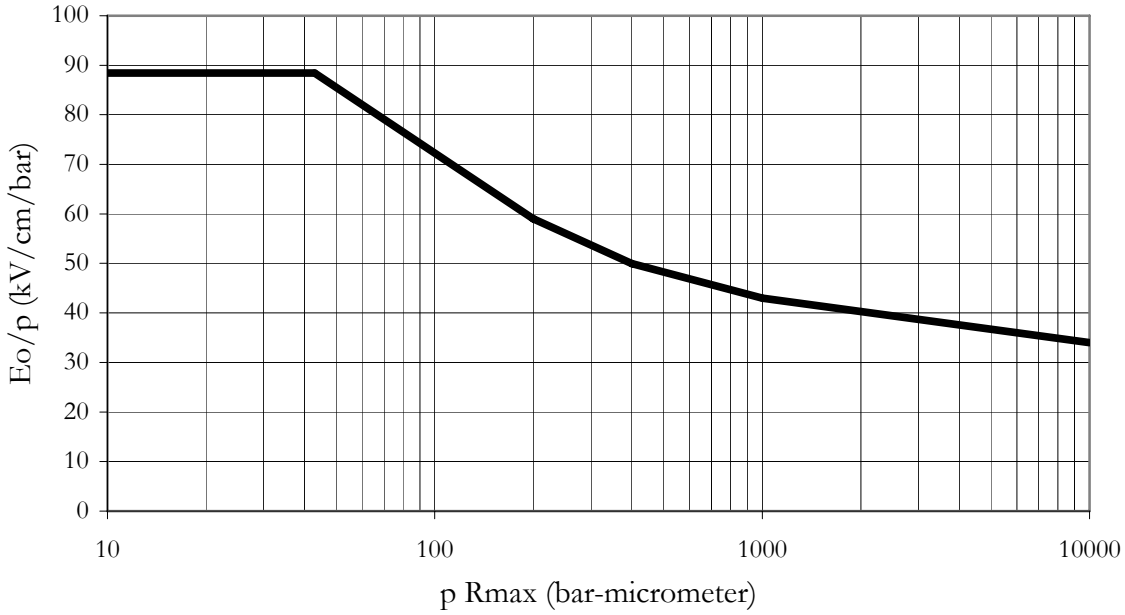

Fig. 6-10. SF_6 reduced dc field due to electrode roughness where roughness is defined as the height of an imperfection above the localized average material height.

(75% tungsten, 25% copper.) Elkonite electrodes were sand blasted to a matte finish and installed in a 3 MV single gap switch. Although the data were not published, the author noted a substantial reduction in jitter that was attributed to the heat treatment of the electrodes. If polished electrodes are used, the large jitter was found to be independent of electrode material or gas type [68].

Electrode surfaces must wear slowly and evenly to reduce extreme field enhancements and to prevent short switch lifetime. Mallory 1000, an (90% tungsten, 6% nickel, 4% copper) alloy was used on the trigger electrode tips of previous Rimfire versions because pure stainless electrodes were wearing too quickly [5]. Heat treating electrodes has a significant effect on reducing electrode wear. Out of several electrodes tested heat treated, Fansteel 77 (tungsten-Ni alloy) was most resistant to wear. It should be noted that the electrode material could have a significant effect on the multichanneling properties of a given gap. Multichanneling was seen to occur in a roughened electrode gap (sandblasted) as opposed to a polished electrode gap in an SF_6 environment [68].

Electrode wear is dependant on material. Brass, aluminum and stainless steel are commonly used electrode materials with very different wear properties. Elkonite (28% copper, 72% tungsten), is also used for its superior electrode wear in non rep-rated gas systems. At 10 Hz, the maximum wear rate for Elkonite electrodes is on the cathode at 8 X 10^{-6} cm^3 C^{-1} [62]. Stainless steel performs similarly with a 9 X 10^{-6} cm^3 C^{-1} wear rate on the anode.

F. Previous Researchers' High Pressure Work

Upon investigation it seems the concept of roll-over when quantifying self-break curves for sub-microsecond pulsed devices is not routinely reported. For many systems,

acceptable self-break voltages are closer to 50% breakdown probability lines than to the low probability E_0 curves. Table 6-1 details a literature search on high-pressure (>100 psia) self-break SF_6 switches and whether or not, under fast pulsed conditions, roll-over was experienced. In this case roll-over is defined as a severe change in slope from 2.5-3 kV/cm/atm to less than 1 kV/cm/atm. As a comparison, this would occur at 100 psia on Fig. 6-7. The only work in this list that indicated severe roll-over was Martin [22]. In this paper, no data are presented and the curve plotted is generic trend labeled "typical large switch" behavior. No roll-over is exhibited in these plots, indicating breakdown occurred above the 0% probability breakdown E_0 curves of Fig. 6-7. This indicates high pressure switching has some viability if a desired prefire probability is known. This is discussed further in the following chapter.

Table 6-1: Literature search for pulsed self-break SF_6 switching above 100 psia A) [22], B) [69], C) MUTTS, D) [68], E) [70].

Ref.	Pulsed Conditions	Pres. (psia)	Electrode Conditions	Roll Over	Source Data
A	N/A	N/A	N/A	yes	Fig. 1
B	6.5 cm, 900 ns to peak, 0.346-3.28 MV, SB	0-115	FE=1.36, brass, hemispherical	no	Fig. 6
B	4.45 cm, 900 ns to peak, 0.346-3.28 MV, SB	0-175	FE=1.2, brass, hemispherical	no	Fig. 7
B	3.1 cm, 900 ns to peak, 0.346-3.28 MV, SB	0-165	brass, hemispherical	no	Fig. A1
C	0.3 cm, 600 ns to peak, 100-250 kV	0-205	brass, uniform	no	Fig. 4
D	1.91 cm, 90 ns rise, 0-1.25 MV	0-90	stainless, hemispherical	no	Fig. 4
E	0.7 mm gap, 55ns rise, 25-80 kV, SB	0-275	FEF=1.04, polished, brass hemispherical	no	Fig. 6

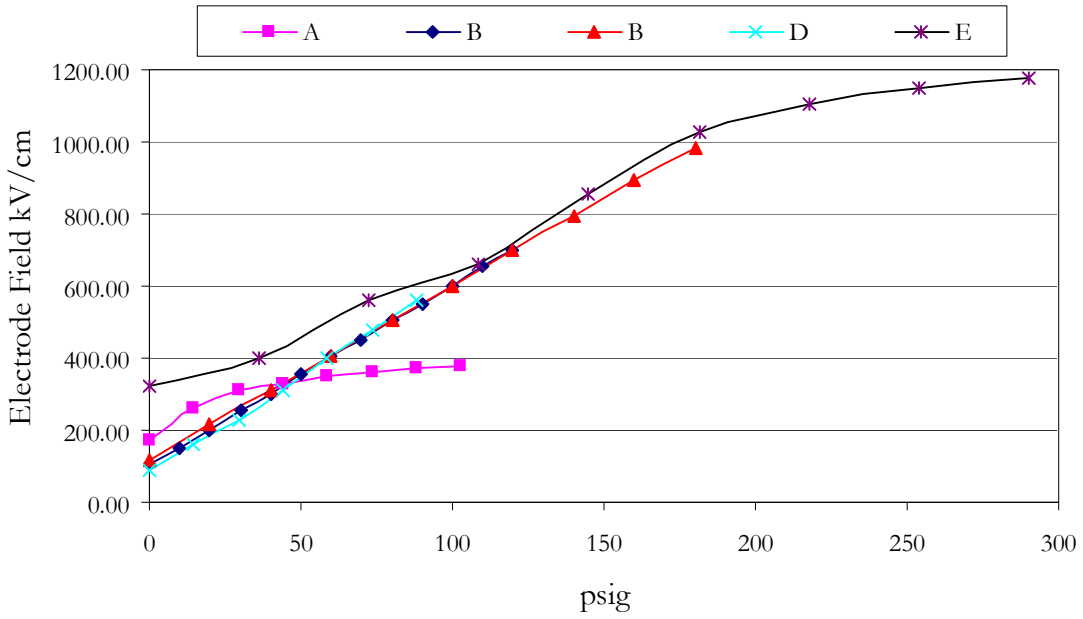

Fig. 6-11. Pulsed self-break field for Table 6-1.

Chapter 7
New Switch Study

This chapter describes a design process for large Rimfire-like SF_6 gas switches. An investigation is presented into a reduced inner to outer conductor ratio and a reduced length 2 MV switch. This switch addresses the low inductance issue, providing a very fast switch that could potentially replace water switches on machines like Z. It also addresses a problem with the location of the gas envelope on current Rimfire designs. The switch is laser triggered and utilizes a completely coaxial design that eliminates the acrylic SF_6 gas envelope. Originally, an all cascade design was to be investigated, but it was abandoned because of issues with the reliability of the triggering scheme. Instead, designs aimed at reducing switching impedance while adding reliability were investigated. This switch was not fabricated.

A. Problems Plaguing Rimfire Switches Today

Reliability requirements for the next generation Rimfire switches have caused a joint effort between many institutions to address unacceptable lifetime problems. ZR, the next machine to utilize Rimfire, requires an astonishing 400 shot lifetime before maintenance with a 2% loss of shots from the entire pulsed power chain [71]. The switch is to operate at up to 6.5 MV and conduct 600 kA with a <2 ns jitter for 36 lines. The design field stress is not to exceed 250 kV/cm with a 1.4 trigger field to cascade field stress ratio. The current 6 MV design cannot meet these requirements electrically because degradation or catastrophic disassembly issues caused by gas envelop flash-over occur after only 22 shots at 5.5 MV.

In 867 shots at the Advanced Pulsed Power Research Module (APPRM) at Sandia, there were 12 cascade envelop failures (flashed housing), one trigger envelope failure (external tracking) and two cascade spacer failures (flashed spacer). Several teams are working on these issues with several approaches to resolve the reliability issues by 2007 [71]. In the Z-20 test bed, there were more failures attributed to the trigger section than to the cascade section envelope.

The design presented in this chapter looks at optimizing switching impedance as well as presents a design that utilizes an I-Store insulator scheme. Instead of having a long gas envelope that is rapidly stressed in parallel with the switching axis, the insulator is moved to a coaxial design so it is stressed with the main forward going voltage wave. This scheme is known to be reliable since it has been adopted on I-Store designs for several decades.

B. Reducing Switching Impedance: Reducing Radius and Reducing Length.

As discussed in the introduction, one goal (besides reliability) for a next generation Rimfire switch is to reduce the inductance for the replacement of problematic water switches. Dramatically lower inductance is required to reduce switch current rise time and make the switches faster. When the question of replacing water switches was posed, there was a generic goal for the inductance requirements of a gas switch replacement. At first this goal was that the switch must have an inductance of 100 nH and operate at 6 MV. This later evolved to reducing the inductance of the current Rimfire design by a factor of two. The first target inductance is nearly impossible using a Rimfire based design. The second target, however, may be achieved.

There are several options for reducing the inductance in a Rimfire switch. Switch inductance relates linearly to length ($L \propto l$) and as a logarithmic ratio of outer (radius b) and

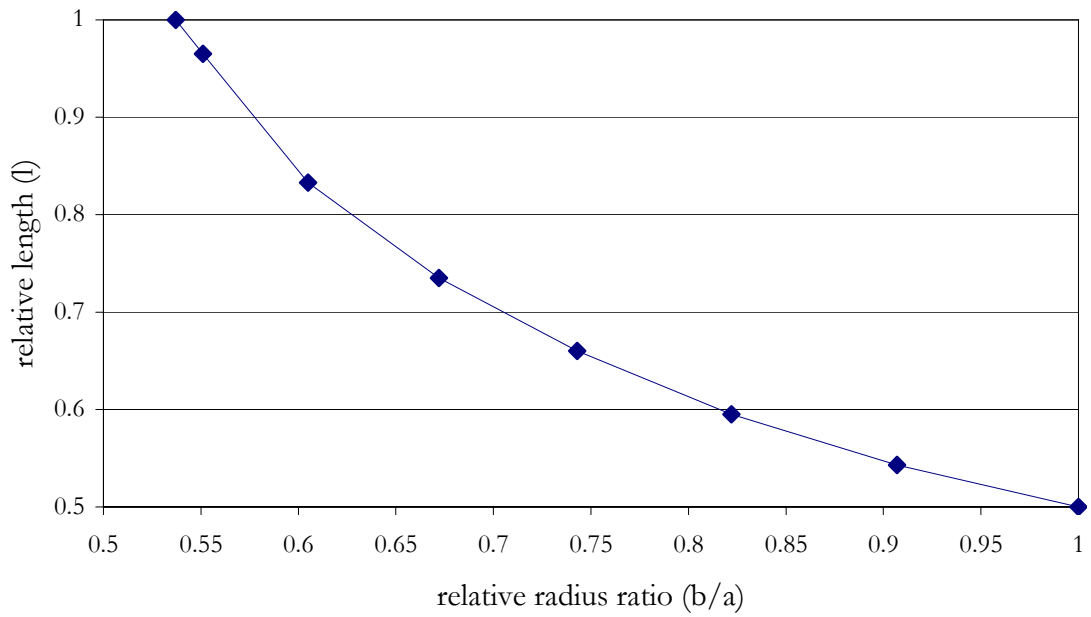

Fig. 7-1. 50% inductance line as a function of geometry.

inner (radius *a*) conductor radii ($L \propto \ln b/a$). Length may be reduced by a factor of two, or b/a may be reduced by a factor of 1.64, or some combination there of, in order to reduce the inductance by a factor of two. The relationship between reducing both length and ratio of radii is plotted in Fig. 7-1. This is a plot of inductance for a single channeling switch. As the number of channels increases the line becomes more steep (a given b/a will tolerate a larger length for the same inductance in Fig. 7-1). In a design where the outer conductor radius *b* is fixed, radius *a* may be increased and *l* may be decreased.

The limiting design factor for radius is based on the electric field requirements for SF_6 at a given pressure. Increase in radius *a* is limited by the breakdown strength of the gas between the inner and outer conductor. At Rimfire operating pressures (50 psig SF_6), the breakdown field is 250 – 300 kV/cm. This will dramatically limit the practical increase in *a,* without also requiring an increase in radius *b*. For example, the 6 MV Rimfire has a measured inductance of 600 nH [71]. Approximately 150 nH of this is contributed by an

external ground shroud and is not considered switching inductance. In addition, approximately 100 nH of what is left over comes from the single channeling trigger section and is not considered reducible without abandoning the Rimfire concept. Therefore, 350 nH must be reduced by 300 nH to have the effect of reducing the total inductance by a factor of two. This leaves an inductance of 50 nH for the cascade section. For this inductance, the ratio of the radii would need to be 0.35 of its nominal value and results in an infinite inner conductor radius. If all the inductance were in the cascade section and not in the trigger section or ground shroud, a reduction in the inductance of the 6 MV Rimfire by a factor of two without reducing length, would require b/a to be 0.45 of its nominal value of 7.53 (81.3 cm outer radius, 10.8 cm inner) [72]. The radius of the inner conductor would grow to 29 cm (11.4") and the outer conductor to 99 cm (39"). This radius growth would apply to every conductor that is included in the inductance estimation of 600 nH and does not consider that each gap does not have an inductance of a solid sheath, but rather some number of non-uniformly spaced arcs. The factor-of-two reduced design would only apply using a gas envelope like the current Rimfire switches with an oil surround dielectric. For an all coaxial design, it is impossible to use SF_6 as the insulating dielectric and achieve a b/a ratio of 0.45 its nominal value without elevating switch pressure beyond 50 psig. Essentially, it is impossible to meet both design goals without altering the switch design and without altering the operating gas pressure.

SF_6 dielectric strength requirements are the limiting factor in the reduction in length. The review of high pressure SF_6 switching given in Chapter 6 and the data presented there were used in the following shortened switch design. In order to achieve the goals for future Rimfire switch design, SF_6 switching at elevated pressure must be reviewed in Rimfire switch geometry.

C. Shortened Design

The following is a design for a coaxial, shortened SF_6 switch. This is a description of a design that was not fabricated so not all mechanical specifications are made. It is designed for a breakdown strength of 470 kV/cm at a conservatively high 270 psia (vapor pressure of SF_6 is approximately 310 psia). Fig. 7-2 depicts the 0.003% breakdown lines based on the Nitta and Solvay data that are averaged to determine a design breakdown field. All insulators in the new design will experience fields of no more than 100 kV/cm at peak voltage (2 MV). The triggered gap will have > 30% of the overall voltage and will have a field enhancement factor of 1.5. It will have a field 1.2 larger than in any cascade gap. The outer conductor radius is fixed due to the constraint of flashover in oil of the plastic surface. The fields in the cascade section on average are 380 kV/cm and vary by less than 15%. At 2 MV this is roughly 10" for a 3" diameter center conductor. The outer to inner return conductor ratio will be minimized. Peak voltage in the case of no breakdown (ring back) event is 2 MV.

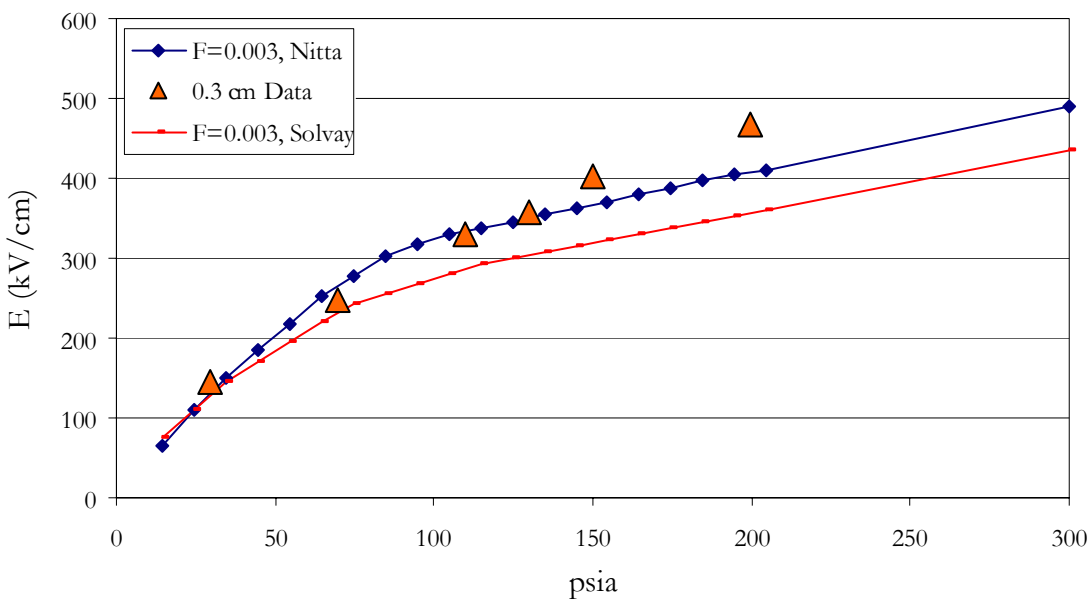

Fig. 7-2. Low Probability Breakdown Lines

Maximum field between inner field shaper and outer conductor at 2 MV is < 400 kV/cm. Peak field in the trigger gap or next cascade gap will be at least 1.1 times larger than the field between any conductor and the outer conductor. The field shaper on the high voltage side will incorporate a cone geometry to minimize *b*/*a* and to reduce fields at the insulator.

A general Rimfire design procedure is as follows. The field shaper at the high voltage side will determine the minimum spacing between the outer conductor and the center conductor at the insulator face. The curvature of the field shaper outer edge must then be addressed. Field shaper radii exceeding 3.81 cm (1.5") are necessary to ensure low field enhancement. Maintaining a low *b*/*a* is preferred over extending the length of this field shaper. The switching gaps are then placed with the appropriate field in the cascade and trigger sections, starting with the trigger section. This process will reduce fields at the high voltage side insulator. When simulating electrostatically, the load-switch conductor should be held at zero potential. Fig. 7-3 depicts the shortened design. dv/dt in all gaps at the time

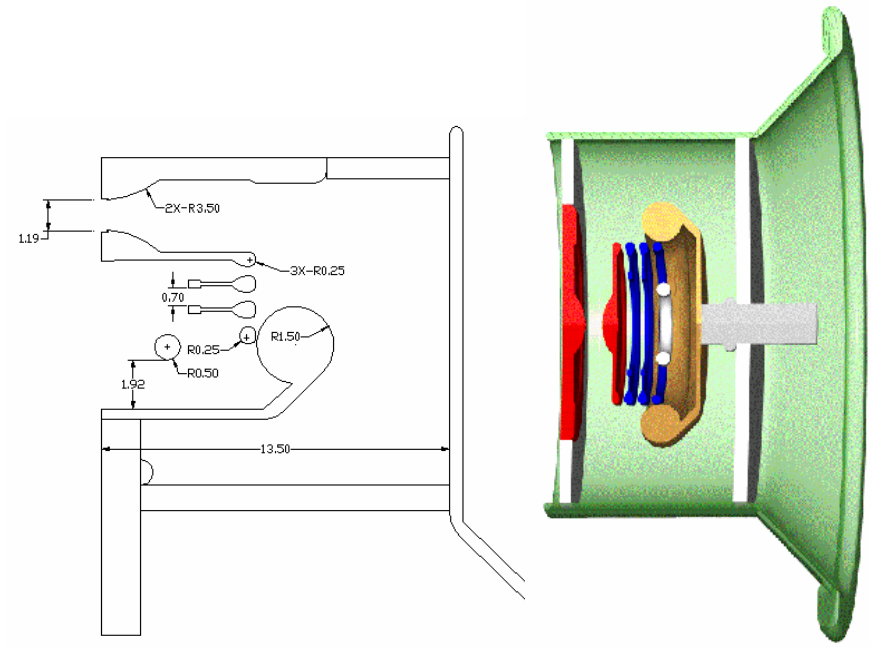

Fig. 7-3. New Switch Dimensions (image at right rotate 90 degrees with respect to image at left).

of laser triggering is above 90 kV/ns with over 900 kV/cm in each gap. Plots of the fields, dv/dt and time to breakdown are depicted in Fig. 9-5, Fig. 9-6, and Fig. 9-7. The inductance of this design is roughly 90 nH, compared to the regular Rimfire inductance of 240 nH at 2 MV. This reduces the rise time of current through the MUTTS output section from roughly 73 ns down to 62 ns, a 15% decrease. The peak current also increases by a factor of 13%. A comparison of each current is depicted in Fig. 7-4.

For a switch in which the long resistive decay time described in Chapter 5 is removed, i.e. the switch transitions to an on state very quickly (<5 ns), the risetime of a Rimfire switch that is not reduced in inductance may be reduced to < 65 ns. This is as effective in reducing switch risetime as reducing the inductance by a factor of two. If the transition state is effectively removed and the inductance reduced by a factor of two, the risetime of the switch decreases to less than 45 ns. That is nearly a 40% reduction in switching rise time. Reducing the resistive turn on phase, however, would likely require the use of a different gas, which is precluded because of the superior breakdown strength of SF_6.

There is very little data, if any, on multichanneling SF_6 switches above a few

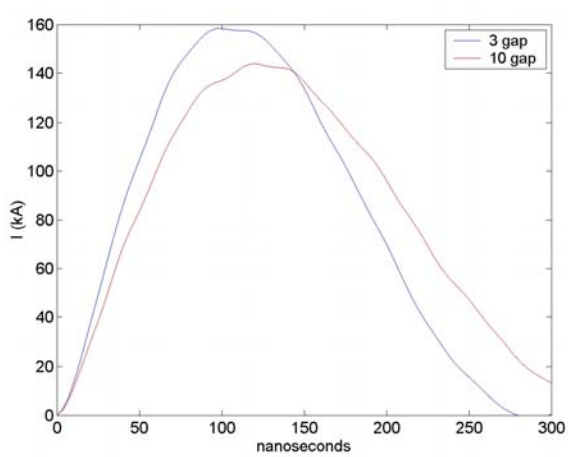

Fig. 7-4. Current comparison of shorted switch to original Rimfire at a breakdown voltage of 1.6 MV.

atmospheres. Producing one to three channels per gap is readily common at 18 – 50 psig SF_6 for the fields that are experienced at MUTTS, sufficient to substantially reduce inductance. A risk exists that the switch may have reduced channel formation in every gap at very high pressures. Approximately 50% of the cascade section inductance is due to metal electrodes if two arcs are assumed in each gap for a canonical Rimfire geometry. Each gap must channel with two channels or more to have a 50% reduction in inductance for the cascade section arcs as is depicted in Fig. 7-5. In this generic example, two theoretical switches are considered one with half the length of the other. The inductance for the reduced length case is less than the longer case for any number of channels as long as each gap has two channels. Two channels will form if dv/dt on each gap is increased not to be less than 20 kV/ns on each cascade gap at the time of closing [36].

A large face electrode may be preferable for reduced wear with multiple mildly field enhanced edges. This larger area should not become so large as to dramatically reduce the

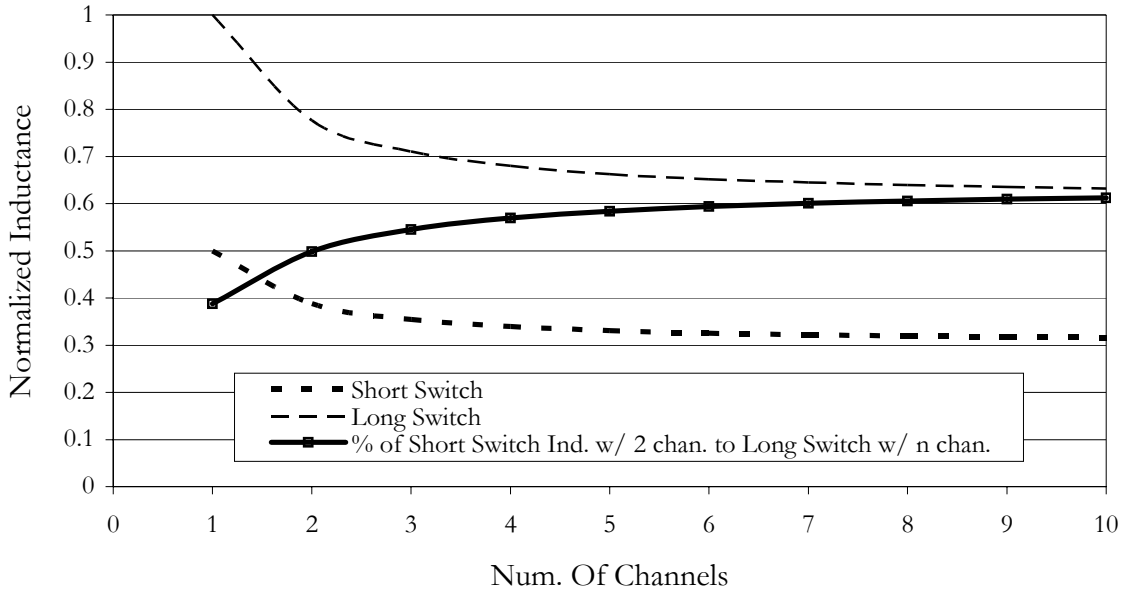

Fig. 7-5. Normalized inductance for two generic cases.

breakdown field [73]. More severe field enhancement would require an unacceptable increase in gap spacing [5]. MUTTS data indicates that the original electrodes are the most prone to multichanneling due to evenly grated fields throughout the inter gap spacing and uniformity across entire active electrode areas. Therefore, electrodes with a larger active area and two 1.1 field enhanced ridges would likely encourage at least two channels in all cascade gaps and reduce electrode wear. Multichanneling is very important when considering both impedance and electrode erosion. It should be noted that the ability of helium (electron affinity of 0) to multichannel is known to increase with pressure, thus making it a likely candidate for a multichanneling gas buffer gas for high pressure SF_6 experiments. If multichanneling at very high pressures in pure SF_6 is not possible, and if the reduction in breakdown strength of the SF_6 – Helium mixture is acceptable, this may be a path forward along with very high pressure SF_6 – Argon mixtures [38].

If fabricated, the new switch would have Elkonite electrodes for superior wear characteristics as described in Chapter 6, Section E. For a shot with a peak current of 500 kA, 300 ns square pulse and an assumed arc diameter of 2 mm, the anticipated ablation depth per shot is 10 μm for Elkonite. The lifetime of the switches cascade electrodes would be roughly 1200 shots for operation on the Nitta E_0 curve. At MUTTS, peak currents at a charge of 1.5 MV are on the order of 100 kA for 200 ns, thus the average ablation depth per shot is 2 μm. This corresponds to a lifetime of 6000 shots for Elkonite electrodes at MUTTS. Electrode wear will have the most effect on a single channeling trigger section. For either example, a single channel in the trigger section reduces the lifetime by a factor of two. Implementing a dual laser triggered section may prove to be the most viable option electrically, but it increases the cost of a large system substantially (36 lasers at $25k per laser is a total $900k increase).

Ideally, a laser trigger would be preferred that completely shorted the entire switching length (tens of centimeters) instantaneously. Or in other words, the ratio of the length of the gap to the length of the laser spark should be unity for low jitter. This is not currently possible, however, with relatively inexpensive commercially available UV lasers and working voltages in the megavolt regime. MUTTS is fitted with a Nd:YAG frequency quadrupled (266 nm), 5 ns, 35 mJ pulsed laser that is focused with a 31 cm UV coated lens. Only 25mJ reaches the trigger gap due to lens and mirror losses. The current switch, operated at 2 atm, requires a minimum power density of 3 X 10^9 W/cm^2. At 20 atm (294 psia), the minimum power density necessary to ionize SF_6 with UV is 1 X 10^{10} W/cm^2 and should be focused to the center of the triggered gap [6,74]. This means for a beam divergence of roughly 8 mrad (very large), and a factor of n times over the minimum ionization level, the energy required to ionize the gas may be related to the spot size by,

$$n \cdot P_{d\min} = \frac{E}{t_p \cdot \pi \cdot w_0^{\ 2}} \qquad \text{Eq. 7-1}$$

where P_{dmin} is 1 X 10^{10}, E is 25 mJ, t_p is 5 ns, and w_0 is the diameter of the spot size. The diameter of the spot relates to the focal length of the focusing lens via,

$$w_0 = f\theta \qquad \text{Eq. 7-2}$$

where f is the focal length of the lens and θ is the beam divergence. Substituting in all values for the Nd:YAG laser, the focal length in cm is,

$$f_{(cm)} = \frac{15}{\sqrt{n}} \qquad \text{Eq. 7-3}$$

The length of the ionized channel d is,

$$d = \frac{2}{\tan^{-1}\left(\frac{0.75}{f_{(cm)}}\right)} \cdot \sqrt{\frac{E}{t_p \cdot P_d \cdot \pi}} \qquad \text{Eq. 7-4}$$

where P_d is n times P_{dmin} and all constants are chosen for this particular laser in this particular system. For a 50 cm focal length, the ionization channel would be over 3 cm at 2 atm, but the energy would not be sufficient at this focal length to ionize the 20 atm case. The maximum allowable focal length for a 1 cm arc at 20 atm is 31 cm. The trigger gap of the new switch is 2.54 cm, so 40% of this length would be ionized using dual Tempest lasers.

A significant challenge is the mechanical design of large vessels with polymer faces operated at hundreds of psi. There is mechanical danger associated with large vessels at this pressure with potential energy storage of that of a small explosive. The energy potential energy associated with a compressed gas is given by,

$$U = \frac{P_1 V_1}{k-1}\left[1 - \frac{P_2}{P_1}^{\frac{k-1}{k}}\right] \qquad \text{Eq. 7-5}$$

where P_1 and V_1 are the vessel pressure (megapascals) and volume (cubic centimeters), P_2 is the outside pressure, and k is the specific heat ratio (1.09 for SF_6 at 1 atm) [75,76]. For a vessel the approximate size of the switch discussed in the previous section, Eq. 7-5 would yield a stored energy of 200 kJ, or 1/10 of a pound of TNT. This issue may prove to be the most difficult to address.

High pressure SF_6 switching must be explored if dramatically reduced inductance is desired. Though there are certainly relevant design concerns for high pressure SF_6 switching, exploration into this area may yield viable designs when implementation of a laser trigger is considered. This issue has never been researched, to my knowledge, using UV laser triggering. With exceptional trigger control possible using advanced and commercially

available lasers, jitter and prefire rate mitigation are possible. It is possible to utilize very high pressure SF_6 switches if some established prefire level is acceptable.

Chapter 8
Conclusions

The University of Missouri Terawatt Test Stand was constructed and made operational by a dedicated team of students, both graduate and undergraduate under the supervision of the author. The result of their efforts produced one of the worlds most powerful and practical university operated pulsers with arguably the most modest development and operational cost in the nation. It was developed in order to research large laser triggered gas switching with the specific purpose of analyzing methods to improve turn on time in these devices. This was conducted by general observation and statistical analysis of data including effects of multichanneling, electrode geometries, and other switch variables on electrical performance.

Generally, for large laser triggered gas switches in an under-damped RLC environment, a larger number of channels affected ringing period more dramatically than switch risetime, when the number of channels was larger than two channels per gap. This indicated that dense multichanneling is more beneficial for reduction in erosion than for the reduction of switch risetime in a typical Rimfire application. This is probably due to a large off to on resistive transition time for both dense multichanneling (six channels per gap) and sparser multichanneling (above two and below six channels per gap) arrangements that dramatically impacted switch risetime in both cases.

Electrode geometries designed to force uniform multichanneling generally did so in air filled environments, but did not do so in SF_6 filled environments. Increasing electrode radius did not have adverse effects on multichanneling nor the hypothesized beneficial effects on inductance. This is likely due to the variation in capacitive matrices not being

sufficient to adversely affect dv/dt, which influences the number of channels. The ratio of outer to inner conductor decreased by only 1.5 in the cases tested. It has a marginal effect on switch inductance and was not sufficiently different between cases to be detected.

Utilization of a laser trigger improved multichanneling performance for air, but not for SF_6. These differences in performance are due to the nature of the electronegativity of SF_6 and the much higher electron affinity of this gas compared to air. Air is therefore much more susceptible to increases in dv/dt than SF_6, resulting in more multichanneling. Larger inductance and risetime was experienced for testing configurations that more frequently singled channeled. For SF_6 most gaps experienced only 1 to 3 channels per gap where as in air this number was frequently larger than six channels per gap. Elevating SF_6 pressure had no adverse effects on multichanneling, nor did improving dv/dt by as much as a factor of two.

A linearly increasing dependence of breakdown voltage on SF_6 pressure was found up to 200 psig. This is encouraging for the development of shortened switches to address impedance reduction, since increasing channel number and decreasing outer to inner conductor radius are impractical. Though mechanical concerns are an issue for such a design, there are no other realistic avenues to pursue when developing very low impedance laser triggered gas switches.

Below is a list of nearly 40 conclusions from results of research and experimentation that support these generalities. All statistical statements are with 95% confidence. References are made to pages in the text from which the conclusions were drawn. Conclusions are for SF_6 filled environments unless stated otherwise.

A. Self-Break Conclusions

- The number of channels did not necessarily increase as the charge voltage was increased from ± 30 kV to ± 40 kV (Fig. 4-2, page 46).
- The all sphere and 2-ball experiments multichanneled worse than all others (page 46).
- There was an increase in the number of channels between the 2-ball and 3-ball experiments (page 46).
- Field enhancement points dramatically effect multichanneling for all data sets in an air environment (page 46).
- The 2-90 experiments multichanneled better than the 2-ball and at ± 40 kV the 2-90 experiments dual channeled for all shots (page 46). This is because increased inductive path length between arc locations provided increased time for which a given gap was stressed before voltage collapse.
- Ringing period depends on inductance if an under-damped sinusoid is assumed. Inductance has a 1/n dependence (Fig. 4-3, page 48).
- di/dt is strongly dependant on breakdown voltage and di/dt and rise time did not statistically steadily increase as the number of channels increased. Risetimes were generally 10-15% larger for the 1-ball experiments than all others (page 49).
- Hundreds of shots are required to determine a difference in di/dt and risetime when the number of multichanneling locations is increased beyond two channels per gap (page 48). This indicates dense multichanneling may have little effect in an under-damped environment on these parameters within the desired lifetime of Rimfire switches.

- Inductance impacts late time switch characteristics more than early time. Period effected more by the number of channels than risetime (Fig. 4-6, page 52).

B. Laser Triggered Conclusions

- Fewer channels formed in the gaps closest to the trigger and all gaps single channeled at least once (Fig. 5-3, page 60). This was observed in previous Rimfire experiments [17].
- Holes capped the number of channels for SF_6 and did not encourage uniformity, rather they worsened performance. There was a fewer number of channels that formed in the holes case, with similar variance in the number of channels in all cases (Fig. 5-3, page 60). No predictable number of channels formed with field perturbations in an SF_6 environment (page 60).
- Increased electrode radius did not worsen multichanneling performance (page 60).
- dv/dt greater than 60 kV/ns is required for multichanneling (page 61). dv/dt increases as the runtime increases when the resistive transition from off to on is assumed instantaneous across each gap (page 62).
- The switch breaks down sequentially starting at the laser triggered end and runtimes in oil compare well with the work of Rosenthal (Fig. 5-6, page 63) [7].
- Resistance drops several orders of magnitude in 50 ns and to a conduction value in an additional 30 ns. This was seen for all shots. This is consistent with other researchers' work [41,42,45]. Conduction values obtained are reasonable based on calculations (Fig. 5-8, page 65).
- There is no significant difference between conduction resistance in the triggered and untriggered data. This is due to the laser spark length being not nearly as long as the

trigger gap and having a focused spark radius less than the radius the channel grows to in both cases (page 65).

- As electrode radius increased, the inductance did not decrease.
- There is a larger inductance for the hole experiments than all others because of a larger number of single channeling events. There is no difference in inductance between the 6.67 cm and 10.16 cm electrode tests, therefore the number of channels is more significant in determining inductance than electrode radius (page 65).
- The spread in the inductance value and the number of channels increased slightly as the electrode radius increased. The inductance spread increased with each size, but the number of channels did not, possibly indicating there is an effect on measured inductance other than the number of channels (Fig. 5-3, page 60, Fig. 5-10, page 68).
- The normalized risetime generally decreased as inductance decreased (Fig. 5-12, page 68).
- Compared to inductance, switching resistance has less dependence on number of channels (Fig. 5-13, page 70). The trigger gap constitutes 40 to 50% of switching resistance and 25 to 40% of switching inductance. This is a major drawback to Rimfire design (along with erosion issues) (Fig. 5-14, page 71).
- Most gaps experienced between 1 and 3 channels irrespective of electrode arrangement. This suggests increasing the number of channels as a reasonable avenue for reduced inductance in SF_6 Rimfire switching is unlikely (page 73).
- Long resistive fall times have significant implications for decreasing switch risetime (page 71).

- Dense channeling was observed for the self-break case in the first few gaps in air but not in other gaps. When the laser was implemented, dense channeling occurred throughout. For SF_6 dense channeling was never observed (Fig. 5-15, page 73) because of its electronegativity. Adding SF_6 to an excellent multichanneling gas decreases multichanneling performance, though it increases breakdown voltage.
- dv/dt has a more pronounced effect in air for multichanneling in all gaps. There is an observed increased in the number of channels in laser triggered data compared to self-break. This is not the case for SF_6 (Fig. 5-15, page 73). When dv/dt exceeds 5 kV/ns dense multichanneling was observed in air, consistent with others work [52,53].
- Field enhancement holes did force a more uniform breakdown in air experiments, but created a cap on the maximum number of channels that formed (page 76). Laser triggering reduced the spread in the number of channels increasing multichanneling reliability.
- The operational percent of self-break a laser triggered experiment was triggered at did not influence multichanneling substantially for SF_6 (page 77).
- The over voltage value (defined as dv/dt at the time of breakdown multiplied by the time over which the voltage exceeds the breakdown threshold, or in other words the multichanneling window) more succinctly describes the breakdown pattern than dv/dt by itself. For a larger over voltage value more channels form (a value of at least 60 kV was necessary for multichanneling in SF_6).
- There was no observed decrease in the number of channels as pressure increased from 35 to 50 psig in the shortened Rimfire. This was the case even though dv/dt

was roughly a factor of two larger compared to shots at 18 psig and 25 psig (page 77).

- In self-break mode the cascade section breaks down virtually instantaneously. Therefore breakdown that occurs close to self-break decreases dv/dt in I-Store side gaps. This was observed in Fig. 5-21. Large dv/dt had a more dramatic effect in air compared to SF_6 (page 79).
- Inductance exhibits a 1/n dependence in the laser triggered experiments (page 81, Fig. 5-24).
- There is a difference in inductance between SF_6 laser shots at 18 psig and all other data, including the SF_6 laser shots at 25 psig. This is due to a larger number of single channeling events at 18 psig (page 81).
- There is a difference in inductance for the laser air shots compared to SF_6 laser shots due to extreme multichanneling in air (page 82).
- There is no difference in inductance between the air self-break shots and the SF_6 laser shots at 25 psig indicating that above 4 channels per gap there is no advantage for inductance (page 82).
- Conduction resistance exhibits a 1/n decrease up to approximately 26 channels, after which it is approximately constant (Fig. 5-26, page 85). This is because and individual arc's radius will decrease as there more arcs are formed, thus increasing each arc's individual resistance.

C. New Switch Conclusions

- With a given acceptable prefire likelihood, the use of high pressure SF_6 in a new shortened switch is possible. Gap transit time and triggering methods must be

considered when designing such a switch (page 101). Under pulsed conditions, these parameters will begin to factor heavily into jitter and prefire likelihood more heavily than at lower pressures.

- Rimfire switches may theoretically be reduced in length by a factor of two if elevated pressures are used and still maintain the same prefire probability.
- Roll-over is experienced in the pulsed SF_6 breakdown curve at the 0% prefire level, but several researchers have reported data with no roll-over under "real world" pulsed conditions [22], [68], [69], [70].

Chapter 9
Appendix

This section contains equations, calculations, and experimental data that address assumptions that were made when designing both phases of the test stand.

A. Inductance Formulas

The inductance of a circuit consisting of an array of individual conductors inside a solid cylindrical return sheath is given by,

$$L_{array} = 2\,l\left[\ln\frac{\rho_1}{a} + \frac{2\left(\frac{\rho_2}{\rho_1}\right)^2}{1-\left(\frac{\rho_2}{\rho_1}\right)^2}\ln\frac{\rho_1}{\rho_2} + \frac{1}{n}\ln\frac{a}{n\rho} + \ln\zeta_1 + \frac{1}{4n} - 1\right]nH \qquad \text{Eq. 9-1}$$

where l is length in centimeters, ρ_1 is the return sheath outer radius in centimeters, ρ_2 is the return sheath inner radius in centimeters, a is the array radius in centimeters of n conductors each of a radius of ρ in centimeters [26]. This geometry is depicted in Fig. 9-1. $\ln\zeta_1$ is a term that is determined from a look up table based on the ratio of ρ_1 to ρ_2 [26]. For a thin return sheath ($\rho_1 \approx \rho_2$), $\ln\zeta_1 = 0$ and Eq. 9-1 reduces to,

$$L_{array} = 2\,l\left[\ln\frac{\rho_1}{a} + \frac{1}{n}\ln\frac{a}{n\rho} + \frac{1}{4n}\right]nH \qquad \text{Eq. 9-2}$$

For an arrangement of a cylindrical conductor within a cylindrical return sheath, the inductance may be calculated using,

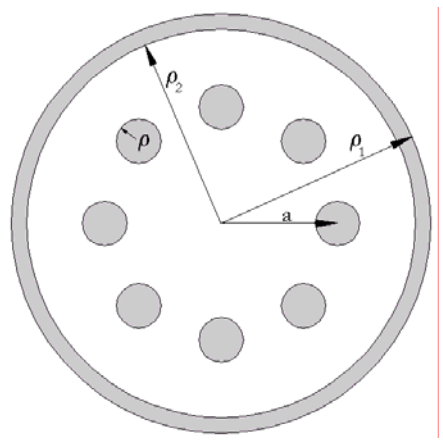

Fig. 9-1. Geometry for Eq. 1.

$$L_{cylindcial} = 2\,l\left[\ln\frac{\rho_1}{\rho_3} + \frac{2\left(\frac{\rho_2}{\rho_1}\right)^2}{1-\left(\frac{\rho_2}{\rho_1}\right)^2}\ln\frac{\rho_1}{\rho_2} - 1 + \ln\zeta_1 + \ln\zeta_3\right]nH \qquad \text{Eq. 9-3}$$

where l, ρ_1, and ρ_2 are defined as in Eq. 9-1. In Eq. 9-2, ρ_3 is the radius of the inner conductor and $\ln\zeta_3$ is a term based on the ratio of the inner conductor outer radius, ρ_3, to the inner conductor inner radius. $\ln\zeta_3$ is 0.25 for a solid inner conductor with frequencies in the megahertz range. For a thin return sheath ($\rho_1 \approx \rho_2$), $\ln\zeta_1 = 0$ and Eq. 9-3 reduces to,

$$L_{cylindrical} = 2\,l\left[\ln\frac{\rho_1}{\rho_3} + 0.25\right]nH \qquad \text{Eq. 9-4}$$

For the case where a cylindrical conductor is surrounded by n return conductors of radius ρ, the inductance is given by,

$$L_{return} = 2\,l\left[\ln\frac{a}{\rho_3} + \frac{1}{n}\ln\frac{a}{n\rho} + \ln\zeta_1 + \frac{1}{4n}\right]nH \qquad \text{Eq. 9-5}$$

where a is the return conductor array radius (cm) and ρ_3 is the center conductor outer radius (cm). For pulsed conditions, in which the skin depth is very small compared to the radius of the conductor, $\ln\zeta = 0$. If the inner conductor is solid and the skin depth is large, $\ln\zeta = 0.25$. Under typical shot conditions the skin depth is much larger than the electrode radius.

A full continuous sheath ground return would be ideal on a coaxial switch design. Practically, however, it must be approximated using discrete conductor elements in the test stand. The following is an analysis of what is an acceptable number of conductors to approximate a full sheath for a given thin sheath radius up to 122 cm (48").

The calculated inductance of a system using discrete return conductors to a system using a continuous cylindrical return sheath (comparing Eq. 9-3 to Eq. 9-5) was compared for several values of n. For a radius ρ_3 of 15.24 cm (6") and a length of 91.4 cm (36"), and with n = 3, 6, and 8, a plot of inductance versus return conductor radius is depicted in Fig. 9-2. This indicates for six return conductors the inductance is roughly 16% larger than for a full sheath. For eight return conductors the inductance is 12% higher. Eight is the largest practical number of return conductors and will be considered the minimum number in future designs.

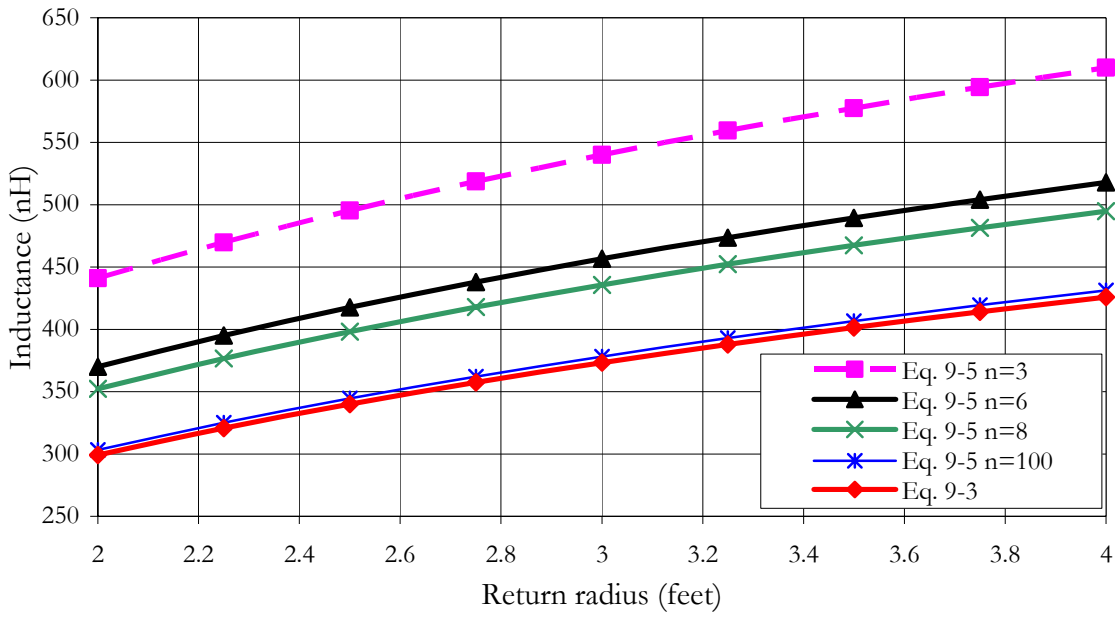

Fig. 9-2. Approximation of a continuous coaxial return with individual conductors.

B. Luminol Pulsed Breakdown

Luminol is a new transformer oil made by Petro Canada. It biodegrades faster than traditional transformer oils and it may be stored in polyethylene containers. It is not nearly as pungent or irritating to the skin as Shell Diala AX. In mid 2001, Diala was roughly $2/gallon and as of mid 2003 it was up to $3.75/gallon. Ten thousand gallons of Luminol was purchased in mid 2003 for $3.55/gallon, delivered.

Tests were conducted on Luminol transformer oil to benchmark its' pulsed oil breakdown and pulsed surface flashover characteristics. The first set of tests consisted of two hemispherical electrodes 3.81 cm (1.5") in diameter spaced 0.432 cm apart (0.17"). One electrode was grounded and the other was pulsed negative. A summary of the breakdown data is shown in Table 9-1. Static field simulations indicate the breakdown field for an

average –200 kV pulse is roughly 485 kV/cm. On the low side, for shot 3 the breakdown field is 390 kV/cm. All future designs will stay below 330 kV/cm.

The next set of tests included surface flashover in a coaxial geometry between a 10.16 cm (4") stainless steel disc and a 22.54 cm (8.875") stainless ring. Four shots were collected before unanticipated destructive disassembly. A summary is shown in Table 9-1. It should be noted that apparently the acrylic became conditioned and breakdown did not initiate until an increasing t_{eff} was reached. Static field simulations indicate a peak field of 450 kV/cm on the cathode and 200 kV/cm on the anode were experienced for an average breakdown voltage of -260 kV. All future designs will keep fields under 150 kV/cm across an entire plastic surface.

Table 9-1. Luminol Breakdown Results

A) Bulk Breakdown

Shot	V (kV)	Rise (ns)
1	-262	15.8
2	-201	13.8
3	-168	10.8
4	-207	13.7
5	-181	12.5
Average	-203.8	

B) Surface Breakdown

Shot	V (kV)	Rist (ns)	Teff (ns)
1	-304	20	16
2	-328	17.6	20
3	-350	18.4	110
4	-305	18.4	318
Average	-257.4		

C. Intermediate Store Stress Analysis

For a conservatively stressed area of 6000 cm^2, the time above 63% of peak, t_{eff}, of 300 ns the estimated water breakdown is empirically given by [49],

$$E_+ = \frac{0.23}{t^{1/3} A^{0.058}} \quad MV/cm, \textit{positive polarity} \qquad \text{Eq. 9-6}$$

$$E_- = \frac{0.56}{t^{1/3} A^{0.070}} \quad MV/cm, \textit{negative polarity}. \qquad \text{Eq. 9-7}$$

For a negative initial pulse the breakdown E field is 454 kV/cm. For a positive pulse, the breakdown field is 207 kV/cm. A full charge of the intermediate store will produce a peak field of 225 kV/cm, well below the theoretical maximum, although in practice the water bottle I-Stores have failed because of damage on the center conductor due to arcing internally. For a maximum 100 kV/cm on the face of the I-Store, the maximum voltage the polycarbonate face may experience is 2.8 MV.

D. Laser System Timing and Noise Issues

Table 9-2: Laser Timing Information

Label	What	Length (feet)	Delay (ns)	Notes
A	Marx CVR to Tank Bulkhead	30.0	46.2	
B	Tank Bulkhead to Diagnostic Bulkhead	61.8	95.2	
C	Diag. Bulkhead to Screen Box	4.2	6.4	
D	Screen Box to Scope 3	3.0	4.6	
E	Scope 3 to 222A	3.0	4.6	
F	Delay from current sense in to 222A input		20.0	Measured
G	Internal delay to process input for 222A		45.0	Measured
H	222A delay to output (variable)		50-500	**Nominally 100**
I	222A cable run to laser Q switch input	45.0	69.3	
J	Q switch in (at laser) (0 V) to laser pulse out		106.0	Measured
K	Q switch sync to laser pulse out		93.0	
L	Q switch in (0 V) to Q sync out (at full laser energy)		13.0	Manual says ~50 ns
M	FL in on laser and FL sync out			Manual says ~9.25 us
N	Laser light travel	9.0	13.9	
O	Delay between Marx current and I Store voltage		2.5	Due to in tank cable differences
P	Anticipated delay between laser trigger and switch conducting		10.0	Also delay between breakdown point and laser arrival noticed
Q	Cable run from photo diode to scope 3		121.0	
R	Total time between Breakdown point and 222A sync out on Scope 3 (called "Trip Duece" position.		**421**	Sum of A,B,C,D,E,F,G,I,N,O
S	Total time delay between Breakdown point and Photo diode in on Scope 3 (called "PhotoD" position.		**300**	Same as R subtracting Q

The laser triggering system was highly susceptible to noise issues, both because of EMI and noise induced on the case of the laser via the attached cables. The only solution to the noise issue was to put the laser in an entirely enclosed, self grounded cabinet. A nicely constructed screen box did not address the issue. A tall double door cabinet was used to shield the laser. The laser would turn off before any light would be emitted if the laser

cabinet doors were left open. The cabinet was connected to a 6' copper ground stake that was driven into the earth. No other components were connected to this ground stake. The laser was grounded to the case internally.

Coaxial trigger connections were in the process of being replaced with fiber optic cable. An Agilent HBFR-1404 transmitter was used with its recommended drive circuit for both the Q switch and the flash lamp triggers. It was connected via fiber to a Thorlabs DET110 photo diode detector that drives the trigger signals high. The receiver end may possibly need an amplifier depending on the transmitter output power for < 10 ns trigger times. This system was in the testing phase at the time this document was written. It was learned through experience that it is absolutely necessary to use such a system, including fiber connections and fully shielded, nicely grounded, cabinets when using laser triggered gas switches.

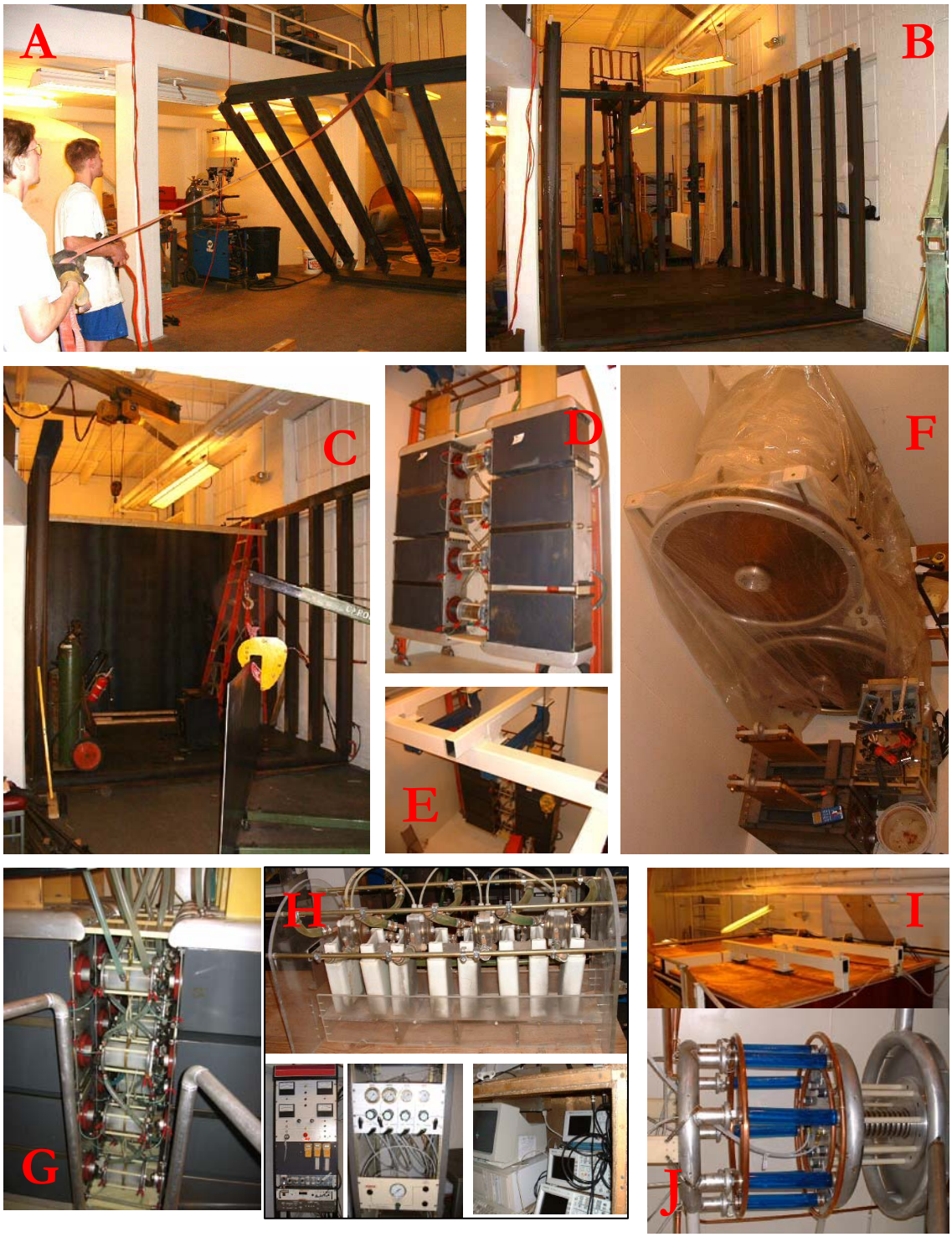

Fig. 9-3. Laboratory photographs. A) South wall assembly, B) Rib assembly, C) plate assembly, D) & E) Marx assembly, F) I-Store assembly, G) Marx complete, H) MTG assembly, control rack, gas rack, data acquisition system, I) Finished tank, J) Phase I output section.

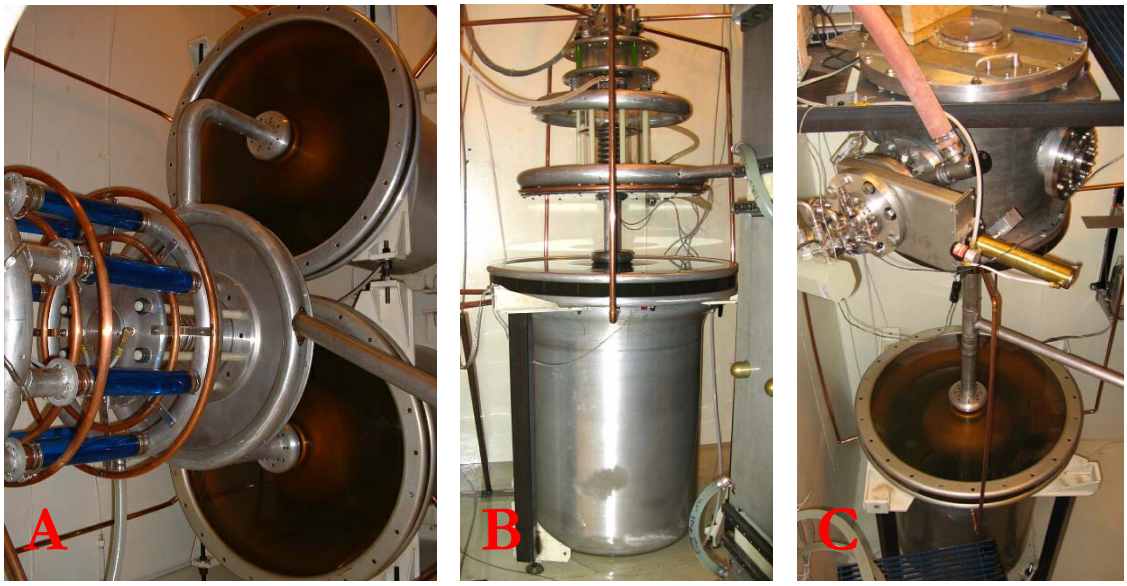

Fig. 9-4. Laboratory photographs. A) Phase I output section front view, B) phase II – tower 1, switch tower, C) phase II – tower 2, magnetic flashover inhibition tower.

E. Electrical Software Description

All electric fields were solved using a student version of Ansoft's Maxwell 2D. This program utilizes CAD drawings from Autocad in which each object is drawn with "polylines" so they are considered separate objects by Autocad and not objects composed of individual lines. These objects are imported into Maxwell with at least 50 lines to complete an arc (frequently used in excess of 100). Objects must not overlap and if they do, an error will be encountered when trying to exit the drawing portion of the Maxwell program. There are several options to combat this frequent error. I have found the most useful is used the "Boundary" command on each object that overlaps and replace the old object with the new one that is formed by the command.

Once objects are imported and all materials are defined. All conductors are described as either floating conductors or having voltage values. All conducting objects must be defined as "signal" objects for a complete capacitance matrix. If the "died abnormally" error is encountered upon simulating, this typically means there are either to many surfaces defined or too complex a shape is being rotated. The solution to this is to start over and import objects with less surfaces or to delete all objects that truly will not influence the simulation results of interest.

Once solutions are obtained there is a possibility that voltage gradients will appear across conductors. This is a result of a glitch in the program that is caused by the assignment of conductors operations. The solution to this is to delete all defined boundary conditions and start over. Exiting the program helps this error. If all else fails, starting over from importing the drawing stage is necessary.

All circuit simulations were conducted using Spectrum Software's MicroCap 6.0 (MC6). This is a SPICE-like program with similar features. Two of the most useful are "Macro" definitions and "User Source" files. Manufacturer discussion of MC6 capabilities is found at www.spectrum-soft.com.

F. New Switch Simulations

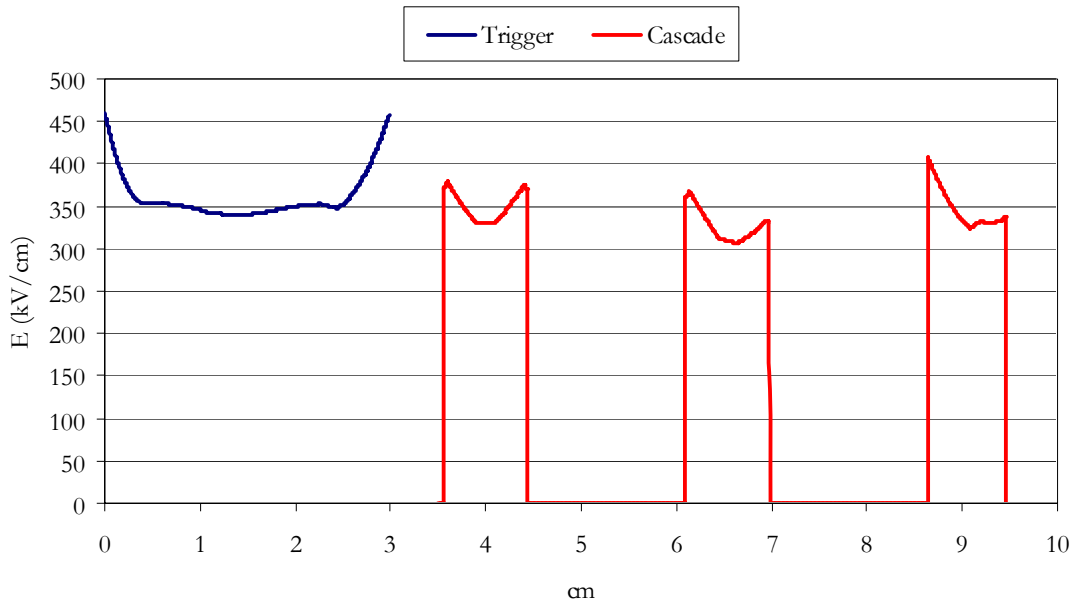

Fig. 9-5. Charging field plots for a 2 MV charge.

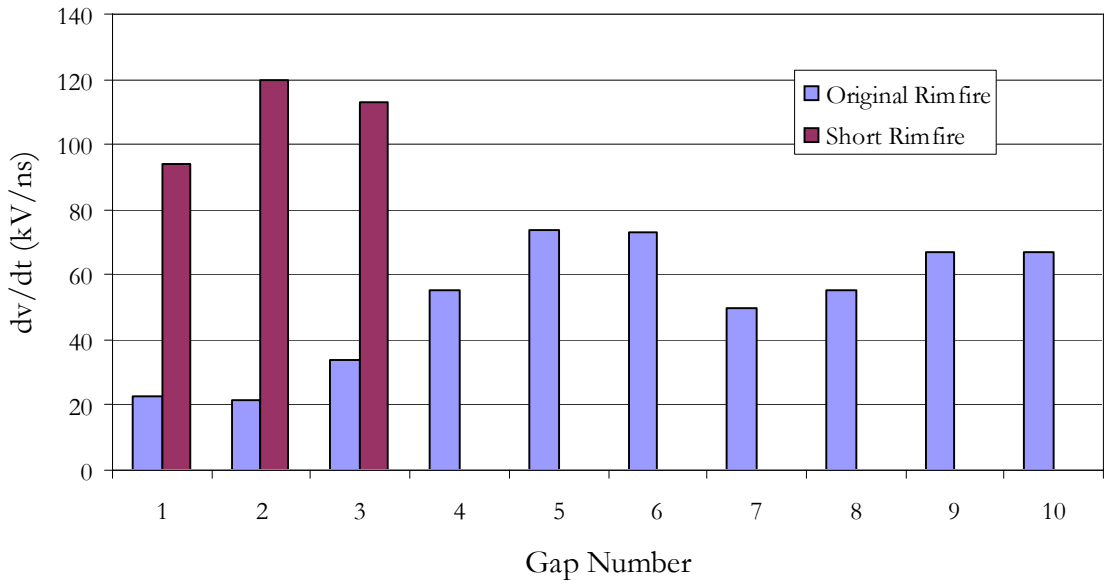

Fig. 9-6. dv/dt at the time of trigger close for a 1.6 MV (80% self-break) simulation.

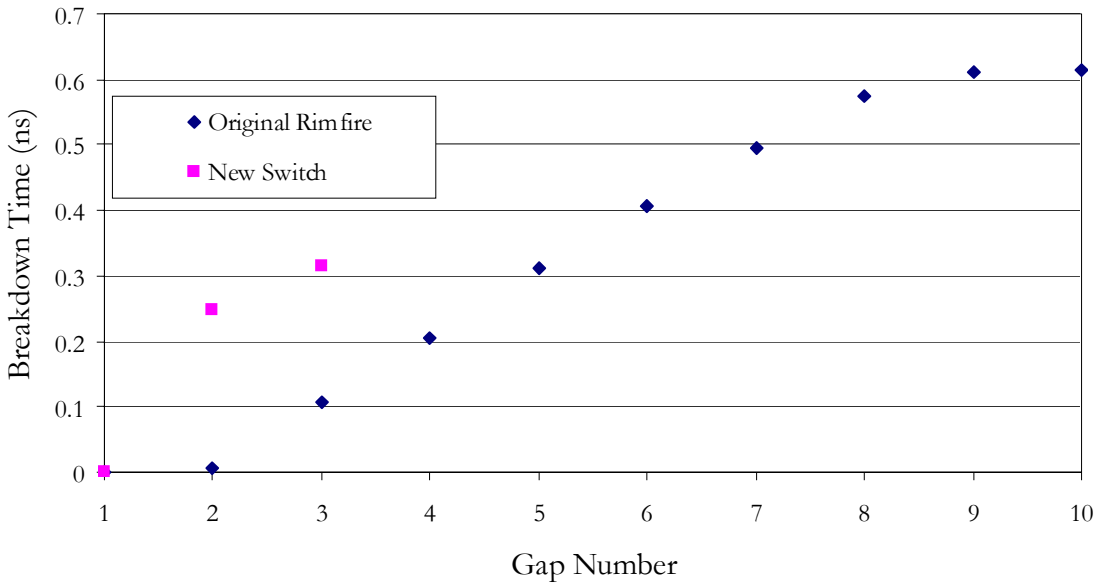

Fig. 9-7. Time to breakdown for the new switch and original Rimfire at 1.6 MV.

G. Self-break Photographs

Images captured using a Canon PowerShot A75 with a Kodak ND 4.0 filter. Color in the images is inverted for clarity.

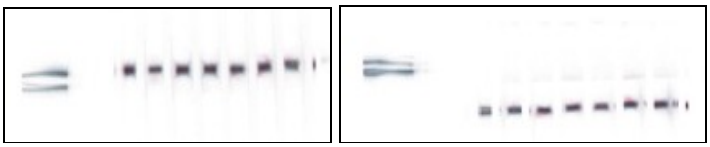

Shot 58 (±30 kV) Shot 59 (±30 kV)

Shot 60 Shot 61 Shot 62

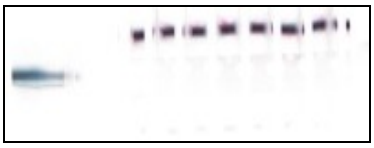

Shot 63

Fig. 9-8. ±40 kV (except where labeled otherwise) all-sphere. Seven cascade gaps visible, trigger gap at left.

Shot 31 (±30 kV) Shot 33 (±30 kV)

Shot 35 Shot 36 Shot 37

Fig. 9-9. ±40 kV (except where labeled otherwise) 6.67 cm radius original electrodes. Seven cascade gaps visible, trigger gap at left.

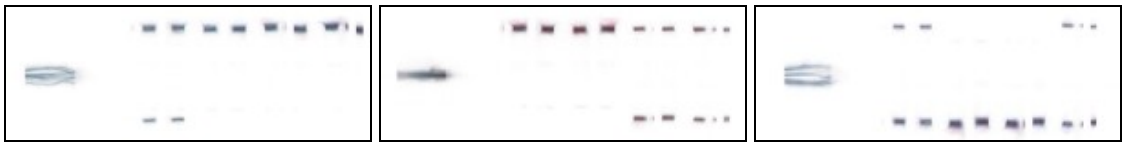

Shot 94 Shot 95 Shot 96

Shot 97 Shot 98 Shot 100

Fig. 9-10. ±30 kV, 2-ball. Seven cascade gaps visible, trigger gap at left.

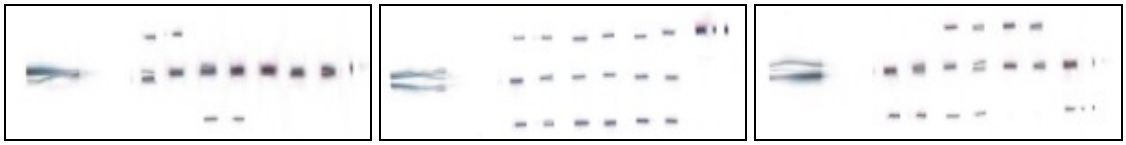

Shot 70 Shot 71 Shot 72

Shot 78 Shot 79 Shot 80

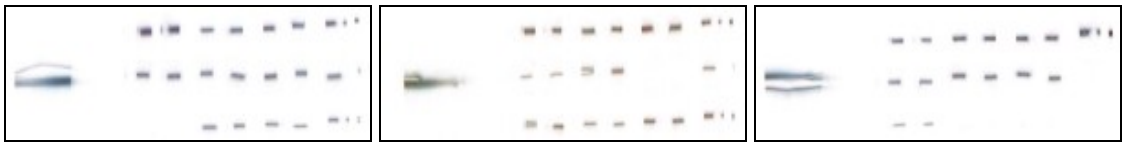

Shot 86 Shot 87 Shot 88

Fig. 9-11. ±30 kV, 3-ball. Seven cascade gaps visible, trigger gap at left.

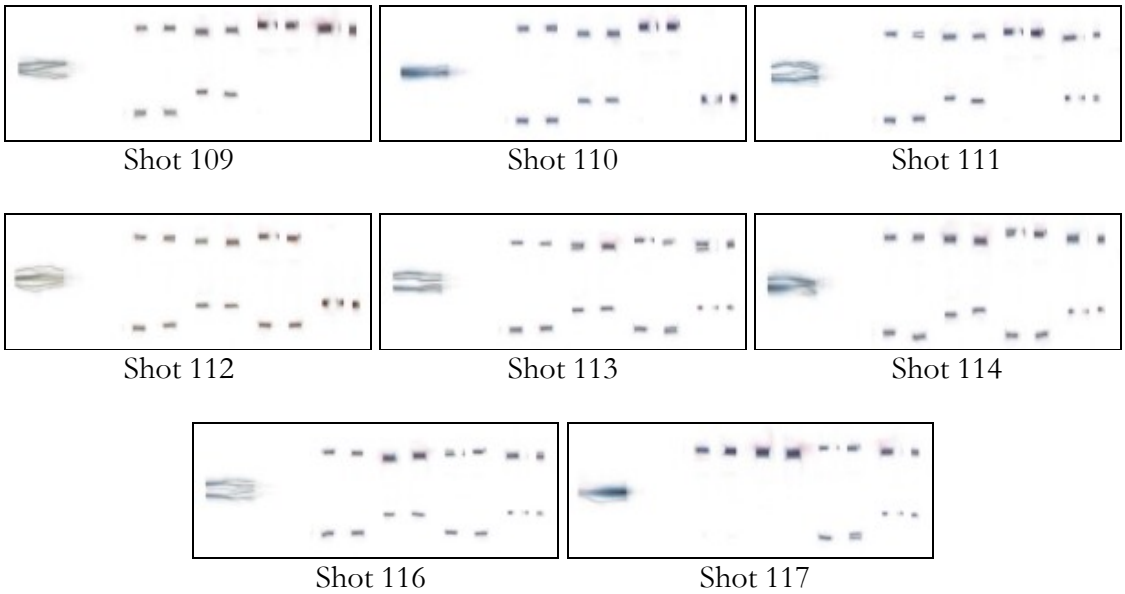

Fig. 9-12. ±30 kV, 2-90. Seven cascade gaps visible, trigger gap at left.

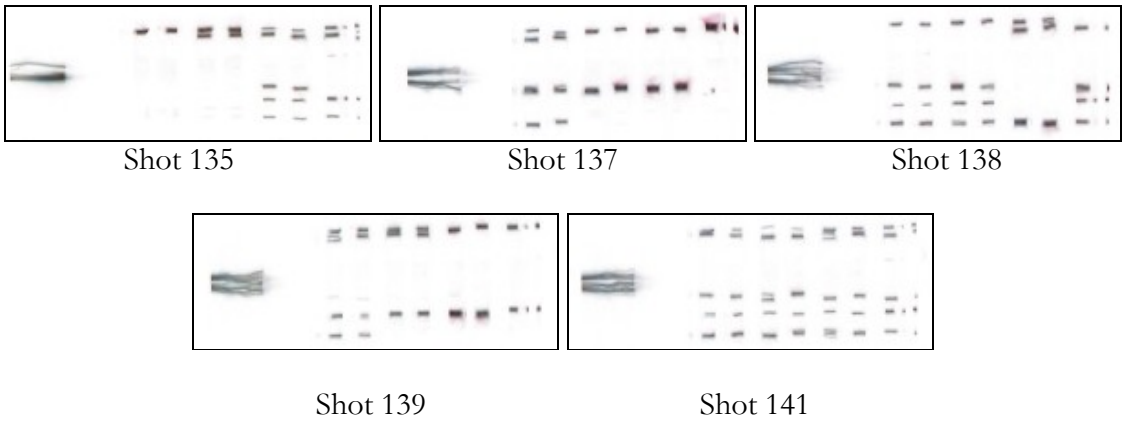

Fig. 9-13. ±30 kV, 6-ball. Seven cascade gaps visible, trigger gap at left.

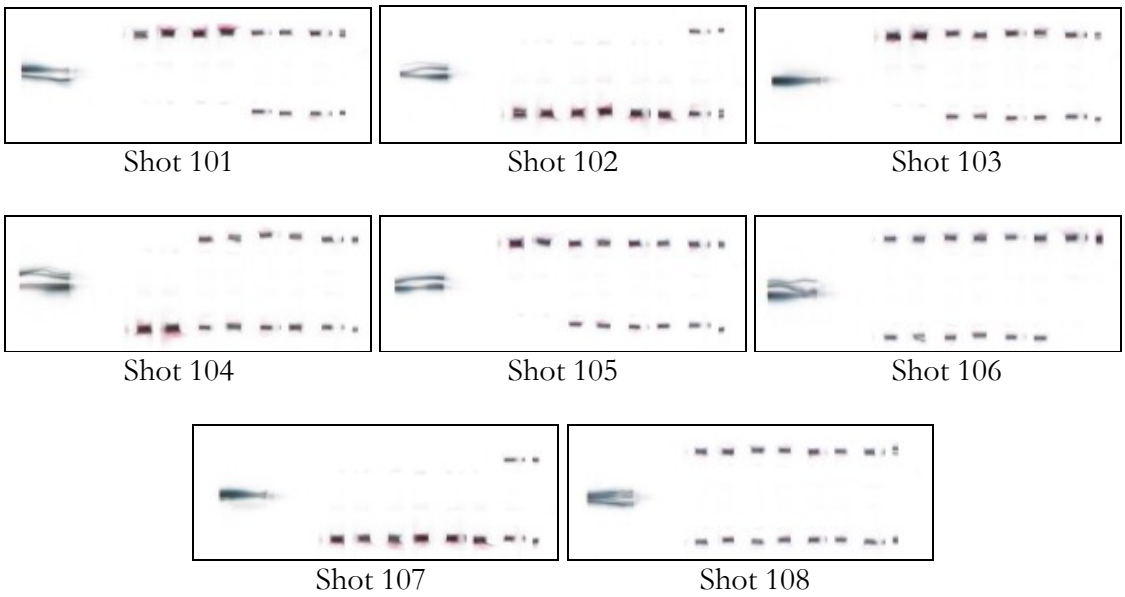

Fig. 9-14. ±40 kV, 2-ball. Seven cascade gaps visible, trigger gap at left.

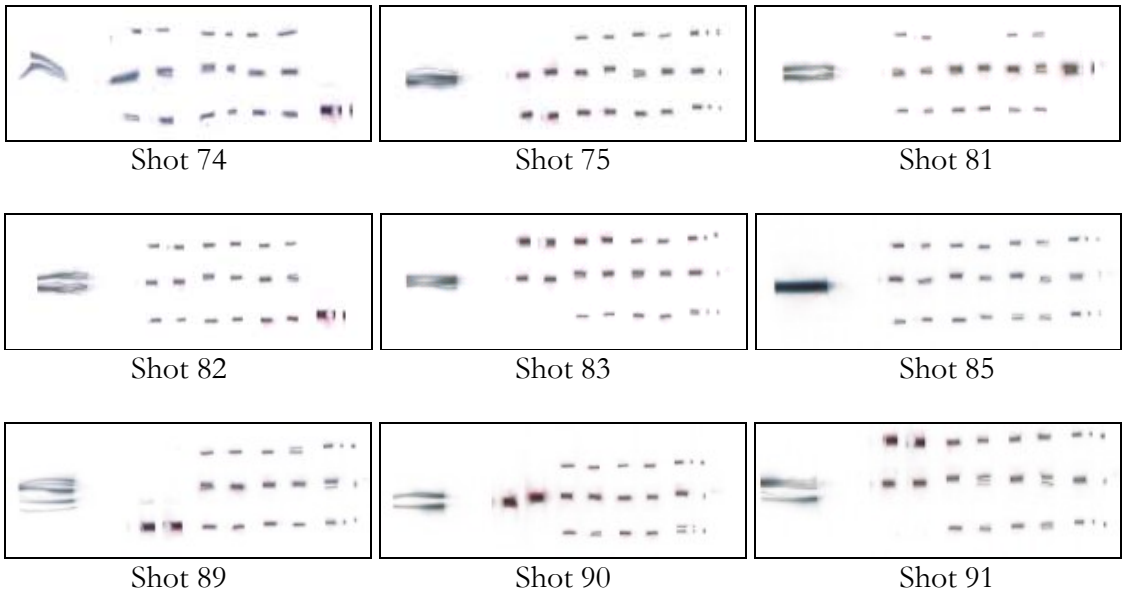

Fig. 9-15. ±40 kV, 3-ball. Seven cascade gaps visible, trigger gap at left.

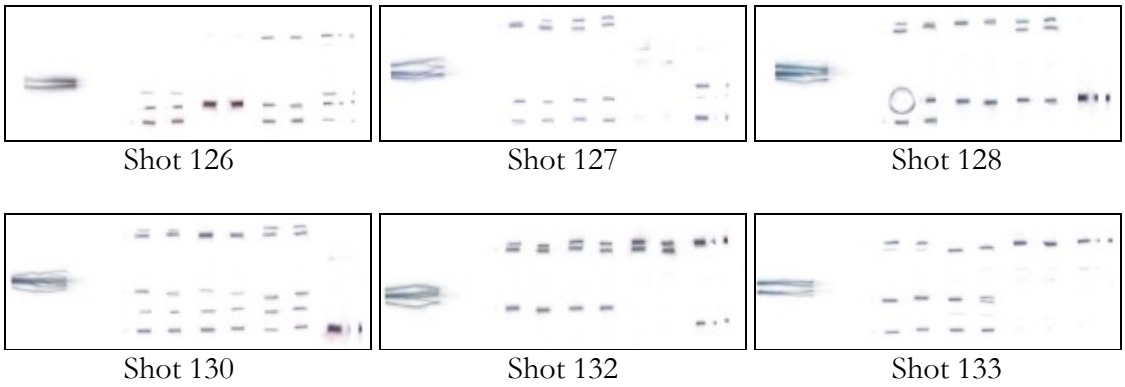

Fig. 9-16. ±40 kV, 2-90. Seven cascade gaps visible, trigger gap at left.

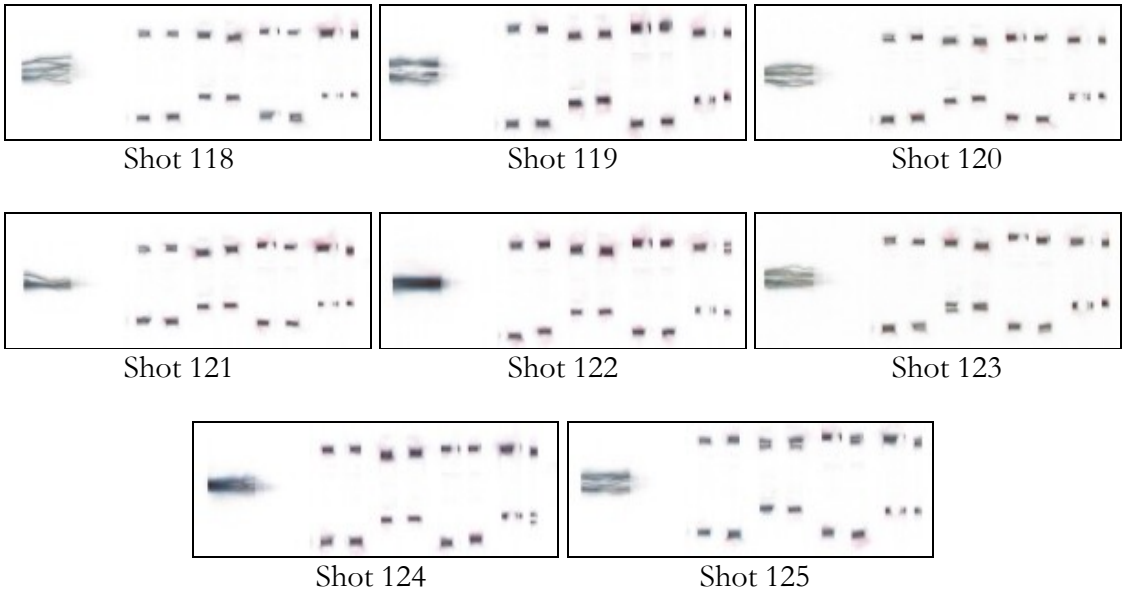

Fig. 9-17. ±40 kV, 2-90. Seven cascade gaps visible, trigger gap at left.

H. Laser Triggered Photographs


Shot A119


Shot A120


Shot A121


Shot A122


Shot A123


Shot A124


Shot A125

Fig. 9-18. ±54 kV, 6.67 cm. Ten cascade gaps visible, trigger gap at left.


Shot A126


Shot A127


Shot A129


Shot A130


Shot A131


Shot A133


Shot A134

Fig. 9-19. ±54 kV, 6.67 cm with holes. Ten cascade gaps visible, trigger gap at left.

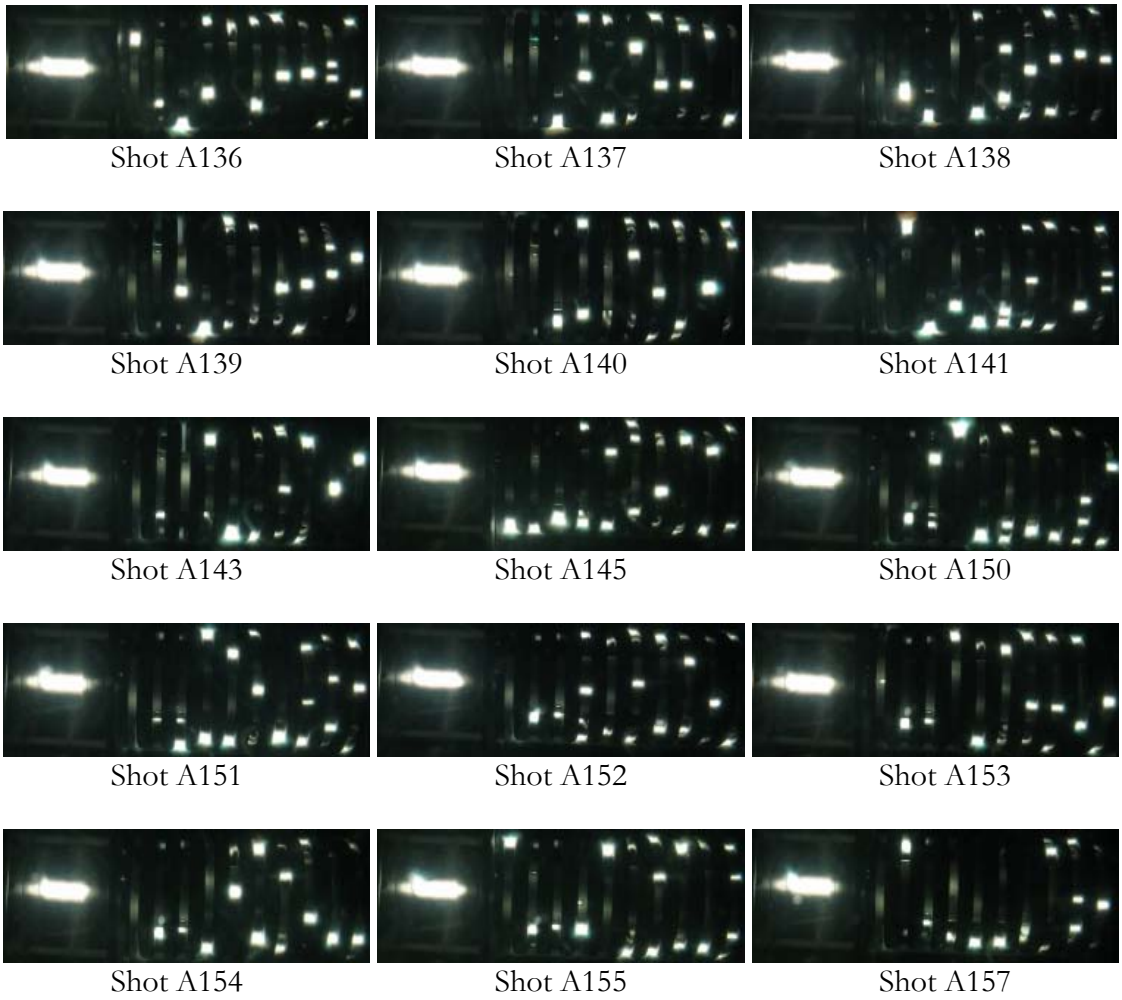

Fig. 9-20. ±54 kV, 8.26 cm. Ten cascade gaps visible, trigger gap at left.

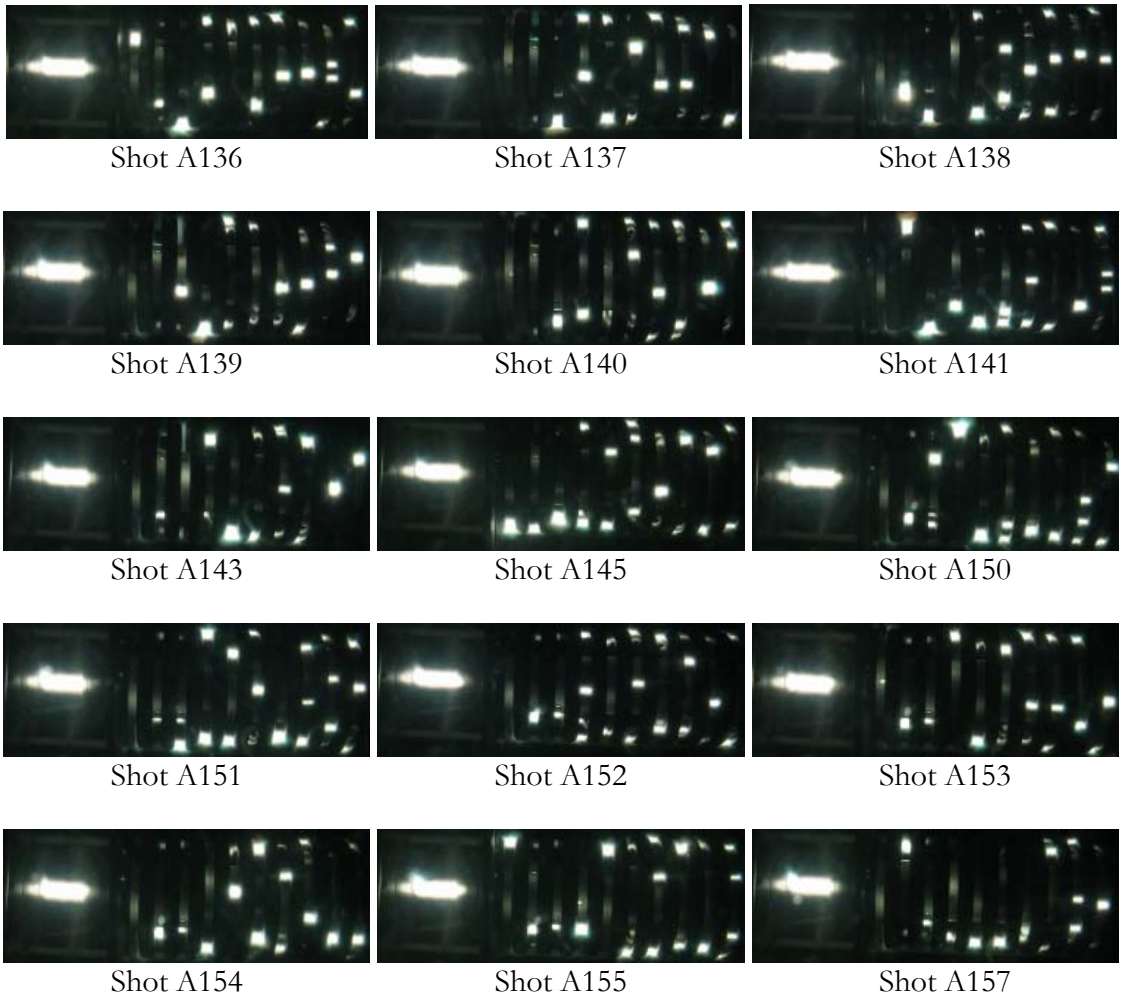

Fig. 9-21. ±54 kV, 8.26 cm. Ten cascade gaps visible, trigger gap at left.

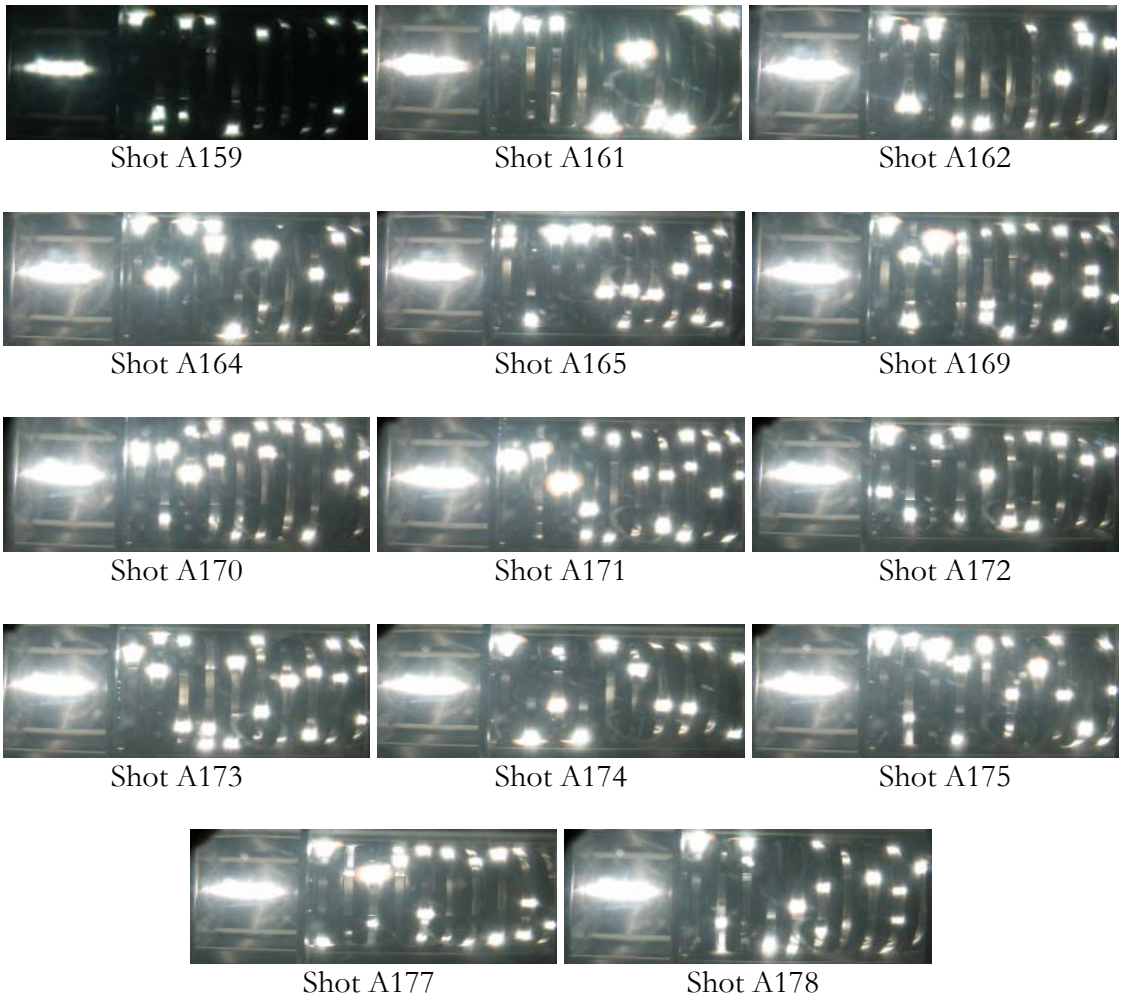

Fig. 9-22. ±54 kV, 8.26 cm. Ten cascade gaps visible, trigger gap at left.

Shot A56 Shot A61 Shot A62

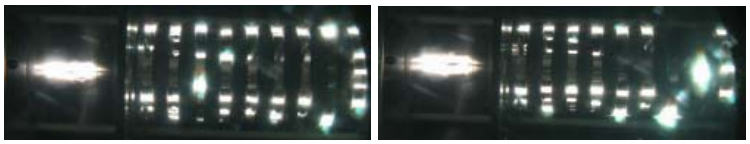

Shot A63 Shot A66

Fig. 9-23. ±26 kV, 30 psig, Air 6.67 cm with holes, self-break. Nine cascade gaps visible, trigger gap at left.

Shot A57 Shot A58 Shot A59

Shot A60 Shot A64 Shot A65

Fig. 9-24. ±26 kV, 30 psig, Air 6.67 cm with holes, laser triggered. Nine cascade gaps visible, trigger gap at left.

Shot A67 Shot A68 Shot A69

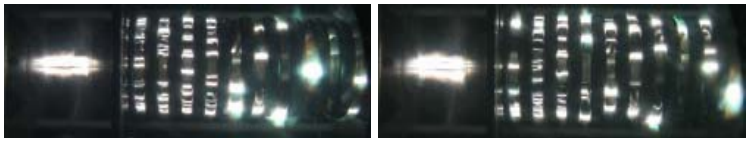

Shot A70 Shot A71

Fig. 9-25. ±26 kV, 26 psig, Air 6.67 cm, self-break. Ten cascade gaps visible, trigger gap at left.

Shot A80 Shot A81 Shot A82

Shot A83 Shot A85

Fig. 9-26. ±57 kV, 25 psig, SF_6 6.67 cm, laser. Ten cascade gaps visible, trigger gap at left.

Fig. 9-27. ±26 kV, 35 psig, Air 6.67 cm, laser trigger. Ten cascade gaps visible, trigger gap at left.

Fig. 9-28. ±45 kV, 35 psig, SF_6 6.67 cm, laser trigger. Ten cascade gaps visible, trigger gap at left.

Table 9-3: Phase I Shot Log

Shot	Date	Marx Charge +/- kV	Marx psig (A-air, S-SF6)	TG-70 charge kV	TG-70 psig(SF6)	Switch psig (A-air,S-Sf6)	MTG Charge +/- kV	MTG charge (A-air,S-Sf6)	Oscope 1 (1-4) settings	Oscope 1 (5-8) settings	Oscope 1 (9-12) settings	notes
1	22-Apr-04	20	2A	-25	6	1A	10	2A	TR1-14mV, 500 mV/div,1us	TR1-2.4V,5V/div,0.5us	1V/div,50us	refer to AR3 for settings, time/voltage scales need adjusting
2	24-Apr-04	20	2A	-25	6	1A	10	2A	TF1-250mV,1V,1us	TR1,1&4-10V,2&3-20V,0.5us	TF2,1-10V,2-.5V,3-1V,4-2V,1us	oscope levels adjudsted, data not saved
3	24-Apr-04	20	2A	-25	6	1A	10	2A				data saved, load currents 6 and 7 noisy, 6 and 7 exchanged with 5 and 8, respectively
4	24-Apr-04	20	2A	-25	6	1A	10	2A	TF1-720mV,2V,250ns	same as 1	TF2,1-.96V,1-2mV,2-2V,3-5V,4-.5V,1us	6 triggered scope when Marx shorted, no other normal channels do this, 6 7 9 10 11 12 saved
5	24-Apr-04	20	2A	-25	6	1A	10	2A	6 and 7 tightened at bulkhead near tank, 6 looks dramatically better, no change on 7, bulkhead near tank wrapped in screen, hole where cables feedthrough plugged, 9 tightened			
6	24-Apr-04	20	2A	-25	6	1A	10	2A	9 looks great, 7 no change, scope 3 time widened to find voltage pulses, 10,11,12 look bad			
7	24-Apr-04	20	2A	-25	6	1A	10	2A	channels 1-4 look same as always and not saved, channels 5-12 saved, 7 still bad, 6 exchanged with 1, 7 with 2, 11 with 3 and 12 with 4, triggered off 10 with widened time scale, waveform saved order on scopes is 6 7 11 12 | 5 1 2 8 | 9 10 3 4			
8	24-Apr-04	20	2A	-25	6	1A	10	2A	Tank BULKHEAD problem at: 6 7 11 12, replace ASAP			need at least 2.5 us on V and current plots on Oscope 3, potential proble with VM load. Load currents shold have the same time scale
9	27-Apr-04	20	2A	-25	6	1A	10	2A	load VM remade and moved to IS plate, all VM resistors measured			
10	29-Apr-04	20	2A	-25	6	1A	10	2A	RINGUP 1, Data Saved on 9 11 12, charged at 20% current			
11	29-Apr-04	20	2A	-25	6	1A	10	2A	RINGUP 2, Data Saved on 9 11 12, charged at 20% current			
12	2-May-04	20	2A	-25	6	6A	10	2A	Self Break data for 20 kV-1, 6 psig A, Data saved on 6 9 11 12			
13	2-May-04	20	2A	-25	6	6A	10	2A	Self Break data for 20 kV-2, 6 psig A, Data saved on 6 9 11 12, VM moved back			
14	2-May-04	20	2A	-25	6	16A	10	2A	Self Break data for 20 kV-1, 16 psig A, DID NOT BREAK DOWN, NO DATA SAVED			
15	2-May-04	20	2A	-25	6	12A	10	2A	Self Break data for 20 kV-1, 12 psig A, Data saved on 6 9 11 12			

16	3-May-04	20	2A	-25	6	20A	10	2A	RING UP 3, DATA SAVED ON 6 9 11, Charging current drastically effects Marx V, 35% charge	
17	3-May-04	20	2A	-25	6	12A	10	2A	Self Break data for 20 kV-2, 12 psig A, Data saved on 6 9 11 12	
18	3-May-04	30	5A	-25	6	30A	10	2A	SB data for 30 kV-1, 30 psig A, 35% charge current, charge current	
19	3-May-04	38	5A	-25	6	50A	10	2A	Tank bulkhead replaced	SB data for 40 kV-1, 40 psig A, 35% charge current, Marx self broke, needed more pressure
20	6/1/2004	30	5A	-25	2	20A	10	2A	MTG VM removed, VM10 now at IS, VM11 at Marx, VM12 at load, I-4 no signal, I-7 Messy, pic looks great, apeture 6, 5 sec shutter, no data saved	
21	6/1/2004	30	5A	-25	2	20A	10	2A	exchaged at tank, 5 w/ 11, 6 w/ 12, 1 w/ 7, 2 w/ 8, 3 w/ 4, great pic, VM saved,	
22	6/2/2004	30	5A	-25	2	20A	10	2A	apeture 5.3, L-7 noisy (screen box issue, moved to open port), L-4 dead (short in tank), L-12 dead (short in tank), L-11 noisy still a mystery	
23	6/2/2004	30	5A	-25	2	20A	10	2A	1, 2, 3, 5, 6, 7, 8 back to original config, T11 on B4, T9 on B12, T12 on B9, T4 on B11	
24	6/2/2004	30	5A	-25	2	20A	10	2A	great pic, no data saved, do shot again	
25	6/2/2004	30	5A	-25	2	20A	10	2A	great pic, all data saved, all signals moved back to correct positions, top screen box feedthrough noisy, VM12 short, drain tank	
26	6/21/2004	30	5A	-25	2	20A	10	2A	HV attenuators refurbished, no data saved, pic saved	
27	6/21/2004	30	5A	-25	2	20A	10	2A	Channel 10 fixed, all data saved but channel 10, including duds actual number of shots closer to 60	
28	6/21/2004	30	5A	-25	2	20A	10	2A	FIRST SHOT OF 12 GOOD CHANNELS OF DATA, NO PIC, BEGIN FULL TESTING	
29	7/1/2004	30	5A	-25	2	20A	10	2A	Camera computer changed, no pic, data saved, channel 6 messy off and on	
30	7/2/2004	30	5A	-25	2	20A	10	2A	no pic, data saved, current matlab file	
31	7/6/2004	30	5A	-25	2	20A	10	2A	pic and data saved, TG-70 repaired, PT55 resistor shorted to one pack, 30kV 20A good shot 1	
32	7/6/2004	30	5A	-25	2	35A	10	2A	no pic, data saved, pic must be taken from memory card, switch did not breakdown at 30 KV with 30A psig	
33	7/6/2004	30	5A	-30	12	50A	10	2A	good pic, data saved, 30kV 20A good shot 2	
34	7/6/2004	40	10A	-30	12	35A	10	2A	good pic, data saved, 40kV 35A good shot 1a	
35	7/6/2004	40	10A	-30	12	35A	10	2A	Time scale at 250 ns/div for all, Scopes 1 and 2 set to 2V/div, Scope 3 set to 5V/div for 10 11 and 12 and 2V/div for 9	good pic, data saved, 40kV 35A good shot 2a
36	7/6/2004	40	10A	-30	12	35A	10	2A		good pic, data saved, 40kV 35A good shot 3a
37	7/6/2004	40	10A	-30	12	35A	10	2A		good pic, data saved, 40kV 35A good shot 4a
38	7/21/2004	50	15A	-30	12	50A	10	3A	current OK, pic great, V no good, time sync off channel 1	
39	7/21/2004	50	15A	-30	12	50A	10	3A	all waveforms saved, good pic	
40	7/21/2004	50	15A	-30	12	50A	10	3A	switch immediately hissed (gas leak) when fired	
41	7/21/2004	50	15A	-30	12	50A	10	3A	no pic	
42	7/21/2004	40	10A	-30	12	8S	10	3A	opposite direction ring before breakdown, no pic, air must have lingered in switch as no other 40 kV shots possible at 8	
43	7/21/2004	50	15A	-30	12	8S	10	3A	normal breakdown (interesting pic)	

44	7/21/2004	50	15A	-30	12	8S	10	3A	
45	7/21/2004	50	15A	-30	12	8S	10	3A	
46	7/26/2004	60	18A	-30	12	12S	10	3A	added 10X to channel 10, 2X to channel 11, 2X to channel 12
47	7/26/2004	60	18A	-30	12	12S	10	3A	same attenuator arrangement
48	7/26/2004	75	25A	-30	12	20S	10	3A	Marx self broke at 71 kV
49	7/26/2004	75	25A	-30	12	24S	10	3A	Loud noise, switch did not breakdown, diagnostic cables arc to wall, kicked out pvc pipe supporting load
50	7/29/2004	30	5A	-30	12	20A	10	3A	took off 2X, 2X and 10X attenuators (trigger section shorted), SYNC RESET
51	7/29/2004	30	5A	-30	12	20A	10	3A	good
52	7/29/2004	30	5A	-30	12	20A	10	3A	good
53	8/2/2004	30	5A	-30	12	35A	10	3A	possibly had 10A in Marx, camera aperture set to 7.1
54	8/2/2004	30	5A	-30	12	2S	10	3A	possibly had 10A in Marx, camera aperture set to 7.1
55	8/2/2004	30	5A	-30	12	2S	10	3A	possibly had 10A in Marx, camera aperture set to 7.1
56	8/2/2004	40	10A	-30	12	22M	10	3A	2 psi SF6-20 psi Air for 22 psi total
57	8/18/2004	30	5A	-30	12	20A	10	3A	Sphere ball Trodes, shot 22 setup
58	8/18/2004	30	5A	-30	12	20A	10	3A	good
59	8/18/2004	30	5A	-30	12	20A	10	3A	good
60	8/18/2004	40	10A	-30	12	35A	10	3A	good, two paths
61	8/18/2004	40	10A	-30	12	35A	10	3A	good
62	8/18/2004	40	10A	-30	12	35A	10	3A	good
63	8/18/2004	40	10A	-30	12	22M	10	3A	shot 56 setup
64	8/18/2004	30	10A	-30	12	20A	10	3A	Tiny hole Trode with quad first trode, shot 22 setup, channel 8 removed and changed with channel 12 at screen box
65	8/18/2004	30	5A	-30	12	20A	10	3A	
66	8/18/2004	30	5A	-30	12	20A	10	3A	
67	8/18/2004	40	10A	-30	12	35A	10	3A	
68	8/18/2004	40	10A	-30	12	35A	10	3A	
69	8/18/2004	40	10A	-30	12	35A	10	3A	
70	9/3/2004	30	5A	-30	12	20A	10	3A	no channel 6 or 8, sphere-plate sandwich trodes 1, good pic move current to 100ns/div
71	9/3/2004	30	5A	-30	12	20A	10	3A	
72	9/3/2004	30	5A	-30	12	20A	10	3A	
73	9/3/2004	40	10A	-30	12	35A	10	3A	no channel 5,6 or 8, OK to replace any load current waveform with 2, 3, 4
74	9/3/2004	40	10A	-30	12	35A	10	3A	

75	9/3/2004	40	10A	-30	12	35A	10	3A	
76	9/7/2004	30	5A	-30	12	20A	10	3A	
77	9/7/2004	30	5A	-30	12	20A	10	3A	lost pic and data
78	9/7/2004	30	5A	-30	12	20A	10	3A	
79	9/7/2004	30	5A	-30	12	20A	10	3A	
80	9/7/2004	30	5A	-30	12	20A	10	3A	
81	9/7/2004	40	10A	-30	12	35A	10	3A	
82	9/7/2004	40	10A	-30	12	35A	10	3A	
83	9/7/2004	40	10A	-30	12	35A	10	3A	
84	9/7/2004	40	10A	-30	12	35A	10	3A	purge Marx every three shots, no pic, prefire 37 kV
85	9/8/2004	30	5A	-30	12	20A	10	3A	
86	9/8/2004	30	5A	-30	12	20A	10	3A	
87	9/8/2004	30	5A	-30	12	20A	10	3A	
88	9/8/2004	30	5A	-30	12	20A	10	3A	
89	9/8/2004	40	10A	-30	12	35A	10	3A	
90	9/8/2004	40	10A	-30	12	35A	10	3A	
91	9/8/2004	40	10A	-30	12	35A	10	3A	
92	9/8/2004	50	15A	-30	12	50A	10	3A	10X attenuation on channels 10 and 11, 2X on channel 12, marx prefire at 50kV
93	9/8/2004	50	16.5A	-30	12	50A	10	3A	
94	9/9/2004	30	5A	-30	12	20A	10	3A	original setup, 2 ball alligned
95	9/9/2004	30	5A	-30	12	20A	10	3A	
96	9/9/2004	30	5A	-30	12	20A	10	3A	
97	9/9/2004	30	5A	-30	12	20A	10	3A	
98	9/9/2004	30	5A	-30	12	20A	10	3A	
99	9/9/2004	30	5A	-30	12	20A	10	3A	no pic
100	9/9/2004	30	5A	-30	12	20A	10	3A	
101	9/9/2004	40	10A	-30	12	35A	10	3A	
102	9/9/2004	40	10A	-30	12	35A	10	3A	
103	9/9/2004	40	10A	-30	12	35A	10	3A	
104	9/9/2004	40	10A	-30	12	35A	10	3A	good two channel
105	9/9/2004	40	10A	-30	12	35A	10	3A	
106	9/9/2004	40	10A	-30	12	35A	10	3A	

107	9/9/2004	40	10A	-30	12	35A	10	3A	
108	9/9/2004	40	10A	-30	12	35A	10	3A	great pic, prefire 39 kV
109	9/13/2004	30	5A	-30	12	20A	10	3A	2 balls offset 90 degrees from gap to gap
110	9/13/2004	30	5A	-30	12	20A	10	3A	
111	9/13/2004	30	5A	-30	12	20A	10	3A	
112	9/13/2004	30	5A	-30	12	20A	10	3A	
113	9/13/2004	30	5A	-30	12	20A	10	3A	
114	9/13/2004	30	5A	-30	12	20A	10	3A	no channels 9-12
115	9/13/2004	30	5A	-30	12	20A	10	3A	switch did not breakdown, no pic
116	9/13/2004	30	5A	-30	12	20A	10	3A	IS ring back, pressure to high
117	9/13/2004	30	5A	-30	12	20A	10	3A	
118	9/13/2004	40	10A	-30	12	35A	10	3A	prefire 40 KV
119	9/13/2004	45	12A	-30	12	35A	10	3A	prefire 45 kV
120	9/13/2004	45	14A	-30	12	35A	10	3A	
121	9/13/2004	45	14A	-30	12	35A	10	3A	
122	9/13/2004	45	14A	-30	12	35A	10	3A	
123	9/13/2004	45	15A	-30	12	35A	10	3A	purge Marx every shot at 45 kV charge and beyond
124	9/13/2004	45	15A	-30	12	35A	10	3A	
125	9/13/2004	45	15A	-30	12	35A	10	3A	
126	9/14/2004	30	5A	-30	12	20A	10	3A	6 ball
127	9/14/2004	30	5A	-30	12	20A	10	3A	mike 2 first shot, apeture 6.3
128	9/14/2004	30	5A	-30	12	20A	10	3A	mike 1first shot
129	9/14/2004	30	5A	-30	12	20A	10	3A	prefire 29 kV, data saved, no pic
130	9/14/2004	30	5A	-30	12	20A	10	3A	
131	9/14/2004	30	5A	-30	12	20A	10	3A	
132	9/14/2004	30	5A	-30	12	20A	10	3A	pre fire 29 kV
133	9/14/2004	30	5A	-30	12	20A	10	3A	
134	9/14/2004	40	12A	-30	12	35A	10	3A	no pic
135	9/14/2004	40	12A	-30	12	35A	10	3A	
136	9/14/2004	40	12A	-30	12	35A	10	3A	no pic
137	9/14/2004	40	12A	-30	12	35A	10	3A	
138	9/14/2004	40	12A	-30	12	35A	10	3A	

139	9/14/2004	40	12A	-30	12	35A	10	3A	
140	9/14/2004	40	12A	-30	12	35A	10	3A	
141	9/14/2004	40	12A	-30	12	35A	10	3A	

Table 9-4: Phase II Shot Log

Shot	Date	Nom. Marx Charge +/- kV	Marx psig (A-air, S-SF6)	TG-70 charge kV	TG-70 psig(SF6)	Switch psig (A-air,S-Sf6)	MTG Charge +/- kV	MTG charge (A-air,S-Sf6)	notes
A1	22-Dec-04	20	3.0	25	12	30A	12.5	4A	storage tank gaskets replaced with VITON, RING UP 1
A2	22-Dec-04	20	3.0	25	12	30A	12.5	4A	No Marx V, RoxBox current sense in noisy
A3	22-Dec-04	20	3.0	25	12	30A	12.5	4A	RING UP 2
A4	22-Dec-04	20	3.0	25	12	30A	12.5	4A	RING UP 3, long time frame
A5	22-Dec-04	20	3.0	25	12	18A	12.5	4A	Shot 1, 4 ball-hole, camera set to 8" and 6.3, pic awefully dark, will turn out to need a lighter filter, probably should retake shots
A6	22-Dec-04	20	3.0	25	12	18A	12.5	4A	increased camera to 7.1
A7	27-Dec-04	20	3.0	25	12	18A	12.5	4A	4 hole with quad trode 1, no voltage waveforms, camera set to 5.6
A8	27-Dec-04	20	3.0	25	12	18A	12.5	4A	
A9	27-Dec-04	20	3.0	25	12	18A	12.5	4A	camera set to 5
A10	27-Dec-04	20	3.0	25	12	18A	12.5	4A	need to change camera filter to ND 2, camera set to 5.6
A11	27-Dec-04	20	3.0	25	12	18A	12.5	4A	
A12	27-Dec-04	20	3.0	25	12	18A	12.5	4A	
A13	27-Dec-04	20	3.0	25	12	18A	12.5	4A	
A14	8-Jan-05	20	3.0	25	12	18A	12.5	4A	filter changed to ND 2, camera set to 6.3, no channel 9, LT system still noisy on current sense in
A15	8-Jan-05	20	3.0	25	12	18A	12.5	4A	camera set to 8.0, LT has lots of noise
A16	8-Jan-05	20	3.0	25	12	18A	12.5	4A	added ND1 to ND2 filter, camera set to 7.1, LT still noisy, must be shielded or power source independent
A17	8-Jan-05	20	3.0	25	12	18A	12.5	4A	remove ND1, need to see reflections on electrodes, leave camera at 8, many arcs
A18	8-Jan-05	20	3.0	25	12	18A	12.5	4A	
A19	8-Jan-05	20	3.0	25	12	18A	12.5	4A	good
A20	8-Jan-05	20	3.0	25	12	18A	12.5	4A	slight bang

A21	8-Jan-05	20	3.0	25	12	18A	12.5	4A	louder bang
A22	8-Jan-05	20	3.0	25	12	18A	12.5	4A	very loud bang, might be flashing Istore, tank drained, switch rod removed, load conductivity checked 10 mS/cm
A23	1/12/2005	20	3.0	25	12	18A	12.5	4A	Channel 10 noisy
A24	1/12/2005	20	3.0	25	12	18A	12.5	4A	
A25	1/12/2005	20	3.0	25	12	18A	12.5	4A	
A26	1/19/2005	20	3.0	25	12	18A	12.5	4A	Noise interfering with laser triggering unit ROXBOX. Putting 5-10 V on "ground".
A27	1/25/2005	20	3.5	25	12	18A	12.5	4A	TG-70 polarity changed-decreased noise to 2V, ROXBOX screened-decreased noise to 1.8V, ROXBOX powered from battery-noise dec. to 200 mV. TG-70 now runs on SF6 at 14 psi. Tank top screens added
A28	1/26/2005	20	3.5	25	16	18A	12.5	4A	
A30	1/26/2005	20	3.5	25	16	18A	12.5	4A	OK, camera 7.1
A31	1/26/2005	20	3.5	25	16	18A	12.5	4A	no pic, switch did not breakdown
A32	1/26/2005	20	3.5	25	16	18A	12.5	4A	Marx not breaking down upon trigger. MTG and TG-70 appear to be working correctly
A33	2/3/2005	30	5	25	16	27A	12.5	4A	First row Marx gaps changed and minimum breakdown voltage changed to 24 kV, no channel 4-cable undone
A34	2/3/2005	30	4	25	16	27A	12.5	4A	no pic, Marx prefire at 24 kV at 4 psi
A35	2/4/2005	28	4	25	16	27A	12.5	4A	First Attempt to laser trigger, laser did not fire on time, should fire when Marx is at 580 kV and switch at 800 kV for 75% operation. Good pic, higher voltage only factor in more arcs.
A36	2/4/2005	28	4	25	12	27A	12.5	4A	Loud noise like before
A37	2/9/2005	25	4	25	12	27A	12.5	4A	drained tank-no bubbles found in IS, moved channel 10 VM away form return conductor, scope added upstairs, laser possibly fired, time between FL and Marx needs to be 178 us
A38	2/9/2005	25	4	25	12	27A	12.5	4A	no channels 1-4, laser possibly fired
A39	2/9/2005	25	4	25	12	27A	12.5	4A	laser fired to early
A40	2/12/2005	25	4	25	12	27A	12.5	4A	no pic
A41	2/12/2005	25	4	25	12	27A	12.5	4A	laser firing way to early, long run DC comparator line detached, all cable runs double checked
A42	2/12/2005	25	4	25	12	27A	12.5	4A	laser should fire 230 ns before breakdown on upstairs scope and 440 ns before breakdown on downstairs
A43	2/12/2005	25	4	25	12	27A	12.5	4A	no channel 12, laser still to early,
A44	2/14/2005	25	4	25	12	27A	12.5	4A	Marx self broke, laser system worked timing wise, no MTG or TG-70, did not breakdown switch because there was no laser FL
A45	2/14/2005	25	4	25	12	27A	12.5	4A	laser timing good, fired 240 ns before upstairs broke, 430 ns before downstairs, FIRST LASER SHOT, IS pump was turned off for a few second perhaps added bubbles to IS.
A46	2/14/2005	25	4	25	12	26A	12.5	4A	26 psi air, loud bang like before, IS monitor noisy, lower breakdown V, load current noisy, no laser shot, laser light photo taken- no spark
A47	2/16/2005	26	4	25	12	35A	12.5	4A	try to trigger at 1MV, that is 1.1V on current pulse, laser fired 260 ns before breakdown upstairs, no channel 11 and 12
A48	2/16/2005	26	4	25	12	35A	12.5	4A	laser possibly a little early, 390 ns before breakdown upstairs, tried 1.2 V on current pulse
A49	2/16/2005	26	4	25	12	35A	12.5	4A	brought back to 1.1V, laser fired 470 ns before breakdown upstairs, laser not breaking down switch

A50	2/16/2005	26	4	25	12	35A	12.5	4A	loud bang, looking at Marx voltage determined it is the swing arm making bang, must be kept to 60 psi and checked every shot, one spark gap in row 2 changed
A51	2/17/2005	26	4	25	12	35A	12.5	4A	upstairs broke down 464 ns before breakdown (no laser trigger), no pic, triggered at 1.55 V marx current
A52	2/17/2005	26	4	25	12	35A	12.5	4A	laser fired 340 ns before breakdown upstairs, 540 downstairs, channel 12 is Q switch control signal
A53	2/17/2005	26	4	25	12	35A	12.5	4A	V set to 0.9 V, broke down 556 ns early upstairs, 720 ns downstairs, no laser shot, either laser not focused properly or timing system way off
	2/17-3/26								**3X beam expander added, laser repaired at New Wave factory, 1" optics replaced with coated 2" optics**
A54	3/28/2005	26	4	27	10	29A	14	6A	need triggered data at 850kV-1MV, current sense at 1.1V added 91' of Q switch delay cable pre-Oscope 3, channel 12 is Q switch after delay of 91' (140 ns), 472 ns from Q switch to breakdown, 36 ns from Q noise to breakdown
A55	3/28/2005	26	4	27	10	30A	14	6A	set current sense to 2V, no laser shot, 720 ns early, no pic, 52 ns between Q noise and breakdown
A56	3/28/2005	26	4	27	10	30A	14	6A	476 ns from Q switch rise to Q switch noise and breakdown, no laser breakdown
A57	3/28/2005	26	4	27	10	30A	14	6A	current sense set to 1.1V, 416 ns from Q switch to breakdown, 386 ns from rise to noise, 30 ns from noise start to breakdown
A58	3/28/2005	26	4	27	10	30A	14	6A	444 ns from Q switch rise to breakdown, 416 ns from rise to noise start
A59	3/28/2005	26	4	27	10	30A	14	6A	432 from Q switch to breakdown, 42 ns from noist start to breakdown
A60	3/28/2005	26	4	27	10	30A	14	6A	laser fired, but timing unconfirmed, lots of Q switch early noise
A61	3/28/2005	26	4	27	10	30A	14	6A	352 ns to breakdown from Q switch, no laser shot
A62	3/28/2005	26	4	27	10	30A	14	6A	set current sense in to 1 V, no laser 700 ns before breakdown, peak voltage is 22.5 V on Oscope 3
A63	3/28/2005	26	4	27	10	30A	14	6A	Marx prefire at 24 kV, Q switch at 416 ns before breakdown, no FL, increasing switch pressure
A64	3/28/2005	26	4	27	10	36A	14	6A	laser shot, 396 ns from Q switch rise to breakdown
A65	3/28/2005	26	4	27	10	35A	14	6A	416 ns from Q switch rise to breakdown
A66	3/28/2005	26	4	27	10	35A	14	6A	self break shot, no laser trigger used, used to confirm other shots were in fact laser triggered
A67	3/30/2005	26	5	27	10	26A	14	6A	ORIGINAL TRODES, self break shot 1, channel 12 is load voltage
A68	3/30/2005	26	5	27	10	24A	14	6A	SB shot 2
A69	3/30/2005	26	5	27	10	26A	14	6A	SB shot 3, oil vapor in switch caused burst of flames, cool pic, switch cleaned
A70	3/30/2005	26	5	27	10	26A	14	6A	brokedown at relatively low voltage
A71	3/30/2005	26	5	27	10	26A	14	6A	good
A72	3/30/2005	26	5	27	10	36A	14	6A	652 ns from Q switch rise to breakdown, change current source voltage to 2.5 V
A73	3/30/2005	26	5	27	10	35A	14	6A	656 ns from Q switch rise to breakdown
A74	3/30/2005	26	5	27	10	32A	14	6A	V set to 1.1, change pressure to 33A in switch, 492 ns from Q switch rise to breakdown
A75	3/30/2005	26	5	27	10	33A	21	15A	MTG charge voltage is increased to 21kV, timing much better, 400 ns from Q switch to breakdown
A76	3/30/2005	26	5	27	10	35A	21	15A	448 ns from Q switch to breakdown

A77	3/30/2005	26	5	27	10	36A	21	15A	416 ns from Q switch rise to breakdown
A78	3/31/2005	57	18A	27	10	25SF6	21	15A	added 300' of Q switch delay, removed 6 dB atten. At bulkhead added 10X atten to scope 3 on channels 10 and 11, channel 12 is Q switch, Marx prefire at 55 kV, no pic
A79	3/31/2005	57	18A	27	10	25SF6	21	15A	no Q switch trigger, amazing noise marx flashed to floor, marx self broke at 52 kV, 6 dB at bulkhead put back 6 dB replaced 10 X with 2X at scope 3, **2X ATTEN FROM A79 to Onward with some variations**
A80	4/4/2005	57	6SF6	27	10	25SF6	21	15A	set current sense to 3 V
A81	4/4/2005	57	6SF6	27	10	25SF6	21	15A	added filter to camera, 300' delay cable removed and not needed, laser spark is considerably smaller
A82	4/4/2005	57	6SF6	27	10	25SF6	21	15A	current sense to 1.1 V 440 ns from Q to breakdown, same V break at A81, removed 1 45' delay cable to trigger at 1.7 MV
A83	4/4/2005	57	6SF6	27	10	25SF6	21	15A	laser fired 690 ns before breakdown, laser spark is very small almost a point, laser energy out of laser is 22 mJ, fourth harmonic generator adjusted, laser now back to 30 mJ, **Marx voltage monitor was shortened (channel 11) will overestimate voltages by ~30%, , the near same peak voltage reading at the Marx and IS dates back to shot A10**
A84	5/2/2005	57	8SF6	27	10	25SF6	21	4SF6	added 45' delay cable, Marx prefire 44 kV, 2X atten added to channel 11 and 12, Laser SF6 trial 1, no channel 10 cables draped over monitor, no laser shot
A85	5/2/2005	57	8SF6	27	10	25SF6	21	4SF6	tough to determine if laser worked or not, Q switch 280 ns before break
A86	5/2/2005	45	8SF6	27	10	25SF6	21	4SF6	no laser, switch SB, pressure increased in switch to 33SF6, Q switch 380ns before break
A87	5/2/2005	45	8SF6	27	10	33SF6	21	4SF6	Q switch 668ns before break, laser shot 1, switch broke at same voltage as for 25SF6
A88	5/2/2005	45	8SF6	27	10	33SF6	21	4SF6	SB test, no laser used, switch no self break, back to laser shots
A89	5/2/2005	45	8SF6	27	10	37SF6	21	4SF6	Q switch 650ns before break
A90	5/2/2005	45	8SF6	27	10	33SF6	21	4SF6	Q switch 690 ns before break
A91	5/3/2005	26	5A	27	10	35A	21	4SF6	trigger section only, no laser used, Marx prefire at 22 kV, increase Marx pressure to 7A, switch break at ~600 kV, **removed atten Ch 10 and 11**
A92	5/3/2005	26	7A	27	10	25A	21	4SF6	Marx prefire at 18 kV, switch break at ~600 kV
A93	5/3/2005	26	5SF6	27	10	25A	21	4SF6	laser attempt 1, 25A trigger only break at 400 kV, Q switch same time as V break, no laser shot
A94	7/11/2005	40	6 SF6	27	8	15S	21	10SF6	Laser timing shots, no load current all clipped, 2X attenuators added to channels 10 and 11, pulse generator 2 toasted, Marx current used to trigger pulse generator 3, must be HF filtered, **Marx voltage monitor was shortened (channel 11) will overestimate voltages by ~13-17%**
A95	7/11/2005	40	6 SF6	27	8	15S	21	10SF6	see notes on shot A94
A96	7/11/2005	40	6 SF6	27	8	15S	21	10SF6	see notes on shot A94
A97	7/11/2005	40	6 SF6	27	8	15S	21	10SF6	see notes on shot A94
A98	7/11/2005	40	6 SF6	27	8	15S	21	10SF6	see notes on shot A94
A99	7/14/2005	45	7SF6	27	9	15S	21	10SF6	
A100	7/14/2005	45	7SF6	27	9	15S	21	10SF6	no switch fire

A101	7/14/2005	35	5A	27	8A	15S	25	10SF6	2562
A102	7/18/2005	54	10SF6	45	60	18S	31	10SF6	attempt firing laser at 85% SB, laser timing system seriously altered, SEE AR32 (changed again for shot A103), TG-70 reconfigured to original configuration, no laser, arc down laser tube through optics and out top of tube to CVR cable, may not let cables rest on laser tube
A103	7/20/2005	40	7SF6	45	60	15A	31	10SF6	laser timing test, laser must be 2+3+5+6+7=397ns from desired breakdown voltage, Ch.5=Marx I, Ch.6=222A trig sync, Ch.7=222A out, Ch.8=ISV
A104	7/20/2005	40	5SF6	45	60	15A	31	10SF6	laser timing verification, same as A103, excellent laser timing shot
A105	7/20/2005	54	10SF6	45	60	18SF6	31	10SF6	laser not at right timing, 222 trig in looks good, trig out too early, TG-70 noise may have set it off, tested with TG-70 and MTG and did not trigger 222, rescale scope to 500 ns/div, no laser fire, retake shot
A106	7/20/2005	54	10SF6	45	60	18SF6	31	10SF6	Vb= 2MV, Trip Deuce position 240 ns, not enough time to indicate laser arrival on time
A107	7/20/2005	54	10SF6	45	60	18SF6	31	10SF6	Vb=1.9 MV, delay set on Trip Duece to 200 ns so output is 380 ns from 1.9 MV time which is 85% of 2.2 MV, Marx prefire
A108	7/20/2005	54	10SF6	45	60	18SF6	31	10SF6	4
A109	7/20/2005	54	10SF6	45	60	18SF6	31	10SF6	change scope 1 to Ch.5=Qswitch sync, Ch.6=222 trig sync, Ch.7=222 out,Ch.8=ISV, timing looks good Marx prefire
A110	7/20/2005	54	10SF6	45	60	18SF6	31	10SF6	Marx prefire, must purge every shot
A111	7/20/2005	54	10SF6	45	60	18SF6	31	10SF6	all good, laser fired 530 ns before breakdown and did not trigger switch at any lower voltage, Vb=2MV
A112	7/20/2005	54	10SF6	45	60	18SF6	31	10SF6	delay moved, Trip Duece position 490 ns before break, did not break switch early, Vb=2.03MV, assumption made that the 222 pulse out downstairs should be ~375 ns before breakdown point, if laser triggers switch , more like 450 ns from shot A116 (this is discussed in AR32)
A113	7/22/2005	34	2A	45	60	16A	31	10SF6	used to compare if laser timing is OK or if the laser spark is long enough for SF6 with 12 cm focal length, Vb=1.1 MV, laser timing OK, Qswitch out looks bad, did not respond to 222 pulse out, Vb is too high, SF6 must still be present in switch
A114	7/22/2005	34	2A	45	60	16A	31	10SF6	no data saved, Trip Deuce was 350 ns before breakdown, Vb=1.2MV
A115	7/22/2005	34	2A	45	60	16A	31	10SF6	222 pulse out was 380 ns before breakdown point, picture indicates laser may have influenced shot, Vb does not illustrate this, Vb=1.2MV
A116	7/22/2005	42	6SF6	45	60	16A	31	10SF6	222 out is 450 ns before break, this was almost definitely a laser shot IS voltage indicates so, Vb=1.4MV
A117	7/22/2005	42	6SF6	45	60	16A	31	10SF6	laser not on, Bv=1.68 M, laser worked on shot A116 (in air not SF6)
A118	7/22/2005	42	6SF6	45	60	16A	31	10SF6	no notes on paper, lens changed to have a focal length of 31 cm for next shot, see AR32 for 222 timing info
A119	7/29/2005	54	10SF6	45	60	18SF6	31	10SF6	Original electrodes SF6 laser tests, LASER 1, 222 set to 350 ns delay, new lens installed, arc of ~0.67 cm, PhotoD=270ns, move Q switch trigger earlier, timing explanation in AR32, Vb=1.8 MV, LASER 1, Ch. 5=PhotoD,Ch. 6=222 input sync, Ch.7=222 out sync, Ch.8=ISV,Ch.1-4=Switch I, Ch.9=Marx I, Ch.10=ISV (2X), Ch.11=Marx V (2X), Ch.12=Load V
A120	7/29/2005	54	10SF6	45	60	18SF6	31	10SF6	changed 222 delay to 100ns, Vb=1.78, Trip2=420ns, PhotoD=276ns,222 delay=100ns, LASER 2
A121	7/29/2005	54	10SF6	45	60	18SF6	31	10SF6	Vb=1.74; Trip2=412ns,PhotoD=244ns,222delay=100ns, LASER 3
A122	7/29/2005	54	10SF6	45	60	18SF6	31	10SF6	Vb=1.78, Trip2=428ns, PhotoD=254ns, 222delay=100 ns, LASER 4

A123	7/29/2005	54	10SF6	45	60	18SF6	31	10SF6	Vb=1.79, Trip2=436ns, PhotoD=264ns, 222=100ns, LASER 5
A124	7/29/2005	54	10SF6	45	60	18SF6	31	10SF6	Vb=1.83,Trip2=424ns,PhotoD=268ns,222=100ns, LASER 6
A125	7/29/2005	54	10SF6	45	60	18SF6	31	10SF6	Vb=1.74; Trip2=408ns,PhotoD=240ns,222delay=100ns, LASER 7
A126	8/9/2005	54	10SF6	45	60	18SF6	31	10SF6	5.25" hole electrodes, PhotoD turned on, Vb=1.72; Trip2=400ns,PhotoD=364ns,222delay=100ns, LASER 1
A127	8/9/2005	54	10SF6	45	60	18SF6	31	10SF6	Laser triggered by noise, evident in PhotoD timing, PhotoD on, Vb=1.65; Trip2=380ns,PhotoD=360ns,222delay=100ns, LASER 2
A128	8/9/2005	54	10SF6	45	60	18SF6	31	10SF6	Laser triggering really only working because of chosen operating voltage, SB shot, switch did not break, Vpeak=2, no pic
A129	8/9/2005	54	10SF6	45	60	18SF6	31	10SF6	PhotoD turned off, PhotoD turned off, Vb=1.63; Trip2=464ns,PhotoD=324ns,222delay=100ns, LASER 3
A130	8/9/2005	54	10SF6	45	60	18SF6	31	10SF6	Vb=1.62; Trip2=484ns,PhotoD=324ns,222delay=100ns, LASER 4
A131	8/9/2005	54	10SF6	45	60	18SF6	31	10SF6	Vb=1.62; Trip2=476ns,PhotoD=348ns,222delay=100ns, LASER 5
A132	8/9/2005	54	10SF6	45	60	18SF6	31	10SF6	Vb=1.96; Trip2=640ns,PhotoD=N/A,222delay=N/A, no channels 1-4, not a laser shot or laser fired late, took several button presses
A133	8/9/2005	54	10SF6	45	60	18SF6	31	10SF6	Vb=1.64; Trip2=492ns,PhotoD=352,222delay=100 LASER 6
A134	8/9/2005	54	10SF6	45	60	18SF6	31	10SF6	delay changed to 160ns, Vb=1.64; Trip2=412ns,PhotoD=400,222delay=160ns, LASER 7
A135	8/12/2005	54	10SF6	45	60	18SF6	31	10SF6	6.5" electrode tests, 222 delay set to 120 ns, Marx prefire 52 kV, Marx needs purging on first shot of day, V clipped, SB shot, no pic (no filter), Vmonitor on ISV needs to be rescaled to A134 and a self break shot on 8/9/2005, bubble in ISV (Ch.10), not replaced, Marx charge voltage potentially not exactly what meters say while charging, potentially charged to 65 kV instead of 54 kV, hitting stop charge on power supply does not disconnect the HV connection, Vb=2.94, perhaps a different self break curve?
A136	8/12/2005	54	10SF6	45	60	18SF6	31	10SF6	Vb=2, LASER 1
A137	8/12/2005	54	10SF6	45	60	18SF6	31	10SF6	Vb=1.77,Trip2=392ns,PhotoD=320ns, LASER 2
A138	8/12/2005	54	10SF6	45	60	18SF6	31	10SF6	Vb=1.77,Trip2=416ns,PhotoD=332ns, LASER 3
A139	8/12/2005	54	10SF6	45	60	18SF6	31	10SF6	Vb=1.76,Trip2=376ns,PhotoD=296ns, LASER 4
A140	8/12/2005	54	10SF6	45	60	18SF6	31	10SF6	Vb=1.78,Trip2=396ns,PhotoD=280ns, LASER 5
A141	8/12/2005	54	10SF6	45	60	18SF6	31	10SF6	Vb=1.75,Trip2=364ns,PhotoD=232ns, LASER 6, SF6 bottle changed
A142	8/22/2005	54	10SF6	45	60	18SF6	31	10SF6	Vb=2.2, no pic, data collected
A143	8/22/2005	54	10SF6	45	60	18SF6	31	10SF6	Vb=2, Trip Duece=448ns, LASER 7
A144	8/22/2005	54	10SF6	45	60	18SF6	31	10SF6	no laser fire, data collected, delay set to 100 ns, no PhotoD, laser may be shutting down before it fire switch, Vb=2.7
A145	8/22/2005	54	10SF6	45	60	18SF6	31	10SF6	Vb=1.94, Trip2=460ns, PhotoD=280ns, LASER 8
A146	8/22/2005	54	10SF6	45	60	18SF6	31	10SF6	no pic, data collected, Vb=1.83, Trip2=436ns,PhotoD=236ns
A147	8/22/2005	54	10SF6	45	60	18SF6	31	10SF6	no laser fire according to PhotoD, button issue, SB, Vb=2.68

A148	8/22/2005	54	10SF6	45	60	18SF6	31	10SF6	PhotoD very early, no pic, we have been turning off camera mid data collection, laser did fire, not triggered, Vb=2.2
A149	8/22/2005	54	10SF6	45	60	18SF6	31	10SF6	PhotoD very early, no laser?, many more channels, data saved and pic, Vb=2.45
A150	8/22/2005	54	10SF6	45	60	18SF6	31	10SF6	Vb=1.98,Trip2=436ns,PhotoD=304ns, LASER 9
A151	8/22/2005	54	10SF6	45	60	18SF6	31	10SF6	Vb=1.9,Trip2=444ns,PhotoD=316ns, LASER 10
A152	8/22/2005	54	10SF6	45	60	18SF6	31	10SF6	Vb=1.9,Trip2=452ns,PhotoD=288ns, LASER 11
A153	8/22/2005	54	10SF6	45	60	18SF6	31	10SF6	Vb=1.96,Trip2=464ns,PhotoD=320ns, LASER 12
A154	8/22/2005	54	10SF6	45	60	18SF6	31	10SF6	Vb=1.7,Trip2=420ns,PhotoD=292ns, LASER 13
A155	8/22/2005	54	10SF6	45	60	18SF6	31	10SF6	Vb=1.83,Trip2=440ns,PhotoD=264ns, LASER 14
A156	8/22/2005	54	10SF6	45	60	18SF6	31	10SF6	no laser fire, Vb=2.7
A157	8/22/2005	54	10SF6	45	60	18SF6	31	10SF6	Vb=1.93,Trip2=464ns,PhotoD=288ns, LASER 15
A158	8/23/2005	54	10SF6	45	60	18SF6	31	10SF6	8" trodes, no laser fire, no PhotoD, good SB, hard to count arcs on bottom, Vb=2.76
A159	8/23/2005	54	10SF6	45	60	18SF6	31	10SF6	take off lighter filter, medium filter only, Vb=1.76, Trip2=448ns, PhotoD=384ns, LASER 1
A160	8/23/2005	54	10SF6	45	60	18SF6	31	10SF6	laser not initiated, SB shot 2, Check marx V ring over (see shot A135 charge voltage description), Vb=2.67
A161	8/23/2005	54	10SF6	45	60	18SF6	31	10SF6	Vb=1.64,Trip2=392ns,PhotoD=292ns, LASER 2
A162	8/23/2005	54	10SF6	45	60	18SF6	31	10SF6	Vb=1.64,Trip2=380ns,PhotoD=292ns, LASER 3
A163	8/23/2005	54	10SF6	45	60	18SF6	31	10SF6	Vb=1.63,Trip2=368ns,PhotoD=288ns, laser shot, no pic, delay readjusted to 120 ns
A164	8/23/2005	54	10SF6	45	60	18SF6	31	10SF6	Vb=1.67,Trip2=372ns,PhotoD=328ns, LASER 4
A165	8/23/2005	54	10SF6	45	60	18SF6	31	10SF6	Vb=1.72,Trip2=372ns,PhotoD=296ns, LASER 5, pic on MUTTSSERVER computer for only this shot
A166	8/23/2005	54	10SF6	45	60	18SF6	31	10SF6	Vb=1.6,Trip2=372ns,PhotoD=328ns, LASER 6, no channels 5-8 saved
A167	8/23/2005	54	10SF6	45	60	18SF6	31	10SF6	Vb=1.67,Trip2=376ns,PhotoD=356ns, good laser, no pic, no channels 1-4 obtained
A168	8/23/2005	54	10SF6	45	60	18SF6	31	10SF6	Vb=1.88,Trip2=408ns,PhotoD=308ns, good laser, no pic
A169	8/23/2005	54	10SF6	45	60	18SF6	31	10SF6	Vb=1.88,Trip2=424ns,PhotoD=360ns, LASER 7
A170	8/23/2005	54	10SF6	45	60	18SF6	31	10SF6	Vb=1.74,Trip2=400ns,PhotoD=352ns, LASER 8
A171	8/23/2005	54	10SF6	45	60	18SF6	31	10SF6	Vb=1.74,Trip2=404ns,PhotoD=316ns, LASER 9
A172	8/23/2005	54	10SF6	45	60	18SF6	31	10SF6	Vb=1.68,Trip2=380ns,PhotoD=292ns, LASER 10
A173	8/23/2005	54	10SF6	45	60	18SF6	31	10SF6	Vb=1.77,Trip2=384ns,PhotoD=364ns, LASER 11
A174	8/23/2005	54	10SF6	45	60	18SF6	31	10SF6	Vb=1.64,Trip2=340ns,PhotoD=292ns, LASER 12
A175	8/23/2005	54	10SF6	45	60	18SF6	31	10SF6	Vb=1.68,Trip2=352ns,PhotoD=304ns, LASER 13
A176	8/23/2005	54	10SF6	45	60	18SF6	31	10SF6	Vb=2.49, SB, photoD way early
A177	8/23/2005	54	10SF6	45	60	18SF6	31	10SF6	Vb=1.74,Trip2=384ns,PhotoD=304ns, LASER 14
A178	8/23/2005	54	10SF6	45	60	18SF6	31	10SF6	Vb=1.73,Trip2=380ns,PhotoD=304ns, LASER 15

A179	9/12/2005	42	5SF6	45	60	20SF6	31	10SF6	Shortened trigger section like "2.5 vert short pres 3" in Maxwell. No Marx fire at 6SF6 or 5SF6, Air prefired at 5A, OK at 10A, no pic, Vb=1.8 (should be 1.51 (check adjudstment factor)), laser power down before discharge, Marx dump reset laser, MTG and TG-70 alone also fire laser (Beginning of laser troubles). For shots A179-A184 there is was no note but post hoc laser it believed to NOT fire for these
A180	9/12/2005	42	6A	45	60	20SF6	31	10SF6	Marx prefire at 36 kV, no pic, Vm=1.2, Vb=1.85 (should be 1.63 (determined for a 1.37 ring up) (later note: does not apply except at peak V)) over estimating by 12%, check shots A119-A178 (checked and found IS V needs a 0.85 multiplier Check A119toA178...7.xls)
A181	9/12/2005	50	10SF6	45	60	35SF6	31	10SF6	Vm=1.53, Vb=2.3, should be 2.1
A182	9/12/2005	50	10SF6	45	60	35SF6	31	10SF6	Vm=1.54, Vb=2.4, should be 2.1
A183	9/12/2005	62	12SF6	45	60	50SF6	31	10SF6	Vm=1.91, Vb=3.11 (should be 2.62)
A184	9/12/2005	62	12SF6	45	60	50SF6	31	10SF6	Vm=1.84, Vb=3.03 (should be 2.52) (shots A179-A184 SB line shots)
A185	9/15/2005	50	10SF6	45	60	35SF6	31	10SF6	Added custom built screen box, added varistor and capacitors to isolation transformer, laser did not shut off on 40 kV SB test, Vb=1.9, laser delay=120n, trip duece=428n, photoD=224n, Laser 1
A186	9/16/2005	50	10SF6	45	60	35SF6	31	10SF6	no laser fire, no PhotoD, SB shot, trip2=608, PhotoD=N/a, Vb=2.68
A187	9/16/2005	50	10SF6	45	60	35SF6	31	10SF6	still no laser fire, reduce delay to 100n for next shot, no PhotoD
A188	9/16/2005	50	10SF6	45	60	35SF6	31	10SF6	MTG not lightling up at least 3 switches in Marx not firing, FOR NEXT SHOT=Marx pressure reduced to 8 psi, TG-70 pres increased to 70 psi, Vcharge=58 for next shot
A189	9/16/2005	58	8SF6	45	70	35SF6	31	10SF6	no PhotoD, Uncouple ground from tank (at pipe on West wall) for next shot, SB shot, MTG has oil in it, all refurbed, capacitor and varistors removed from laser
A190	9/16/2005	50	10SF6	45	70	35SF6	31	15SF6	no laser fire on next shot, try again and removed new copper screen box, added old box, PhotoD=156, Vb=1.8, TripD=464, Laser 2
A191	9/20/2005	50	10SF6	45	70	35SF6	31	15SF6	SB, no pic, UPS's installed, no change in laser situation, FL and Qsw external connections disconnected, laser acting like stop button pressed, not like power interuption
A192	9/20/2005	50	10SF6	45	70	35SF6	31	15SF6	antenna in screenbox, box grounded, all signals obtained, SF shot noise, no laser, channels 6&7 added for time reference
LASER NOISE TESTING and Andy taking data 9/25 to 11/8									Laser installed into bottomless full cabinet. Two 0.75" copper ground pipes run 6' into earth, tank connected to 1, laser cabinet to other via 10' ground strap, Full cabinet always kept laser on if doors were closed and no cables ran into the box except UPS power from a transformer on the breaker strip. Since doors must be closed, cabinet is deemed to reduce ambient noise if grounded. Cables must have ground connection internal to cabinet. WIth the Qsw plugged in and strap grounded, laser worked, with FL and Qsw plugged in a grounded worked 3/4 times. Beefy ground strap added internal to the screen box on signal inputs. PhotoD installed to be isolated electrically from laser case, cable run through tygon, braid jacket grounded to laser case.
A194	11/9/2005	50	10AIR	45	60	35SF6	31	15SF6	Purpose of following tests: To compare 18 psi shots A119-A125 (7 shots) to a set of 35 and 50 psi shots. Two laser shots obtained at 35 so far (A185 and A190). Must fire at same % of SB at A119. TripD=436, delay set to 110, Marx prefired at 45 kV, self break, no pic, no laser shot, laser did not stay on, SF6 bottle starting pressure 280 psi., MARX UNKNOWINGLY HAS AIR UNTIL A211

A195	11/9/2005	50	13AIR	45	60	35SF6	31	15SF6	Marx prefire, no laser, bad pic need medium filter, SF6 start pres 260 psi
A196	11/9/2005	50	16AIR	45	60	35SF6	31	15SF6	Using medium and light filter, Vb=2.6 (must multiply by 0.85). SF6 level 250 psi, no pic, Marx prefire
A197	11/9/2005	40	15AIR	45	60	35SF6	31	15SF6	Vb=1.8, TripD=368, PhotoD=72, voltage monitors on power supply thought to be reading too low (turns out this is not the case), Laser 3
A198	11/9/2005	40	15AIR	45	60	35SF6	31	15SF6	laser delay set to 180, 12.5mA charge current, Vb=2, TripD=348, PhotoD=52, SF6 level 220, Laser 4
A199	11/9/2005	40	15AIR	45	60	35SF6	31	15SF6	TripD=352, PhotoD=56, Vb=1.95, SF6=200, Laser 5
A200	11/9/2005	40	15AIR	45	60	35SF6	31	15SF6	scope 3 was reset before data acquisition, Vb=1.86, SF6 level=190, Laser 6
A201	11/9/2005	40	15AIR	45	60	35SF6	31	15SF6	scope 3 reset again, Vb=1.9, SF6=170, Laser 7
A202	11/9/2005	40	15AIR	45	60	35SF6	31	15SF6	takes 31s to charge Marx, tripD=356,PhotoD=60, Vb=1.85, SF6=150, Laser 8
A203	11/9/2005	40	15AIR	45	60	35SF6	31	15SF6	no chan 5-8 but it looked similar to A202, Laser 9
A204	11/9/2005	40	15AIR	45	60	35SF6	31	15SF6	no chan 5-8 but it looked similar to A202, scope 3 has been triggering in chan 3 instead of exterior, change for next shot, Vb=1.85, SF6=120, Laser 10
A205	11/10/2005	40	15AIR	45	60	35SF6	31	15SF6	SF6 bottle changed, TripD=364, PhotoD=68, Vb=1.85, SF6=75, Laser 11
A206	11/11/2005	60	20AIR	45	60	50SF6	31	15SF6	no pic, Vb now contains 0.85 correction factor, self break at 50 kV, self break and peak ringover, set delay to 180 ns, Vb=2.59, new SF6 bottle
A207	11/11/2005	48	20AIR	45	60	50SF6	31	15SF6	change delay to 132 ns, no PhotoD signal (was covered with tape), LASER 1
A208	11/11/2005	48	20AIR	45	60	50SF6	31	15SF6	TripD=360, PhotoD=60, Vb=1.9, LASER 2
A209	11/11/2005	48	20AIR	45	60	50SF6	31	15SF6	delay set to 112 ns, TripD=368, Vb=1.8, LASER 3
A210	11/11/2005	48	20AIR	45	60	50SF6	31	15SF6	TripD=368, Vb=1.8, LASER 4
A211	11/11/2005	48	20AIR	45	60	50SF6	31	15SF6	Loud bang, Istore perhaps flashed outside because there were no bubbles inside IS but there were a collection of bubbles on the surface of the oil around the switch tower, no marks found on IS face, no evidence of breakdown in data or visually, try again
A212	11/14/2005	50	20AIR	45	60	50SF6	31	17SF6	air was unknowingly in Marx from shot A194 to A211, SB shot, Marx and MTG self breaking, laser did not fire, TripD before input
A213	11/14/2005	50	20AIR	45	60	50SF6	31	17SF6	laser did not fire because TripD fired very early like shot A212, TripD delay must increase to put it 360 ns from break point, Marx current has pre blip and is trigger in TripD earlier, increased TripD delay by 152 ns to 264 ns
A214	11/14/2005	50	20AIR	45	60	50SF6	31	17SF6	SB shot, laser did not fire, laser acting like it is shutting off, delay set back to 112 ns, peahaps early current blip is a result of SF6 filled Marx or more likely MTG not firing all gaps simultaneously, went to air in MTG
A215	11/14/2005	50	20AIR	45	60	50SF6	31	17SF6	attached laser cabinet ground back directly to pipe, removed bill's attachment, LASER 5
A216	11/14/2005	50	20AIR	45	60	50SF6	31	17SF6	PhotoD back operational for this shot, switch brokedown late in time, scope 3 time set to 250 ns/div to see if laser firing late, laser turning off, PhotoD very noisy, disconnect exterior ground strap that was added on A214 to Qsw in, SB shot, laser did not fire, PhotoD looks OK as before but laser not staying on

References

1. E.A. Weinbrecht, D.H. McDaniel, and D.D. Bloomquist, "The Z Refurbishment Project (ZR) at Sandia National Laboratories", 14th IEEE Pulsed Power Conference, pp. 157-162, 2003.

2. K.R. LeChien and J.M. Gahl, "Investigation of a Multichanneling Multigap Marx Bank Switch", Review of Scientific Instruments, Vol. 75, No. 1, pp. 174-178, 2004.

3. J.P. Corley, M.A. Dixon, A.A. Kim, et al., "Tests of 6-MV Triggered Switches on APPRM at SNL", 13th IEEE Pulsed Power Conference, pp. 1778-1781, 2001.

4. J.P. Corley, K.C. Hodge, et al., "Development/Tests of 6 MV Triggered Gas Switches at SNL", 14th IEEE Pulsed Power Conference, pp. 875-878, 2003.

5. D.R. Humphreys, K.J. Penn, J.S. Cap, et al., "Rimfire: A Six Megavolt Laser-Triggered Gas-Filled Switch for PBFA II", 5th IEEE Pulsed Power Conference, pp. 262-265, 1985.

6. B.N. Turman, A.E. Rodriguez, and K.J. Touryan, "Experimental and Analytical Study of Laser-Triggering in the Rimfire Switch", 8th IEEE Pulsed Power Conference, pp. 319-322, 1991.

7. S.E. Rosenthal, J.M. Elizondo, J.E. Maenchen, K.W. Struve, et al., "Modeling 6-MV Gas Switches for the ZR Accelerator", 14th IEEE Pulsed Power Conference, pp. 163-166, 2003.

8. D.L. Johnson, "Initial Proto II Pulsed Power Tests", 1st IEEE Pulsed Power Conference, pp. IE2-1, 1976.

9. T.H. Martin, J.P. Vandevender, G.W. Barr, S.A. Goldstein, et al., "Particle Beam Fusion Accelerator-I (PBFA-I)", 1981 Particle Accelerator Conference, Washington, DC, 1981.

10. G.J. Denison, J.A. Alexander, J.P. Corley, et al., "Performance of the HERMES-III Laser-Triggered Gas Switches", 7th IEEE Pulsed Power Conference, pp. 579-582, 1989.

11. D.D. Bloomquist, R.W. Stinnett, D.H. McDaniel, et al., "Saturn, A Large Area X-Ray Simulation Accelerator", 6th IEEE Pulsed Power Conference, pp. 310-317, 1987.

12. B.N. Turman, et al., "PBFA II, a 100 TW Pulsed Power Driver for the Inertial Confinement Fusion Program", 5th IEEE Pulsed Power Conference, pp. 155, 1985.

13. R.B. Speilman, et al., "PBFA II-Z: A 20-MA Driver for Z-Pinch Experiments", 10th IEEE Pulsed Power Conference, pp. 396, 1995.

14. D.D. Bloomquist, G.R. Montry, S.E. Downie, and G.R. Peterson, "Cascade Switch Implementation on PBFA I", 5th IEEE Pulsed Power Conference, pp. 266-269, 1985.

15. B.N. Turman and D.R. Humphreys, "Scaling Relations for the Rimfire Multi-Stage Gas Switch", 6th IEEE Pulsed Power Conference, pp. 347-353, 1987.

16. G.J. Denison, J.P. Corley, D.L. Johnson, et al., "A High-Voltage Multistage Laser-Triggered Gas Switch", 6th IEEE Pulsed Power Conference, pp. 490-493, 1987.

17. B.N. Turman and D.R. Humphreys, "Interstage Closure Times for the Rimfire Multistage Gas Switch", 7th IEEE Pulsed Power Conference, pp. 555-558, 1989.

18. K.R. LeChien, J.M. Gahl, M.A. Kemp, et al., "Development of a Terawatt Test Stand and the University of Missouri for Fast, Multichannel Switching Analysis", 14th IEEE Pulsed Power Conference, pp. 1051-1053, 2003.

19. Sandia National Laboratories, "Proto II Design Drawings", 1980.

20. Rob Sharpe, Private Communication, 2003.

21. Juan Elizondo, Private Communication, 2003.

22. T.H. Martin, "Pulse Charge Gas Breakdown", 5th IEEE Pulsed Power Conference, pp. 74-83, 1985.

23. T.H. Martin, "An Empirical Formula for Gas Switch Breakdown Delay", 7th IEEE Pulsed Power Conference, pp. 73-79, 1989.

24. T. Nitta, N. Yamada, and Y. Fujiware, "Area Effect of Electrical Breakdown in Compressed SF_6", IEEE Transactions on Power Apparatus and Systems, Vol. PAS-93, No. 2, pp. 623-629, 1974.

25. J.C. Martin, "JC Martin on Pulsed Power", Plenum Press, pp. 146, 1996.

26. F.W. Grover, "Inductance Calculations", Dover Publications, pp. 31-44, 1962.

27. Physics International, "Physics International Data Sheet", 1980.

28. K.R. LeChien, J.M. Gahl, M.A. Kemp, et al., "Initial Results from the University of Missouri Terawatt Test Stand", Proceeding of the 2004 Power Modulator Conference, pp. 122-125, 2004.

29. M.A. Kemp, R.D. Curry, and S.D. Kovaleski, "Experimental Study of the Multichanneling Self-Break Section of the Rimfire Switch", IEEE Transactions on Plasma Science, In press, 2005.

30. M.A. Kemp, "Simulation and Experimental Study of the Multichanneling Rimfire Gas Switch", Masters Thesis, University of Missouri-Columbia, 2005.

31. C.R. Hicks, "Fundamental Concepts in the Design of Experiments", Holt, Rinehart and Winston, pp. 259-269, 1973.

32. SAS Institute Inc., "SAS Version 9.", Statistical Software, 2005.

33. J.F. Francis, "High Voltage Pulse Techniques", Plasma Laboratory, Department of Electrical Engineering, Texas Tech University, 1976.

34. M.A. Kemp, R. Curry, and S. Kovaleski, "Experimental Study of the Multichanneling, 3 MV Rimfire Gas Switch in the Self Breakdown Mode", 15th IEEE Pulsed Power Conference, pp. In press, 2005.

35. New Wave Research, "Laser Manual", User Manual, 2003.

36. K.R. LeChien, J.M. Gahl, and K.W. Struve, "Electrical Effects of Multichanneling in the 2.5 MV Rimfire Gas Switch Using a Laser Trigger", 15th IEEE Pulsed Power Conference, 2005.

37. M.A. Kemp, R.D. Curry, J.M. Gahl, K.F. McDonald, and K.W. Struve, "Modeling and Analysis of the Rimfire Gas Switch", IEEE Trans. on Plasma Science, Vol. 33, No. 4, pp. 1245-1251, 2005.

38. S. Furuya, Y. Watanabe, T. Yoshikawa, S. Takano, and J. Irisawa, "Characteristics of Multichannel Arc Gap", Japanese Journal of Applied Physics, Vol. 40, No. 2B, pp. 987-991, 2001.

39. T.H. Martin, J.F. Seamen, and D.O. Jobe, "Energy Losses in Switches", 9th IEEE Pulsed Power Conference, pp. 463-470, 1993.

40. T.W. Hussey, K.J. Davis, J.M. Lehr, N.F. Roderick, R.C. Pate, et al., "Dynamics of Nanosecond Spark-Gap Channels", 12th IEEE Pulsed Power Conference, pp. 1171-1174, 1999.

41. M.J. Kushner, W.D. Kimura, and S.R. Byron, "Arc Resistance of Laser-Triggered Spark Gaps", Journal of Applied Physics, Vol. 58, No. 5, pp. 1744-1751, 1985.

42. H. Akiyama, M. Kristiansen, H. Krompholz, and B. Maas, "Current-Voltage Characteristics of a High-Current Pulsed Discharge in Air", IEEE Trans. on Plasma Science, Vol. 16, No. 2, pp. 312-316, 1988.

43. M.J. Kushner, R.D. Milroy, and W.D Kimura, "A Laser-Triggered Spark Gap Model", Journal of Applied Physics, Vol. 58, No. 8, pp. 2988-3000, 1985.

44. S.I. Braginskii, "Theory of the Development of a Spark Channel", Soviet Physics JETP, Vol. 34 (7), No. 6, pp. 1068-1074, 1958.

45. R. Kalstrom and P. Lehmann, "Resistance Measurements on a Gasdischarge Switching Device and on Projectile Plasma Armatures for EML", IEEE Trans. on Magnetics, Vol. 27, No. 1, pp. 160-164, 1991.

46. "Solvay Flour", Available Online: www.solvay-fluor.com/product/datasheet/0,0-EN-10007005,00.html, 2001.

47. P. Swarbrick, "Composition and Properties of a Sulphur Hexafluoride Arc Plasma", British Journal of Applied Physics, Vol. 18, pp. 419-426, 1967.

48. X.Q. Qiu, I.D. Chalmers, and P. Coventry, "A Study of Alternative Insulating Gases to SF_6", Journal of Physics D: Applied Physics, Vol. 32, pp. 2918-2922, 1999.

49. R. Adler, "Pulse Power Formulary", North Star Research Formulary, 2001.

50. K.R. LeChien, "A Study of a Multichanneling Spark Gap Switch", Master's Thesis, University of Missouri, 2002.

51. R.L. Sandstrom, H. Sheilds, and J.I. Levatter, "Performance Characteristics of a High-Repetition Rate, Multichannel Rail-Gap Switch", Review of Scientific Instruments, Vol. 58, No. 4, pp. 696-700, 1987.

52. G.R. Neil and R.S. Post, "Multichannel, high-energy railgap switch", Review of Scientific Instruments, Vol. 49, No. 3, pp. 401-403, 1978.

53. H.M. von Bergmann, "Triggered Multichannel Surface Spark Gaps", Journal of Physics E: Scientific Instruments, Vol. 15, pp. 243-247, 1982.

54. T.D. Hguyen, H.R. Hiziroglu, and M.S. Dincer, "Breakdown Voltages in SF_6 + Argon Mixtures", IEEE Conference on Electrical Insulation and Dielectric Phenomena, pp. 598-601, 1996.

55. H.R. Hiziroglu, M.S. Dincer, and T.D. Hguyen, "Breakdown Voltages in SF_6 + Argon Mixtures Under Nonuniform Electrostatic Fields", IEEE Conference on Electrical Insulation and Dielectric Phenomena, pp. 579-582, 1997.

56. H.R. Hiziroglu, A. Nutakki, and M.S. Dincer, "Impulse Voltage Breakdown of Argon + SF_6 Mixtures Under Non-Uniform Electric Fields", IEEE

Conference on Electrical Insulation and Dielectric Phenomena, pp. 448-450, 2003.

57. W. Khechen and J.R. Leghari, "Breakdown Studies of SF_6/Argon Gas Mixtures", IEEE Transactions of Electrical Insulation, Vol. 24, No. 6, pp. 1141-1146, 1989.

58. T. Hinterholtzer and W. Boeck, "Breakdown in SF_6 Influenced by Corona-Stabilization", Conference on Electrical Insulation and Dielectric Phenomena, pp. 413-416, 2000.

59. A. Guenther and M. Kristiansen, "Gas Discharge Closing Switches", edited by Gerhard Schaefer, Electrical Breakdown in Gases in Electric Fields, Plenum Press, pp. 20, 1990.

60. V.A. Lisovskiy and V.D. Yegorenkov, "Electron-Drift Velocity Determination in CF_4 and SF_6 in a Strong Electric Field from Breakdown Curves of Low-Pressure Discharge", Journal of Physics D: Applied Physics, Vol. 32, pp. 2645-2648, 1999.

61. Ansoft Corp., Maxwell SV 9 static field solver, 2002.

62. J.M. Koutsoubis, S.J. MacGregor, and S.M. Turnbull, "Triggered Switch Performance in SF_6, Air, and an SF_6/Air Mixture", IEEE Transactions on Plasma Science, Vol. 27, No. 1, pp. 272-281, 1999.

63. V.A. Avrutskii, G.M. Goncharenko, et al., "Effect of Electrode Roughness on the Electrical Strength of Compressed Gas", Soviet Physics Technical Physics, Vol. 18, No. 3, pp. 386-388, 1973.

64. L. Bradley, "Preionization Control of Streamer Propagation", Journal of Applied Physics, Vol. 43, No. 3, pp. 886-889, 1972.

65. A. Dick, S. MacGregor, et al., "An Investigation into High Speed Gas Breakdown in Pulsed Power Switches", Proceedings of the IEEE Power Modulator Symposium, pp. 202-205, 1998.

66. A. Pederson, "The Effect of Surface Roughness on Breakdown in SF_6", IEEE Transactions on Power Apparatus and Systems, Vol. PAS-94, No. 5, pp. 1749-1754, 1974.

67. S.J. MacGregor, F.A. Tuema, S.M. Turbull, and O. Farish, "The Application of the Paschen Deviation to the Operation of Repetitive High Pressure Gas Switches", 9th IEEE Pulsed Power Conference, pp. 934-937, 1993.

68. J.J. Ramirez, "Effect of Electrode Surface Conditions on the Self-Breakdown Strength and Jitter of a High Pressure Pulsed Gas Switch", Journal of Applied Physics, Vol. 47, No. 5, pp. 1952-1958, 1976.

69. W.K. Tucker, "A 3-Megavolt Sulphur Hexafluoride Trigatron", Sandia Document SC-DR-72 0506, 1972.

70. A. Dick, S. MacGregor, et al., "Breakdown Phenomena in Ultra-Fast Plasma Closing Switches", IEEE Transactions on Plasma Science, pp. 1456-1461, 2000.

71. J. Maenchen, "An Introduction to ZR Gas Switching", Internal Sandia Workshop Note, 2005.

72. J. Elizondo, "ZR Tech Note 5, Inductance Calculations for the Rimfire Multichannel Switch", Sandia Internal Tech Note, 2003.

73. M.J. Mulcahy, P. Bolin, et al., "Gas Insulation", Ion Physics Corp., Note from the High Voltage Technology Seminar, 1969.

74. W.R. Rapoport, J. Goldhar, and J.R. Murray, "KrF Laser Triggered SF_6 Spark Gap for Low Jitter Timing", IEEE Transactions on Plasma Science, Vol. PS-8, No. 3, pp. 167-170, 1980.

75. LLNL, "Document 18.2: Pressure Vessel and System Design", Lawrence Livermore National Lab, ES and H manual, Available online: http://www.llnl.gov/es_and_h/hsm/doc_18.02/doc18-02.html, 2000.

76. Honeywell, "SF6 Technical Reference", Available Online: www.specialtychem.com/sf6/pdf/techbook.pdf, 2005.

VITA

Keith LeChien was born July 17, 1979, in Belleville, Illinois. After attending a well rounded mixture of public, parochial and non-parochial private schools in Belleville, he received B.S. (2001), M.S. (2002), and a Ph.D. (2005) in electrical engineering from the University of Missouri-Columbia. His graduate research was supported Sandia National Laboratories. He is married to the former Mary Porter of Kansas City, Missouri, and he was employed in the Advanced Pulsed Power Technologies division at Sandia following his work at Missouri.